2025 ISOE INTERNATIONAL SYMPOSIUM ON OCCUPATIONAL EXPOSURE MANAGEMENT AT NUCLEAR FACILITIES

WEIHAI, CHINA, 22-24 OCTOBER 2025

PROGRAMME & BOOK OF ABSTRACTS

ORGANIZED BY

- IAEA Technical Centre of the Information System on Occupational Exposure (ISOE)

CO-SPONSORED BY

- International Atomic Energy Agency (IAEA)
- OECD Nuclear Energy Agency (NEA)

HOSTED BY

- Nuclear and Radiation Safety Centre, Ministry of Ecology and Environment of China

COOPERATED AND SUPPORTED BY

- Huaneng Shandong Shidao Bay Nuclear Power CO., LTD.
- China National Nuclear Corporation
- China General Nuclear Power Group
- Chinese Society of Radiation Protection
- China Chamber of International Commerce Weihai Chamber

The IAEA Technical Centre of the Information System on Occupational Exposure (ISOE) is organizing the 2025 ISOE International Symposium on Occupational Exposure Management at Nuclear Facilities in Weihai, China from 22 to 24 October 2025.

The Symposium will be hosted by the Nuclear and Radiation Safety Centre (NSC), Ministry of Ecology and Environment of China in cooperation with the China Huaneng Group Co., Ltd. (CHNG), co-sponsored by the International Atomic Energy Agency (IAEA), the OECD Nuclear Energy Agency (NEA), supported by the China National Nuclear Corporation (CNNC), the China Nuclear Power Group (CGN) and the Chinese Society of Radiation Protection (CSRP).

The Symposium is targeted at all those concerned with radiation protection at nuclear facilities, from utilities, contractors, regulatory bodies as well as international organizations.

The main objectives of the Symposium are:

- to provide a forum of information exchange on occupational exposure concerns in nuclear power plants (practices, management and procedures, dose results and reduction, improvements of techniques and tools, etc.),
- to provide an opportunity to transfer the knowledge and experiences on occupational radiation protection accumulated in the ISOE system to newcomers and embarking countries of NPP.
- to allow vendors to present their recent experience and developments in radiation protection (measurement techniques, operating and plant design improvements, ALARA practices during operation and outages, etc.) in a commercial exhibition.

The Symposium will provide an opportunity for the participants to take part in discussions during plenary sessions and presentations of posters.

A technical visit will be organized on the last day of the Symposium.

We are looking forward to welcoming you in Weihai, China.

Jizeng MA

Head of ISOE IAEA Technical Centre
On behalf of the Programme Committee

PROGRAMME COMMITTEE MEMBERS

Duanjie YANG	*NSC, China*
Junwu YANG	*CGN, China*
Chuan WANG	*CNNP, China*
Jizeng MA	*ISOE IAEA TC*
Hidenori YONEHARA	*ATC, Japan*
Laure-Anne BELTRAMI	*ETC, CEPN, France*
Lucie D'ASCENZO	*ETC, CEPN, France*
Caroline SCHIEBER	*ETC, CEPN, France*
David W. MILLER	*NATC, USA*
Benjamin CHUI	*Darlington NPP, Canada*
Hans MEIJER	*Borssele NPP, the Netherlands*
	ISOE Chair
Akiko SUZUKI	*NRA, Japan*
	ISOE Vice-Chair
Toshikazu SUZUKI	*TEPCO, Japan*
	ISOE Chair Elected
Ye ZHANG	*OECD/NEA, France*
	ISOE Secretariat

SYMPOSIUM VENUE

The Symposium will take place at the Rongcheng Shidao Hotel, Weihai, China.

WORKING LANGUAGE

The symposium will be held in English.

2025 ISOE INTERNATIONAL SYMPOSIUM

22-24, OCTOBER 2025, WEIHAI, CHINA

TABLE OF CONTENTS

PROGRAMME OF THE SYMPOSIUM

WEDNESDAY 22 OCTOBER 2025

08:30 – 09:00	**Registration**

09:00 – 09:50	**Opening Ceremony** 1.Opening remarks *by Youcai Feng from NSC* (Detupy director General of NSC) 2.Opening remarks *by Miroslav Pinak* (Head, Radiation Safety and Monitoring Section, IAEA) 3.Opening remarks *by Mr. Huaquan Lv* (Deputy General Manager of CHNG) 4.Opening remarks *by Akiko Suzuki* (ISOE Vice Chair) 5. Briefing on logistical information *by the host organization* 6.Group Photo

SESSION 1. *Chairpersons*	**RADIATION PROTECTION MANAGEMENT (1)** *André Theune (N.V. EPZ (Borssele NPP), the Netherlands), Duanjie Yang (Nuclear and Radiation Safety Center, China)*
9:50 – 10:50 (60 min)	**Radiation Protection Management System, Dose Management and Performance Indicators at CNPGS** *Iftikhar Ahmad Rana (Chashma Nuclear Power Generating Station, Pakistan)*
	Dose Optimization of Overhaul Critical Work Order: A Pilot Study and Risk Assessment *Zhao Jiang (China General Nuclear Power (Shenzhen) Operational Technology & Radiation Monitoring Co., Ltd, China)*
	Analysis of Occupational Exposure Status and Good Practices in Operating Nuclear Power Plants in China *Yuan Fang (Nuclear and Radiation Safety Center, China)*

10:50 – 11:20 (30 min)	**Coffee-break, Visit of Exhibition, Posters**

SESSION 2. *Chairpersons*	**COMPREHENSIVE APPROACHES TO RADIATION PROTECTION** *Benedicte Clement Walschaerts (Belgium), Xueming Ren (Taishan Nuclear Power Joint Venture Co., Ltd)*
11:20 – 12:40 (80 min)	**Radiation Protection at the Design Stage of Nuclear Installations** *Caroline SCHIEBER (CEPN, France)*
	Application of ALARA Principle in the Radiation Protection Design of HPR1000 Nuclear Power Plant *Qianqian Huang (China Nuclear Power Engineering Co., Ltd, China)*
	The Application of Virtual Reality Technology in Radiation Protection Training *Yanyun Shen (CNNP Nuclear Power Operations Management Co., Ltd, China)*
	Strengthening Occupational Radiation Protection in Nigeria Through Effective Regulatory Oversight *Godwin B. Ekong (Nigerian Nuclear Regulatory Authority, Nigerian)*

12:40 – 14:00 (80 min)	**Lunch Break**

SESSION 3. *Chairpersons*	**RADIATION PROTECTION MANAGEMENT (2)** *Iftikhar Ahmad Rana (Chashma Nuclear Power Generating Station, Pakistan), Hua Li (China Institute for Radiation Protection, China)*
14:00 – 15:40 (100 min)	**Radiation Protection Performance Indicator System of CNNP** *Quanli Chen (CNNP Co., Ltd. Jiangsu Nuclear Power Corporation, China)*
	Radiation Protection – Self-Protection vs. Service-Protection *Loc Nguyen (-, Canada)*
	Discussion on Analysis and Optimization of Collective Dose in China National Nuclear Power Company *Bing Dong (Nuclear Power Operations Research Institute, China)*
	Surface Contamination Control Practices and Refined Management of the Cleanliness Radiation Controlled Area (CRCA) Mode at Taishan Nuclear Power Plant *Xueming Ren (Taishan Nuclear Power Joint Ventrue Co., Ltd, China)*
	A Brief Discussion on a Regeneration and Decontamination Process for Radioactive Waste Resin *Ming Han (Huaneng Shandong Shidao Bay nuclear power Co.,Ltd, China)*

15:40 – 16:10 (30 min)	**Coffee-break, Visit of Exhibition, Posters**

SESSION 4. *Chairpersons*	**SOURCE TERM MANAGEMENT** *Caroline Schieber (CEPN, France), Chuan Wang (Nuclear Power Operations Research Institute, China)*
16:10 – 17:50 (100 min)	**ALARA Impact of a Chemical Decontamination and Design Modification at a BWR in Subsequent Cycles** *René Hoffmeister (Nuclear Power Plant Leibstadt (KKL), Switzerland)*
	Analysis and Optimization of Radioactive Source Terms for Qinshan Nuclear Power Plant *Hao Huang (CNNP Nuclear Power Operations Management Co., Ltd, China)*
	Changes in Ionizing Radiation Field During the First Cycle after Zinc Injection into the Primary Circuit of Operating Nuclear Power Units *Haiju Shen (CNNP Nuclear Power Operations Management Co., Ltd, China)*
	Source Term Control Technologies for Key Radionuclides in Nuclear Power Plants *Yaru Fu (Shanghai Nuclear Engineering Research & Design Institute, China)*
	Investigation and Analysis of Deposition Source Term AP1000 Units *Quanlu Gou (Shandong Nuclear Power Co., Ltd, China)*

CONFERENCE DINNER	
19:00	**Symposium Dinner at Shidao Hotel**

THURSDAY 23 OCTOBER 2025

SESSION 5. *Chairpersons*	**MEASUREMENT & MONITORING TECHNOLOGY** *Rene Hoffmeister (Nuclear Power Plant Leibstadt, Switzerland), Quanlu Gou (Shandong Nuclear Power Co., Ltd, China)*
09:00 – 10:40 (100 min)	**Preliminary Comparison Study on the Dosimetric Characteristics of Personal Neutron Dosimeters in a Nuclear Power Plant** *Lizhi Zhang (State Nuclear Power Demonstration Plant Co.Ltd, China)*
	Investigation on Weakly Penetrating Radiation and Personal Dose Monitoring for VVER Units *Bingjun Hou (Jiangsu Nuclear Power Corporation, China)*
	Research and Development of Online Monitoring System for Nuclear Power Plant Radioactive Sources under 5G Environment *Bing Qu (Liao Ning Hong Yan He Nuclear Power Co.,Ltd, China)*
	In-situ Gamma Spectroscopy Measurement of Activated Corrosion Products in Nuclear Power Plants and Its Applications *Ruiwen Liu (China Institute for Radiation Protection, China)*
	Implementation and Verification of a free-moving 3-D Compton Imaging System for γ source Term Monitoring in Nuclear Power Plants *Chongyang Wang (China Institute for Radiation Protection, China)*

10:40 – 11:10 (30 min)	**Coffee-break, Visit of Exhibition, Posters**

SESSION 6. *Chairpersons*	**ADVANCED TECHNOLOGIES & DIGITAL TRANSFORMATION (1)** *Toshikazu Suzuki (Tepco, Japan), Jianqi Jiang (CNNP Nuclear Power Operations Management Co., Ltd, China)*
11:10 – 12:30 (80 min)	**An Engineering Approach of Building Effective 3D Radiation Map with Low Cost** *Gaoxiang Xu (Huaneng Shandong Shidao Bay nuclear power Co.,ltd, China)*
	Nuclear Power Plant Radiation Protection Digital Transformation Implementation Path and Application Effect — A Case Study of Taishan Nuclear Power Plant *Weihua He (Taishan Nuclear Power Joint Venture Company Limited, China)*
	Real-time Primary Coolant Isotopic Trending using 3-D Pixelated CZT Spectrometers *Weiyi Wang/David W. Miller (H3D, Inc Palisades Nuclear Plant, China/USA)*
	Study On Digital Refined Management of Radiation Protection in Nuclear Power Plants Based on Wireless Positioning EPD *Yangxing Hu (Huaneng Hainan Changjiang nuclear power Co.LTD, China)*

12:30 – 14:00 (90 min)	**Lunch Break**

SESSION 7. *Chairpersons*	**ADVANCED TECHNOLOGIES & DIGITAL TRANSFORMATION (2)** *Akiko Suzuki (NRA, Japan), Jinfeng Li (China Institute of Atomic Energy, China)*
14:00 – 15:00 (60 min)	**Indoor 3D Gamma Radiation Mapping Based on VSLAM and Its Preliminary Application in Digital Systems** *Hui Li (China Institute for Radiation Protection, China)*
	A New Solution for Occupational Exposure Management at Nuclear Facilities Using SMARP System *Ji Ma (China Institute for Radiation Protection, China)*
	Development of Small and Medium-Sized Robotic Platform System for Nuclear Emergencies and High-Radiation Scenarios *Yanan Hong (China Institute of Atomic Energy (CIAE), China)*

15:00 – 15:30 (30 min)	**Summary of the meeting** **Briefing for the next ISOE International Symposium** **Distinguished Papers and Closure of the Symposium** **Arrangement for the Technical Tour**

FRIDAY 24 OCTOBER 2025

09:00 – 16:00	**Technical Visit** **Shidao Bay Nuclear Power Plant** **Weihai International Exhibition Center** Departure: 9:00 – Finish: around 16:00

POSTER SESSION

■TOPICAL SESSION 1 : RP management

1. Optimization of Radioactive Sources and Radiographic Inspection Management in Nuclear Power Plant Engineering Area
   Yangxing Hu (Huaneng Hainan Changjiang Nuclear Power Co., Ltd, China)
2. Practical Experience of Limiting Radiation Field in a Nuclear Power Plant
   Pingwei Li (Yangjiang Nuclear Power Co., Ltd., China)

■TOPICAL SESSION 2 : Comprehensive Approaches To Radiation Protection

3. Research on Mitigation of Radioactive Contamination
   Shen Fu (China Institute for Radiation Protection)

■TOPICAL SESSION 3 : Source Term management

4. Experimental Study on Graphite Dust Deposition in Pipelines under Simulated HTGR
   Shulong Huang (China Institute for Radiation Protection, China)
5. Analysis of the Current Status of Research on Neutron Shielding Materials
   Caixia Miao (China Institute of Atomic Energy, China)
6. Development of a Novel Neutron Spectrometer for Application in Boron Neutron Capture Therapy (BNCT)
   Zhenglin Huang (China Institute for Radiation Protection, China)

■TOPICAL SESSION 4 : Measurement & Monitoring Technology

7. Envisioned Automation of Thermoluminescent Measurement System
   Haijiang Shi (China Institute of Atomic Energy, China)
8. Domestic Commercial VDMOS as a High Radiation Doses Sensor
   Zhiji Pan (China Institute for Radiation Protection, China)
9. Research on Screening Method of Heavy Charged Ions in Solid State Nuclear Track Detector
   Qi Zhang (China Institute for Radiation Protection, China)
10. Design and Validation of a Single-Sphere Neutron Spectrometer with Nearly Isotropic Response for Workplace Spectroscopy
    Bowen Sun (China Institute for Radiation Protection, China)
11. Analysis of Weakly Penetrating Radiation Dose Distribution in Heavy-Ion Therapy Based on GATE Simulation
    Yingguo Li (China Institute for Radiation Protection, China)
12. Development of a Total Organic Carbon Analyzer Based on Supercritical Water Oxidation and Preliminary Experimental Validation
    Anyuan Hu (China Institute of Atomic Energy, China)
13. β-γ Discrimination Using a Phoswich Detector for Radiation Monitoring
    Qianyu Pan (China Nuclear Power Research and Design Institute)
14. Study on α Energy Spectrum Fitting Technology for Radioactive Aerosols
    Tao Ma (China Institute for Radiation Protection)

15. Establishment of a Mobile Pulsed γ-Ray Generation Device

    Jiaoyu Zhang (China Institute for Radiation Protection, China)

■TOPICAL SESSION 5 : Advanced Technologies & Digital Transformation

16. 3D Radiation Mapping Using 3-D Pixelated CZT Detectors

    Weiyi Wang / David W. Miller (H3D, Inc/Palisades Nuclear Plant, China/USA)

■TOPICAL SESSION 6 : Internal Exposure management

17. The Development of the Self-Service WBC System and Its Application

    Xiaodun Li (China Institute for Radiation Protection, China)

18. Design of Thyroid/Lung Counter and Monte Carlo Simulation Study on Detection Efficiency

    Yunpeng Wang (China Institute for Radiation Protection)

19. Development Of a New Skull Phantom for Calibrating In Vivo Monitoring Systems for Pb-210 Internal Contamination

    YiCong Liu (China Institute for Radiation Protection)

20. Standardization Research on Analytical Monitoring Technology for 241Am in Urine

    Yipin Zhang (China Institute of Atomic Energy (CIAE))

21. Study on the Standardization of Tritium Analysis in Urine and Internal Exposure Dose Assessment

    Jinfeng Li (China Institute of Atomic Energy, China)

22. Analysis Of the Establishment of Monitoring Period and Measurement Duration for Personal Dose of Internal Exposure

    Zheng Lu (China Institute of Atomic Energy, China)

23. Impacts of Legacy Uranium Sites on Agricultural Ecosystems

    Chenxiao Wang (China Institute of Atomic Energy, China)

■TOPICAL SESSION 7 : Waste Management & Decontamination

24. Optimization Suggestions for Classified Collection and Treatment Methods of Scrapped Protective Articles in Nuclear Power Plants

    Yu Zhang (Shandong Nuclear Power Company Ltd, China)

25. A Brief Introduction of Thermal Treatment and Clearance Technology of Radioactive Wastes for Nuclear Power Plants

    Ming Han (Huaneng Shandong Shidao Bay nuclear power Co., Ltd, China)

26. Introduction To a Plasma Melting Treatment Process for Radioactive Sludge

    Ming Han (Huaneng Shandong Shidao Bay nuclear power Co., Ltd, China)

BOOK OF ABSTRACTS

TABLE OF CONTENTS

ORAL PRESENTATIONS

POSTERS

SESSION 1. Radiation Protection Management System, Dose Management and Performance Indicators at CNPGS"

Iftikhar Ahmad Rana

Chashma Nuclear Power Generating Station, Pakistan

Abstract / Outlines

Radiation Protection Management System

a) CNPGS Organization (Overall headed by General Manager)
b) Plant Organization (Headed by Plant Manager, who Reports to General Manager)
c) Responsibilities of Manager Health Physics (Reports to Plant Manager)
d) Responsibilities of Head Radiation Protection (Reports to Manager Health Physics)
e) Quality Assurance Department (each plant / unit has own quality assurance department)
f) Corporate Oversight (independent multi-stage oversight at corporate i.e. DNPO/ DQO/ DOS)

Dose Management

a) External Dosimetry Management (EPDs / TLDs etc.)
b) Internal Dosimetry Management (WBC etc.)
c) Radiation Work Permit
d) Special Radiation Work Permit
e) ALARA Committee (independent committee at each plant / unit)
f) RFO Dose Target
g) Dose Management at Multi-unit site (at all four units of CNPGS)

Performance Indicators

a) Collective Radiation Exposure etc.
b) Fleet Management System (i.e. CFAM & SFAM)
c) Over Achievement (WANO 1st Position in CRE)

SESSION 1. Dose Optimization of Overhaul Critical Work Orde: A Pilot Study and Risk Assessment

Zhao Jiang

China General Nuclear Power (Shenzhen) Operational Technology & Radiation Monitoring Co., Ltd., Shenzhen, China

Abstract: This study proposes a radiation dose optimization framework tailored for maintenance operations in nuclear power plants. By establishing and maintaining CGN's Overhaul Critical Work Order Database, which incorporates benchmark and excellence evaluation criteria for work orders, the methodology provides robust technical support for optimizing collective dose management. Through systematic application during overhauls, we constructed a Key Operations Database and implemented Grubbs' criterion for outlier elimination to develop a standardized dose assessment model. The framework was validated through overhaul practice, successfully identifying critical dose optimization intervals. This approach delivers actionable solutions for radiation protection optimization under the ALARA (As Low As Reasonably Achievable) principle in nuclear facility maintenance management.

SESSION 1. Analysis of Occupational Exposure Status and Good Practices in Operating Nuclear Power Plants in China

Yuan Fang, Duanjie Yang, Bing Li

Nuclear and Radiation Safety Center, MEE, Beijing, China

Abstract: Radiation protection is an important part of nuclear and radiation safety supervision. Occupational exposure personal dose monitoring is the foundation of radiation protection and safety assessment. The personal dose situation and its changes directly reflect the optimal level of radiation protection and the effectiveness of radiation protection, providing effective early warnings for the radiation safety conditions of various facilities.

In 2018, the Nuclear and Radiation Safety Center of the Ministry of Ecology and Environment completed the China Information System of Occupational Exposure (CISOE), which was officially launched and put into operation. This marked a solid step forward for China in achieving unified supervision and management of occupational exposure dose control and personnel protection. Realize centralized control of occupational exposure information and form a hierarchical management network system at the national, provincial and enterprise levels. Achieve full coverage of personal dose data for nuclear facilities, uranium mining and metallurgical facilities, nuclear technology utilization, and radiation safety supervision.

This article sorts out the annual collective dose and overhaul dose of China's nuclear power units in operation from 2018 to 2024 and conducts a summary and analysis by different models. It is found that the collective dose of HPR1000, AP1000, VVER, and CNP600 units is relatively low. The average collective dose for major overhauls of CNP600, VVER and AP1000 units is relatively low.

In the radiation protection management of operating nuclear power plants, each power plant has been striving to implement the principle of optimal protection. In recent years, a large amount of work has been carried out in various aspects such as radiation source item control, personnel dose control, radiation risk control, and information exchange, forming good practices and continuously improving the optimal level of radiation protection and radiation protection efficiency of the country and batteries.

Keywords: Nuclear power plant; Occupational exposure; Collective dose; Outage dose

SESSION 2. Radiation Protection at the Design Stage of Nuclear Installations

Caroline SCHIEBER

CEPN, France

A multi-stage approach is required when taking radiation protection into account in the design of a nuclear facility:

1. Identify the radiological risks (i.e. exposure of workers) that may be encountered during all phases of the facility's life, as well as during various operating situations (including incidental or accidental operation).

2. Assess radiological hazards, such as external exposure and airborne and surface contamination.

3. Determine design provisions (risk-related countermeasures) to eliminate risk or achieve residual risk levels as low as is reasonably achievable, including zoning and monitoring actions, and specific provisions for internal and external exposure (action on sources, time, screening and distance).

4. Select optimum parade(s) based on qualitative or quantitative criteria, using decision support methods where necessary.

This presentation will outline the different stages and illustrate the protective measures relating to the design of buildings, layouts and equipment in particular. It will also highlight some of the specificities and challenges associated with the design of small modular reactors.

SESSION 2. Application of ALARA Principle in the Radiation Protection Design of HPR1000 Nuclear Power Plant

Qianqian Huang，Weifeng Lv
[1]China Nuclear Power Engineering Co., Ltd., Shenzhen, China

Abstract: Occupational radiation exposure during normal operating is one of the key concerns in the field of radiation safety at nuclear power plants. This paper systematically elaborates on the methodology for demonstrating the optimization of radiation protection based on the "As Low As Reasonably Achievable (ALARA)" principle during the design phase of the HPR1000 nuclear power plant. The approach involves steps such as reviewing the design process, analyzing compliance with international standards, incorporating operational experience (OPEX) feedback, and risk-ranking high-dose tasks to identify design aspects that are both optimizable and most worthy of optimization. The ERIC-PPE method is employed to determine the feasible optimal design solutions. The results indicate that through comprehensive measures, including zinc injection, structural optimization of high radiation risk equipment, and remote operation, the annual collective dose of the unit is reduced to 0.34 man·Sv. This methodology effectively translates the ALARA design concept into engineering practice during the nuclear power plant design phase, providing valuable references for occupational radiation protection design in future nuclear power plants.

Keywords: ALARA, Occupational Radiation Protection, Radiation Safety

SESSION 2. The Application of Virtual Reality Technology in Radiation Protection Training

Yanyun Shen

CNNP Nuclear Power Operations Management Co., Ltd., China

Abstract: This presentation proposes a Virtual Reality (VR) training system to address critical radiation protection challenges within work organizations. Traditional training methods are hampered by excessive theory, insufficient practical skill development, high costs, long cycles, low knowledge retention, passive learning, and inadequate coverage of essential RP procedures. These limitations contribute to increased risks of unplanned radiation exposures and contamination events. The solution is a VR-based platform accessible via standard office computers or tablets. It utilizes gamified story-lines within immersive 3D simulations of radiation-controlled environments, enabling risk-free repeated practice of complex RP tasks outside actual control areas. Crucially, this eliminates trainee radiation exposure during learning. Multiple story-lines cater to different experience levels, comprehensively covering radiation work organization processes.

SESSION 2. Strengthening Occupational Radiation Protection in Nigeria Through Effective Regulatory Oversight

Godwin B. Ekong

Nigerian Nuclear Regulatory Authority, Nigeria

Nigeria is embarking on a nuclear power programme and has indicated its readiness for the peaceful application, assented to a number of international instruments covering nuclear safety, security and safeguards. Nigeria through the Nigerian Nuclear Regulatory Authority (NNRA) conducted the IRRS Mission in 2017, to strengthen its national regulatory infrastructure for nuclear, radiation, radioactive waste, and transport safety by providing a peer review against IAEA Safety Standards and is implementing its recommendations. Furthermore, its Human Resources Development in enhancing staff competence and productivity in the 19 key infrastructure issues for a new nuclear power program is ongoing and thus preparing to regulate its first NPP in Nigeria. Consequently, Occupational Radiation Protections (ORP) infrastructure to protect occupational radiation workers in nuclear and radiological facilities is well placed in the NNRA with the conclusion of ORPAS mission to Nigeria. Occupational workers can be exposed to both internal and external radiation dose in varying amounts, depending on their jobs and sources involved. The body cell system of exposed individuals interacts with the radiation particles thus resulting in biological damaging effect, such as impairment, permanent alteration and death of the cell. The NNRA has established regulatory infrastructure for occupational radiation protection requiring operators of these facilities to make adequate arrangements with an accredited Dosimetry Service Providers (DSPs) to maintain, submit and make available occupational dose records of its workers on regular basis. To ensure Quality Assurance of dose records, the NNRA has provided procedures for Performance Testing/Intercomparison (PT/IC) of the dosimetry systems to verify traceability with regards to linearity, accuracy, repeatability, and reproducibility for DSPs utilizing products such as Thermo-luminescence Dosimeters (TLD), Optically Stimulated Luminescence (OSL) badges for occupational dose monitoring. Subsequently, Eight (8) DSPs provided 20 badges each to Secondary Standard Dosimetry Laboratory (SSDL) for the PT//IC exercise which were exposed with mono-energetic source of Cs-137 blind doses, and later sent back to DSPs

for readings, details of the read badges were then compared with blind doses of SSDL with tolerance/acceptable limit kept at ±30%. Consequently, results showed that for deep dose exposure with a standard low dose of 0.4 mSv, the range of dose recorded were (4.56 to 559.38) mSv while exposure with a standard high dose of 6.0 mSv the range of dose recorded was (6.55 to 374.63) mSv. For shallow dose exposure with a standard low dose of 0.4 mSv, the range of dose recorded were (2.31 to 528.13) mSv while exposure with a standard high dose of 6.0 mSv the range of dose recorded was (5.40 to 362.04) mSv. Therefore, Three (3) out of Eight (8) DSPs with 20 badges each were found to be within the tolerance/acceptable limit of ±30% during the Performance Testing/Intercomparison exercise. It was recommended that DSP facilities having higher tolerance/acceptable limit should put its dosimetry system in place on or before the next cycle of accreditation year. Finally, it is seen that regulatory standard instituted by the NNRA can considered as good practice, to ensure that occupational radiation protection is well strengthened for safety of radiation workers in Nigeria.

SESSION 3. Radiation Protection Performance Indicator System of CNNP

Quanli Chen

CNNP (China National Nuclear Power Co., Ltd.) Jiangsu Nuclear Power Corporation
Lianyungang, Jiangsu, China

Abstract: A suitable and effective radiation protection indicator system is very important for nuclear power plants. It enables radiation protection personnel and plant managers to better identify performance deviations, detect management deficiencies, prevent accidents and incidents, and benchmark against peer plants using the same indicators to assess whether the plant has performance shortcomings.

CNNP currently operates 25 reactors (with additional units under construction), from a fleet management perspective, this indicator system enables clear oversight of radiation protection performance across all member NPPs. Should performance deviations occur at any member plant, timely experience feedback can be organized among other plants, and preventive measures can be developed to enhance radiation protection performance across the entire fleet.

This presentation outlines the primary basis for establishing CNNP's (China National Nuclear Power Co., Ltd.) radiation protection indicator system, its structure, specific definitions of indicators, and evaluation criteria. It also analyzes the overall operational results following the implementation of this indicator system.

SESSION 3. Radiation Protection – Self-Protection vs. Service-Protection

Loc Nguyen, M.Sc., CHP

Ajax, Ontario, Canada

Abstract: This paper presents the differences between self-protection and service protection models of radiation protection that are being implemented in Canada. The paper focuses on the pros and cons between the two protection models with respect to the implementation, effectiveness and alignment with regulatory and industry practices. Self-protection refers to systems and practices wherein individual workers are responsible for monitoring and limiting their radiation protection utilizing the skills learned from training, personal protective equipment (PPE) and dosimetry. In contrast, service protection involves direct oversight from qualified radiation protection (RP) staff. The expectation from this model is that individual workers shall follow the direction from the assigned qualified RP staff in regard to work area, PPE, dosimetry, exposure duration and back-out when called upon. Each model has its own strength and limitations from good practices, compliance, cost, risk mitigation and dose saving perspective. It has been observed that an integrated approach, combining the proactive responsibility of self-protection with service protection, yields the most effective outcomes in ensuring radiation safety and achieving the As Low As Reasonable (ALARA) goals in radiological workplaces.

SESSION 3. Discussion on Analysis and Optimization of Collective Dose in China National Nuclear Power Company

Bing Dong, Weimin Liang, Enwei Shen*, Chuan Wang*

Nuclear Power Operations Research Institute, Shanghai, China

1. Introduction

With the rapid development of China's nuclear power industry, the number of nuclear power plants continues to increase, and nuclear power has become an important component of the national energy strategy. In the process of nuclear energy utilization, radiation protection is a key issue on ensuring nuclear safety. Collective dose, as a significant indicator for assessing occupational and public exposure impacts, is directly related to the healthy and sustainable development of the nuclear power industry [1].

In recent years, the control level of collective dose in China National Nuclear Power Company (CNNP) has generally remained favorable. However, as operational years increase, the accumulation of radiation sources and the management of personnel exposure face new challenges [2]. Against this backdrop, systematically analyzing the current status, characteristics, and trends of collective dose in CNNP, exploring its influencing factors, and proposing optimization methods are of great significance for further enhancing the radiation protection level of CNNP and meeting with international advanced standards [3].

This paper aims to provide a comprehensive review of historical data and the current status of collective dose in CNNP, analyze dose composition and major contributing factors, and explore feasible pathways for dose optimization from both technical and managerial perspectives, thereby offering theoretical reference and practical guidance for radiation protection efforts in China's nuclear power industry.

2. Current Status of Collective Dose in CNNP

2.1 Collective Dose in 2024

The collective dose and normalized dose for operational nuclear power units in China in 2024 are shown in Table 1. For CNP1000, Fangjiashan Unit 2 and Fuqing Unit 2 are under ten-year major maintenance. Due to the change of work guidance, hydrostatic tests were canceled, and a significant amount of work on main loop welds was added, resulting in significant increase of collective doses for both units. The annual collective dose for Fuqing Unit 2 exceeded the management target value. Fuqing Unit 4 conducted extended minor maintenances from January to March and May to October, resulting in an increased annual collective dose. For CANDU6, Qinshan III Unit 1, the OT-212 maintenance involved a special project on investigation of inaccessible instrument tubes, leading to higher annual

collective doses. The collective doses for all other operational units of CNNP remained below the management target values.

Table 1: Collective Dose and Normalized Dose for Operational Nuclear Power Units in CNNP in 2024

Reactor Type	Annual Collective Dose (man·mSv)	Management Target (man·mSv)	Percentage (%)
CNP300	245	500	79.7%
CNP600	245±104	286±119	82.5±16.3%
CNP1000	500±438	588±426	70.0±34.7%
HPR1000	224±198	274±155	63.3±51.5%
VVER1000	230±168	297±170	65.5±28.9%
AP1000	192±206	200±212	94.0±3.7%
CANDU6	402±408	480±481	82.9±2.1%

2.2 Collective Dose Over the Years

From 2002 to 2011, the collective doses for most units in CNNP were better than the WANO median, and some even exceeded the WANO advanced value. After 2011, both the WANO advanced and median values continued to decrease. Since then, most units under maintenance in CNNP have been unable to reach the WANO advanced value, and some have even fallen below the WANO median. In 2024, 18 units had collective doses better than the WANO median, with 7 of them exceeding the advanced value, a performance similar to the previous year.

The WANO advanced value for 2024 was 156 man·mSv, and the median has remained around 340 man·mSv over the past three years. The number of operational nuclear power units globally has remained relatively stable, with most units in the WANO advanced value category being those that were shut down or did not under refueling maintenances during the year.

From the comparison of collective doses for units in CNNP with the WANO advanced and median values from 2002 to 2024, it can be observed that the VVER1000 units at Tianwan had relatively low collective doses, generally better than the WANO median. The CANDU6 and CNP1000 units that under maintenances during the year generally performed worse than the WANO median. The CNP300, CNP600, and AP1000 units were between these two groups, with collective doses better than the WANO median. Figures 1 and 2 illustrate the comparison of collective doses for units in CNNP with WANO values from 2002 to 2024.

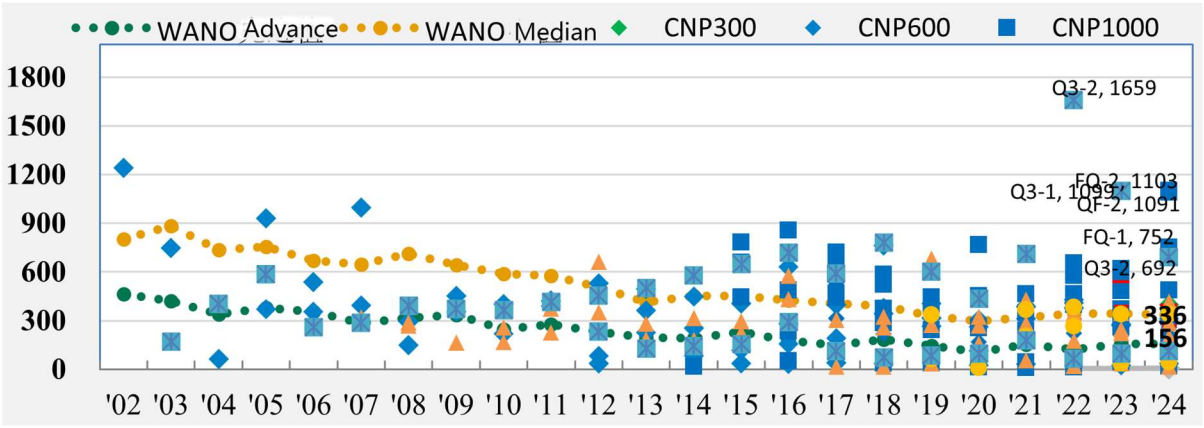

Figure 1: Comparison of Collective Doses for Units in CNNP with WANO Values (2002-2024)

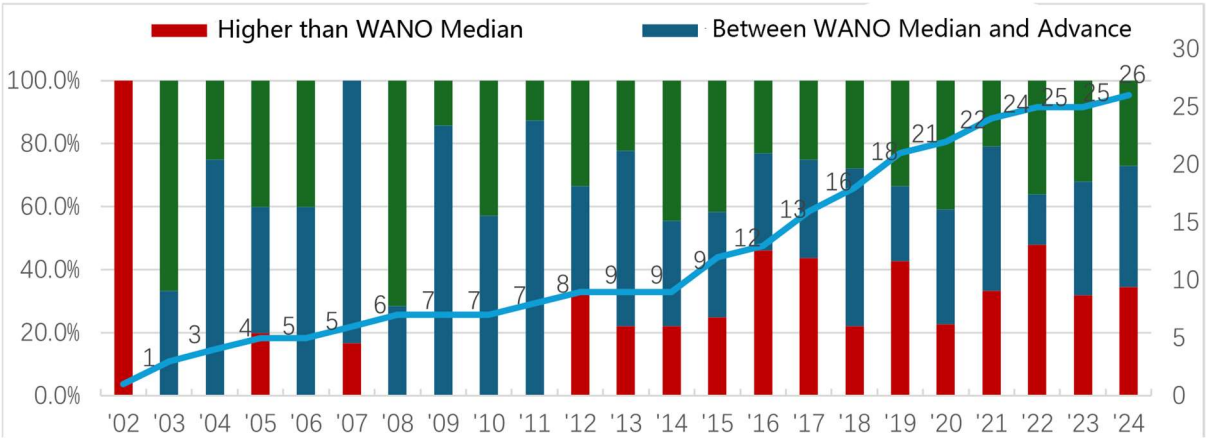

Figure 2: Comparison Results of Collective Doses for Units in CNNP with WANO-Related Values (2002-2024)

2.3 Collective Dose During Maintenances in 2024

In 2024, a total of 26 units were operated by CNNP, with 18 units undergoing refueling maintenances. The annual collective doses for the 8 units that did not undergo refueling maintenances were all below the green light value of CNNP's safety quality indicator (ASP indicator). Among the 18 refueling units, the collective dose during maintenances accounted for approximately 85% to 95% of the annual collective dose for most units. Out of the 26 units, 22 met the green light value of the ASP indicator for annual collective dose, 1 met the yellow light value, and 3 met the red light value.

In 2024, 22 units, or 88%, met the green light value of the ASP indicator, the same as in 2023. However, due to three CNP1000 units undergoing ten-year maintenances during the year, which resulted in higher collective doses, the number of red light units in 2024 was significantly higher than in 2023. The distribution of collective doses during maintenances for units in CNNP in 2024 is shown in Figure 3.

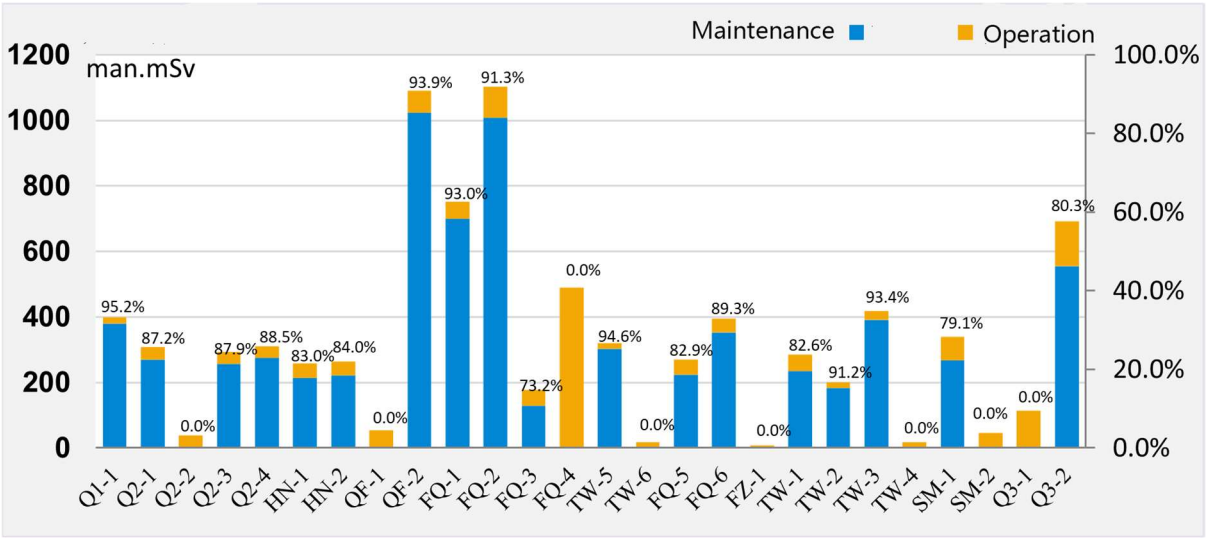

Figure 3: Distribution of Collective Doses During Maintenances for Units in CNNP in 2024

2.4 Individual Dose

In 2024, the maximum individual doses at all operational nuclear power plants under CNNP did not exceed 10 mSv, and none exceeded their respective annual management target values. Over 80% of personnel at operational nuclear power plants received individual doses below 0.5 mSv, and over 90% received doses below 1 mSv. The number of personnel receiving doses above 1 mSv saw a slight overall increase, while the number receiving doses above 5 mSv decreased slightly. At Fuqing Nuclear Power Plant, the proportion of personnel receiving doses above 5 mSv exceeded 1%, which is related to the extensive maintenance activities conducted during the year. The maximum and average individual doses for 2024 are shown in Figures 4.

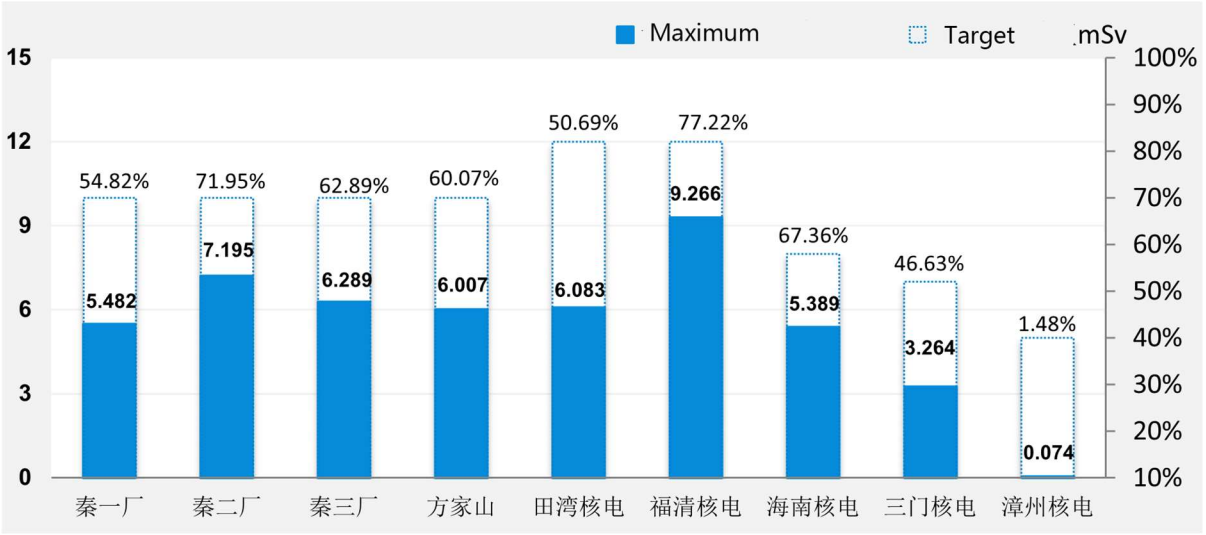

Figure 4: Comparison of Maximum Individual Doses in CNNP in 2024

From 2002 to 2024, the maximum individual doses at operational nuclear power plants in China remained below dose limits and management target values. Since 2012, except for Qinshan III, all plants have maintained maximum individual doses below 10 mSv. The median maximum individual dose across China's operational nuclear power plants was approximately 5.895 mSv, with an average of 5.788 mSv.

3. Directions for Collective Dose Optimization

3.1 Oxidation Operation

During reactor operation, materials such as iron, nickel, and cobalt enter the coolant through corrosion and erosion, forming corrosion products. These products are activated as they flow through the core and exist in a dynamic equilibrium of dissolution-deposition within the primary coolant system. The deposition of activated corrosion products on equipment surfaces outside the core leads to the formation of radiation field outside the core. Empirical data indicate that 90% of the collective dose during maintenances in nuclear power plants is caused by activated corrosion products. To effectively control radiation levels in the primary coolant system, reduce the deposition and release of radiation sources in maintenance areas, and lower the collective dose during maintenances, nuclear power plants adopt various source term control methods during shutdown.

Currently, operational units in CNNP employ oxidation operation for radiation source term control during reactor shutdown. Depending on whether hydrogen peroxide is added manually or oxygen is introduced naturally, it is classified as chemical oxidation or natural oxidation. The main objective is to ensure that activated corrosion products resolution during the oxidation operation and are removed by purification.

However, if there is a high amount of activated corrosion products in the core or insufficient purification time in the chemical and volume control system (CVCS), removal may be incomplete, leading to the deposition of activated corrosion product in the primary coolant system and equipment, thereby significantly increasing radiation levels. Therefore, during reactor shutdown, sufficient purification time and maximum purification flow rates should be guaranteed.

3.2 Informatization and Intelligentization of Radiation Protection

CNNP has begun implementing informatization and intelligentization in radiation protection. The following initiatives help control collective dose:

3.2.1 5G Wireless Radiation Monitoring Application

Leveraging 5G speed supports the informatization of radiation monitoring. During maintenance or oxidation operations, wireless gamma meters are deployed at radiation monitoring points. Utilizing the high speed, low latency, and broad connectivity of 5G signals, dose rate information from monitoring points such as the primary coolant system is transmitted in real time via plant-wide 5G signals. This

achieves visualization of radiation monitoring and controllability of radiation protection, providing timely and effective support for decision-making.

3.2.2 In-Depth Application of 3D Radiation Field Visualization

The 3D radiation field visualization for all four units at Qinshan II has been fully completed. The application of the 3D radiation field platform has been extended to include virtual reality (VR) applications for radiation work organization, the RWP path guidance, and upgrades to ALARA simulation exercises, thereby enhancing personal radiation protection awareness and skills.

3.2.3 Wireless Radiation Monitoring Application

Making full use of the wireless network, wireless transmission modules for gamma dose rate meters are developed. Portable radiation meters connected to these modules can upload monitoring data in real time to the radiation protection platform.

During maintenances, wireless instruments are pre-deployed at locations such as the RCP main pipeline and RRA pipeline to monitor changes in radiation levels during oxidation purification and primary coolant level variations, enabling remote real-time monitoring. Additionally, these are used during critical valve disassembly and seat and core grinding operations in high-dose-rate areas. Radiation protection personnel can monitor changes in radiation levels at maintenance workers' locations from low-dose-rate areas and intervene promptly to ensure personnel radiation safety.

3.3 New Equipment Development

In addition to informatization and intelligentization, the application of new equipment in radiation protection also contributes to collective dose control.

3.3.1 WBC Automated Measurement System

This system enables radioactive workers to autonomously conduct intelligent monitoring of internal gamma exposure, meeting the 24-hour measurement needs of radioactive workers during daily plant operation and maintenances. It fills the gap in automated individual dose measurement in domestic nuclear power plants.

3.3.2 Ultrasonic Decontamination Device

An ultrasonic decontamination device has been developed and applied for flushing hot spot pipelines, addressing the difficulty of flushing adhered radiation-activated products on inner walls. The effectiveness of hot spot flushing has improved from 20%-43% to 46%-83%, effectively reducing on-site radiation levels. Additionally, the application scenarios for ultrasonic decontamination devices are being expanded to include ultrasonic cleaning of valve chambers and small containers, enhancing hot spot elimination capabilities.

3.3.3 Integrated Air Pollution Isolation Chamber for Steam Generators

The integrated air pollution isolation chamber for steam generators has reduced setup time by over 60%, collective dose by over 40%, and waste production by over 50%. This technology has been promoted to Sanmen Nuclear Power Plant and Qinshan Nuclear Power Plant.

4. Conclusion

This paper systematically studies the current status, trends, and optimization measures for collective dose in operational nuclear power plants in CNNP. The results indicate that in recent years, the collective dose in CNNP has generally been well controllable.

However, against the backdrop of increasing operational years and maintenance workloads, some units have experienced collective doses exceeding management targets, particularly during ten-year maintenances and special maintenance activities. Compared with WANO advanced and median values, some units in CNNP have maintained low levels over the long term, but overall, there remains pressure for continuous optimization.

In terms of individual dose control, domestic nuclear power plants generally comply with international and national standards without exceeding limits, reflecting a high level of radiation protection management.

In the direction of collective dose optimization, the rational application of oxidation operation technology, the development of informatization and intelligentization in radiation protection, and the development of new equipment all demonstrate potential for collective dose control. Measures such as the introduction of 5G wireless monitoring, 3D radiation field modeling, and ultrasonic decontamination not only enhance the real-time nature of protection but also help effectively reducing collective dose.

Reference

[1] Wang L, Huang Q, Ye Y, et. al, Suggestions on standardizing collective dose data management of nuclear power plants in China, Radiation Protection, 2023, 43(S1)

[2] Wang C, He J, Shen E, Understanding and thinking about the role of collective dose concept in radiation protection management of nuclear power plants, Radiation Protection, 2023, 43(6)

[3] Peng Y, Wang K, Jiang J, ConstructionandApplicationoftheFour-path ModelforCollective DoseReductioninNPP, China Nuclear Power, 2023, 16(5)

SESSION 3. Surface Contamination Control Practices and Refined Management of the Cleanliness Radiation Controlled Area (CRCA) Mode at Taishan Nuclear Power Plant

Xueming Ren, Yu Xu, Weihua He, Wei Li, Lingqi Lin, Jiawei Bai

Taishan Nuclear Power Joint Venture Co., Ltd., Taishan, Guangdong, China

With nuclear energy playing an increasingly critical role in achieving the China's "Carbon Peaking & Carbon Neutrality" goals, nuclear safety, particularly radioactive contamination control, has become paramount. Among the key challenges in radioactive contamination control—external exposure, airborne contamination, and surface contamination—effective management of surface contamination remains a significant and persistent difficulty for the nuclear industry, despite established protective measures for the former two risks.

This study systematically elaborates on the radiological surface contamination control system and the refined management practices within the Cleanliness Radiation Controlled Area (CRCA) at Taishan Nuclear Power Plant (Taishan NPP). The research first identifies the primary sources of radiological surface contamination and the associated control challenges, highlighting that its management involves complex physicochemical processes and is critically dependent on personnel protection awareness and behavior, making it one of the most difficult safety risks to control in NPPs.

To address this challenge, Taishan NPP established a contamination control system centered on "Technical Barriers" and "Human-Centered Measures." For technical barriers, the plant enhanced contamination control capabilities through the implementation of contamination monitoring barriers, optimization of environmental factors, and application of novel decontamination technologies. For human-centered measures, the plant innovatively implemented a CRCA management mode. This includes the "Three-Forms-One-Signage" program, clearly defined regional management standards, and the execution of contamination region management.

Practice demonstrates that this integrated system has achieved significant results, including reduced contamination of personal protective equipment and decreased generation of technical waste. Data indicate a marked reduction in technical waste volume during outages from 2017 to 2022, with the average alarm rate at the C2 access point consistently below the international average. Furthermore, this paper explores optimization pathways for refined CRCA management, proposing improvements such as enhancing access rules for contamination barriers and standardizing protective measures.

The study concludes that effective radiological contamination control is essential for the safe operation of NPPs. The CRCA mode not only elevates current safety management standards but also promises significant economic benefits for future plant decommissioning. Consequently, this mode warrants widespread adoption and further in-depth research within the nuclear power industry.

Keywords: surface contamination, refined management, Cleanliness Radiation Controlled Area, Three-Forms-One-Signage, Nuclear Power Plant

SESSION 3. A Brief Discussion on a Regeneration and Decontamination Process for Radioactive Waste Resin

Ming Han

Huaneng Shandong Shidao Bay Nuclear Power Co., Ltd., Rongcheng, China

Abstract: This thesis provides an explanation of a patent with the number ZL 2022 1 0667826.8, which is a method for the regeneration and decontamination treatment of radioactive waste resin. It aims to analogize traditional resin regeneration technology and apply the decontamination method of resin elution and regeneration to elute radioactive nuclides, thereby transforming radioactive waste resin into ordinary waste resin for reuse or disposal, and subjecting the resulting concentrated liquid to solidification treatment. This thesis offers a detailed explanation of the apparatus involved in the process to ensure its feasibility and highlights the advantages of this process, which has certain value for promotion and application.

Keywords: Regenerative decontamination, solid-liquid separation, neutralization, evaporation, cement solidification

Introduction

Ion exchange resins are commonly used by pressurised water reactor (PWR) nuclear power units for the purification of the first circuit coolant in the first circuit process systems (e.g., chemical containment system, boron recovery, radioactive waste liquid evaporation system, and spent fuel cooling pools, etc.). The ion exchange resins used in the one-circuit process system are disposed of as solid waste after one overhaul cycle in service (12 to 18 months). For a pressurised water reactor (PWR) nuclear power plant with an installed capacity of 1000 MWe, the actual amount of radioactive waste resin produced annually is about 6 to 8 m3. Currently, the main method used in China to dispose of radioactive waste resin is cement curing, and the volume of the cement curing body after treatment by this method is 2 to 3 times the volume of the waste resin, which amounts to about 1/3 of the annual output of solid waste from the nuclear power plant. The treatment of radioactive solid waste from nuclear power plants follows the principle of minimisation to reduce the cost of disposal at a later stage. Therefore, technologies such as super compression and high integral container dry storage with relatively small volume increase ratio are gradually applied in nuclear power plants. However, the volume increase ratio of these two treatment methods is greater than 1, which does not realise the real meaning of volume reduction.

Ion resin is a special kind of organic waste, China Radiation Protection Research Institute is currently trying to use wet oxidation method of ion exchange resin degradation treatment, has completed the industrial pilot. Supercritical water oxidation treatment is another treatment method for ion exchange resin. However, both wet oxidation treatment and supercritical water oxidation treatment have the problems of complicated process and high requirements on equipment.

The process described in this thesis aims to focus on the ionic existence of the nuclear island cation resin adsorption of radioactive solid impurities in the form of ions, except for a small number of metal ions contained in solid particles, most of the free ionic form by the resin adsorption, so that the addition of sulphuric acid for elution similar to the conventional resin regeneration process can be used, so that the adsorption of the radioactive metal ions from the resin to restore the free form of the resin into the elution residue, so that the radioactive waste resin can be radioactively decontaminated. The radioactive

waste resin can be radioactively decontrolled, and the elution residue containing radioactive ions can be reprocessed using the nuclear island waste evaporation process.

1 Process Flow Description

The unit used in this process is shown below.

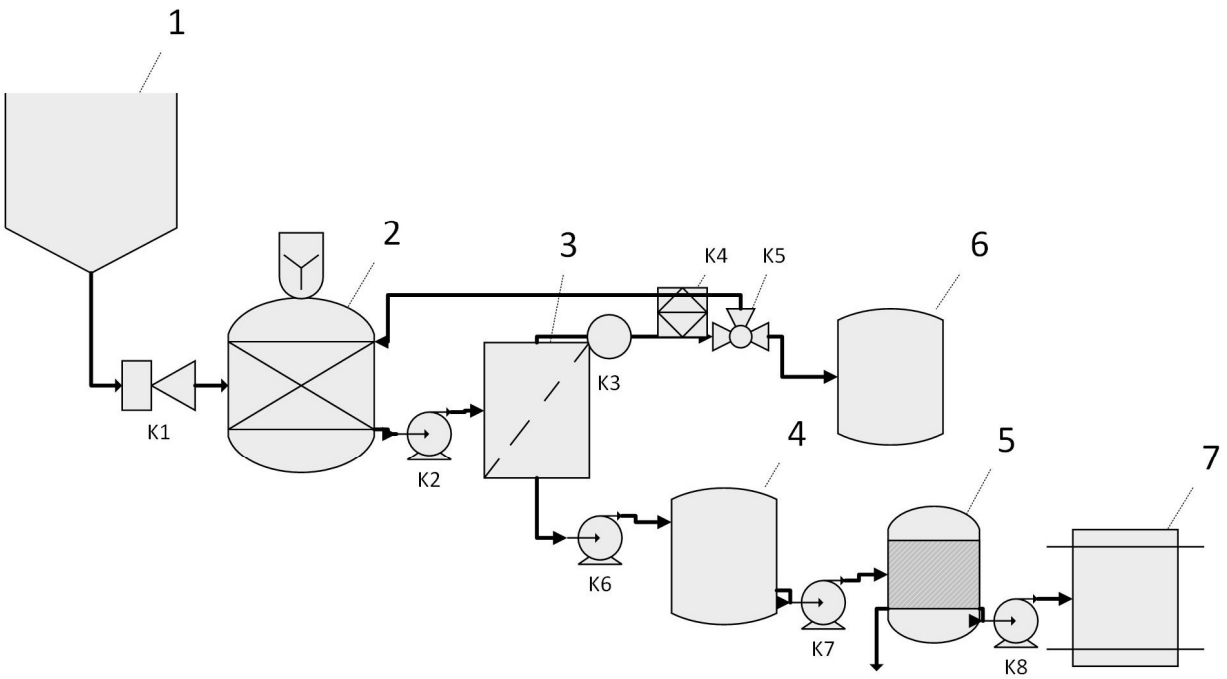

room；**4** H_2SO_4 residual liquid neutralisation room；**5** waste liquid evaporation device；**6** decontamination room；**7** cement curing device；**K1** resin injector；**K2** transfer pump；**K3** transfer pump；**K4** radiation monitoring instrument；**K5** three-way valve；**K6** transfer pump；**K7** transfer pump；**K8** transfer pump

Fig. 1 Process device diagram

The process flow is to use the resin injector K1 to transfer the radioactive waste resin to the H2SO4 elution chamber (2) with agitator through the radioactive waste resin transfer device (1), after the radioactive waste resin is eluted by the full mixing of the H2SO4 solution, the waste resin and the sulphuric acid elution residue are transported to the resin elution residue separation chamber (3) through the transfer pump K2 to separate the solid-liquid separation; the separated waste resin passes through the transfer pump K3 in turn, and the radiation monitoring instrument K4 is set outside the pipeline to monitor the radiation level of the resin when it reaches the decontrol level. After the separation, the waste resin is transported to the resin elution residue separation room (3) by K2 transfer pump for solid-liquid separation; after the separation, the waste resin passes through the transfer pump K3, and the radioactivity level of the resin is monitored by the radiation monitoring instrument K4 set outside the pipeline; when the waste resin reaches the level of decontamination, it is transported to the decontamination room (6) through the three-way valve K5 for temporary storage, and then it will be reused or disposed of in a conventional way when the amount of the temporary storage is more than 2/3, if the radioactivity level does not meet the requirements of the decontamination, the waste resin will return to the H2SO4 elution room (2), elution again; separation of the elution residual liquid through the transfer pump K6 transported to the H2SO4 residual liquid neutralisation room (4) for acid and alkali neutralisation, neutralised residual liquid by the transfer pump K7 sent to the waste liquid evaporation device (5) for evaporation and concentration, evaporation of condensate into the nuclear island liquid

effluent emissions system, the concentrated liquid by the transfer pump K8 sent to the cement curing device (7) for cement curing treatment. Concentrate is sent to cement curing device (7) by transfer pump K8 for cement curing treatment.

2 Detailed explanation of process equipment

2.1 Conveyor pump

Considering that the volume of waste resin is small and the friction resistance is large in the transmission project, the form of conveyor pump adopts the displacement pump to ensure that the waste resin and its elution solution can be effectively pressed and transmitted. It is recommended to use 0.5MPa head displacement pump to ensure effective transport.

2.2 H2SO4 elution chamber

To ensure effective elution, two key elements are used in the H2SO4 elution chamber: the addition of a mechanical agitator and ensuring that the concentration of the sulphuric acid solution is a certain volume fraction (2-3 mol/L). In order to ensure effective elution, sufficient agitation and elution time is required, and for waste resins up to 1/2 the volume of the elution chamber, the waste resin should be immersed and agitated for at least 2 hours and more to ensure that radio-metal nuclides adsorbed on the resin are removed. Adsorbed radioactive metal nuclides are removed from the resin into the elution residue. To ensure the safety of the elution chamber, the interior of the chamber is rubber lined to prevent corrosion. At the same time, the stirrer structure should ensure that the resin structure is not broken, otherwise the stirrer can be deactivated.

2.3 Resin elution residue separation room

Considering the efficiency, the separation room adopts the method of filtering and intercepting to achieve the separation of waste resin and sulfuric acid elution solution, this device needs to pay special attention to the selection of filtration devices, in order to avoid that the filter is not fine enough to lead to the resin can't be completely filtered and separated.

2.4 H2SO4 residual liquid neutralisation chamber

In this device, the separated sulfuric acid elution residual liquid is treated with acid and alkaline neutralisation, and the alkaline solution used is NaOH solution, the concentration of which should be such that the residual H2SO4 can be neutralised, and the pH after neutralisation is equal to 6-9. Therefore, the volume of NaOH solution should be adjusted according to the volume of the sulfuric acid elution residual liquid to be neutralised in order to ensure that the neutralisation is achieved.

2.5 Waste liquid evaporation device

In order to avoid repeated construction of equipment, waste liquid evaporation device (5) is a nuclear power plant radioactive waste liquid evaporation device. That is, the use of high-temperature steam from the top injection port to the lower part of the evaporation device, the waste liquid to be evaporated through the transfer pump from the lower part of the evaporation device to the upper part of the injection, through the countercurrent heat transfer, so that the water in the waste liquid is evaporated, introduced into the condenser, evaporation of the condensate into the liquid effluent emission system of the nuclear island. The condensate is sent to the cement curing unit through a transfer pump.

2.6 Decontamination room

The decontamination room is a steel temporary storage container with a certain volume, which is used for temporary storage of the waste resin qualified by the radiation monitoring instrument K4 for a certain period of time, and then can be used to test whether the conditions of chemical specifications for reuse are met, and if it is not reused, then it will be disposed of in a conventional way.

2.7 Three-way valve

If the waste resin after elution and solid-liquid separation fails to pass the radiation monitoring instrument K4, the three-way valve automatically turns to the H2SO4 elution chamber 2 for re-elution treatment. If the radiation monitoring is qualified, the three-way valve is transferred to the decontrol room to ensure that the waste resin after decontrol into the decontrol room for temporary storage.

2.8 Cement curing device

To avoid duplication of equipment construction, the cement curing device (7) is a cement curing device for radioactive waste liquid concentrate of nuclear power plant. That is, the waste neutralisation concentrate generated by the waste liquid evaporation device enters the cement curing device of the power plant through a transfer pump, and the waste concentrate is fully stirred outside the barrel with a certain proportion of cement curing formula, and then loaded into a 400L steel drum with a seal for temporary storage, and then disposed of as a radioactive waste drum to be transported out of the plant.

3 Superiority of the process

(1) The device chemically elutes the radioactivity from the radioactive waste resin and makes it into common waste resin, avoiding the problem of environmental radiation pollution caused by leaching of nuclides after cement curing of the radioactive waste resin.

(2) The device uses the waste liquid evaporation device common to the waste liquid treatment system of the nuclear island of the power plant to evaporate the waste liquid after neutralisation, and the resulting radioactive concentrate is cement-cured, which reduces the amount of radioactive waste liquid to be processed, and does not produce the waste resin curing body, which is a volume reduction process. Overall, it is a capacity reduction process for radioactive waste resin. At the same time the equipment used are mature equipment, economic safety, high reliability, can be continuous treatment of waste resin, improve the processing efficiency.

(3) The ordinary resin obtained after this process can be further analysed chemically to determine whether it meets the conditions for reuse, and if it meets the conditions for reuse, it can relatively save the purchase cost of nuclear grade resin in the power station. And even if it is disposed of, it is also a conventional disposal method, which greatly reduces the disposal cost.

(4) This device can achieve automated processing, without too much intervention by personnel, reducing the risk of radiation exposure of staff, to protect the health of employees.

4 Conclusion

This process is analogous to the conventional resin regeneration technology, using the decontamination method of waste resin elution and regeneration of radionuclides, making it easy to reuse or dispose of ordinary waste resin, and curing the resulting concentrate. The volume of radioactive waste resin is reduced, and the process does not require too much intervention by personnel, so this process has certain value for popularisation and application.

SESSION 4. ALARA Impact of a Chemical Decontamination and Design Modification at a BWR in Subsequent Cycles

René Hoffmeister

Nuclear Power Plant Leibstadt (KKL), Switzerland

Since the implementation of HWC/OLNC in 2008, KKL has experienced an increase of collective radiation exposure (CRE) and source term. Average dose rates in the Drywell had nearly doubled between 2008 and 2021. Already in 1992, the recirc pump housings and recirc pipes were identified as major Co-source term contributors due to the high content of stellite and the corrosion rate. In 2005, a decision was made to replace part of the recirc pipes and pumps as part of a life extension project. Several measures concerning the ALARA impact like Stellite replacement in the steel used in pipes, pumps and valves, chemical decontamination of the recirc system and adjacent RHR system and the replacement of the flow control valves by an adjustable speed drive were included in the project's scope, together with the electropolishing of new surfaces. The project was executed in a 7-month outage in 2021 and only started after a chemical decontamination that removed 1,27 TBq (34,3 Ci) of gamma emitters, and achieved an average decon factor of 17. The accrued dose for the whole outage in 2021 was 3434 Pers.-mSv (343 p-rem). The chemical decontamination saved an estimated 3 Pers.-Sv. The measures taken to reduce CRE and source term had the following effects in the subsequent outages in 2022, 23, 24 and 25: The saved dose is estimated around 600 Pers.-mSv (60 p-rem). Also, for the first time since 2008 the average Co-source term decreased steadily, currently 45% lower than at its all-time high in 2017, and still 31% lower compared to the 2021 level. The recontamination of the recirc system was much lower compared to the start-up years in the 1980's, most likely due to the electropolishing of surfaces and the improved source term in the reactor water. Dose rate increase on the recirc system almost reached equilibrium after 4 cycles and is still lower than pre-HWC/OLNC. At this point in time, it is still too early to make a final assessment, but the totality of all measures already ensures a reduction of the collective dose in the order of a low 3-digit Pers.-mSv per 3-year average, always assuming that workload stays relatively stable at current levels.

SESSION 4. Analysis and Optimization of Radioactive Source Terms for Qinshan Nuclear Power Plant

Hao Huang

CNNP Nuclear Power Operations Management Co., Ltd., China

Abstract: This article introduces the mechanism of the generation, migration, and deposition of the main corrosion activation products in PWR nuclear power. By conducting radioactive source term investigations during refueling outage at M50, the composition of radioactive source terms and the contribution of radioactive nuclide dose rate in the previous refueling overhaul of Qinshan Nuclear Power Plant were clarified. Furthermore, the trend of changes in the surface activity of key nuclides ^{60}Co, ^{58}CO, and ^{124}Sb that affect the radiation level of the unit was analyzed, and targeted measures such as valve grinding particle cleanliness control, antimony containing material replacement, oxidation operation optimization and hot spot flushing were proposed. These measures have a certain positive effect on reducing the radioactive source term of the unit, reducing the collective dose of major repairs, improving radiation protection performance, and practicing the principle of radiation protection optimization.

Introduction

For the collective dose control in nuclear power plants and the implementation of radiation protection optimization principle, reducing the radioactive source term of the unit is a crucial task. The focus of radioactive source term control is to study the generation mechanism for the radioactive source terms of the unit, track the variation trend of the critical radionuclides, so as to take the targeted measures to reduce the entry of activated radioactive particles into the primary circuit, and prevent their deposition on the surface of pipeline and equipment, thereby reducing the radiation field dose rate level in the nuclear island. Therefore, sorting out and analyzing the composition and variation trends of the radioactive source term of the unit, and defining the elimination measures for the critical radionuclides are of great significance for reducing the collective dose during the major overhaul of the unit, improving the performance of radiation protection, and ensuring the radiation safety of personnel.

The main work of this paper is to sort out and analyze the formation mechanism and composition structure of the radioactive source term of Qinshan Nuclear Power Plant (hereinafter referred to as First Qinshan Plant), track and analyze the variation trends of the main radionuclides of the unit during several cycles and propose the targeted purification measures according to the characteristics of the nuclides.

1. Radioactive Source Term of Unit

1.1 Profile of radioactive source term

The radioactive source term during the operation of the pressurized water reactor nuclear power mainly consists of fission products of fuel elements, neutrons, coolant activation products, and corrosion activated products. Among them, the fission products pose less harm to the personnel. As long as the fuel cladding is not damaged, the vast majority of the fission products will be contained within the fuel assembly, with only a small amount of inert gas and radioactive iodine entering the primary circuit coolant. Neutrons mainly affect the entry of the personnel into the reactor building during the power operation to carry out the work such as defect elimination and leak detection. In addition, the coolant

activation products represented by ^{16}N are mainly short-lived nuclides, with a very short half-life period (7.13s).

After the unit is shut down, the neutrons and the coolant activation products no longer exist, and the fission products are contained within the fuel assembly. Therefore, for pressurized water reactor nuclear power unit, the main radioactive source term is the corrosion activated products. According to the statistical data provided by French EDF [1], more than 85% of the radiation fields in the pressurized water reactor nuclear power units are caused by corrosion activated products.

1.2 Corrosion activated products

During the operation of the reactor, the materials such as iron-nickel alloy in the primary circuit materials enter the primary circuit coolant by means of corrosion and wearing to form the corrosion products. These corrosion products enter the reactor core with the coolant and are activated by neutrons, generating the corrosion activated products. Then, such corrosion activated products flow with the coolant and deposit outside the reactor core, forming a deposition source term. The deposition source term can directly affect the level of radiation at the operation site. Therefore, close attention shall be paid to the changes in and the elimination measures for the deposition source term. The nuclear reaction equations for the main corrosion activated products of the pressurized water reactor nuclear power are shown in Table 1.

Table 1 Formation of Main Corrosion activated Products of Pressurized Water Reactor Nuclear Power

Nuclide	Half-life Period	Activating Reaction
^{60}Co	5.27a	$^{59}Co(n,\gamma)^{60}Co$
^{58}Co	70.88d	$^{58}Ni(n,p)^{58}Co$
^{110m}Ag	249.8d	$^{109}Ag(n,\gamma)^{110m}Ag$
^{124}Sb	60.2d	$^{123}Sb(n,\gamma)^{124}Sb$
^{54}Mn	312.1d	$^{54}Fe(n,p)^{54}Mn$
^{59}Fe	44.51d	$^{58}Fe(n,\gamma)^{59}Fe$
^{95}Zr	64.02d	$^{94}Zr(n,\gamma)^{95}Zr$
^{65}Zn	243.8d	$^{64}Zn(n,\gamma)^{65}Zn$

2. Variation Trends of Radioactive Source Term of Unit

2.1 Measurement of deposited radioactive source term

In order to understand the types of radionuclides deposited on the inner surface of the pipeline and their contribution to the dose rate outside the pipeline and to analyze the sources of radionuclides, during the very low water level period for major overhaul of OT116, OT118, OT119 and OT122, the deposition source term is surveyed with the high-purity germanium and cadmium zinc telluride detector for the

relevant primary circuit pipeline in the reactor building and the nuclear auxiliary building at First Qinshan Plant.

2.2 Nuclide analysis of deposition source term

First, the current deposition source term of the unit is analyzed. The data from the survey of the radioactive source term during the major overhaul of Q1-OT122 is sorted out. The dose rate contribution proportions of the nuclides are shown in Table 2. ^{60}Co, ^{58}Co, ^{124}Sb, ^{54}Mn, ^{110m}Ag and other nuclides are the main nuclides in First Qinshan Plant. The surface radioactivity of the other nuclides does fall on the same order of precedence as the above-mentioned nuclides, and their dose rate proportion is very low.

Table 2 Ranking of Dose Rate Contribution of Main Deposited Nuclides on Inner Wall of Pipelines

Survey Point	Dose Rate Contribution of Deposition Source Term on Inner Wall of Pipelines
Main System	Co-60、Co-58、Sb-124、Mn-54 Co-60, Co-58, Sb-124, Mn-54
Chemical and Volume Control System	Co-60、Ag-110m、Co-58、Sb-124 Co-60, Ag-110m, Co-58, Sb-124
Shutdown Cooling System	Sb-124、Co-60、Co-58、Ag-110m Sb-124, Co-60, Co-58, Ag-110m
Cooling and Purification System for Waste Fuel Pool	Co-60、Co-58、Sb-124、Mn-54 Co-60, Co-58, Sb-124, Mn-54

In conclusion, ^{60}Co has the highest surface activity in the primary circuit system pipeline and makes the greatest contribution to the radiation field dose rate of the unit. The dose rate contribution of ^{58}Co is also among the top. In addition, ^{124}Sb has the highest surface activity in the reactor shutdown cooling system. Next, the formation, migration, deposition and variation trends of such three critical radionuclides in the system are analyzed.

2.2.1 Critical Radionuclide ^{60}Co

2.2.1.1 Source and physical properties of ^{60}Co

In pressurized water reactor nuclear power, the target nuclei of ^{60}Co mainly include ^{60}Ni, ^{59}Co and ^{63}Cu, and their nuclear reaction equations are shown in Table 3.

Table 3 Nuclear Reaction Equation of ^{60}Co

Radionuclide	Target Nucleus	Nuclear Reaction Equation	Reaction Cross Section (b)
^{60}Co	^{60}Ni	n, p	2.0E-3
^{60}Co	^{63}Cu	n,α	6.0E-4
^{60}Co	^{59}Co	n,γ	37.45

First, ^{63}Cu is less used in the primary circuit material of pressurized water reactor nuclear power, and the reaction cross-section of its reverse (n,α) reaction is very small, making it impossible to serve as the main source of ^{60}Co. Second, despite the small natural abundance and the small reaction cross section, ^{60}Ni is widely used as a nickel-based alloy for steam generator heat transfer tubes (Inconel800), spring bolts and other equipment in the nuclear power plant and is one of the main sources of ^{60}Co. In addition, ^{59}Co with a (n,γ) reaction cross-section up to 37.45bar is also a major target nucleus for radioactive ^{60}Co [3]. ^{59}Co is mainly used for two purposes in nuclear power: One is the steam generator heat transfer tubes (Inconel800), and the other is the Stellite hard alloy used for the sealing surface of valves, as shown in Table 4.8

Table 4 Materials of SG Heat Transfer Tube and Sealing Surface of Valve in First Qinshan Plant

Element	Stellite Hard Alloy	Inconel800
Ni	2%~4%	32%~35%
Cr	27%~31%	20%~30%
Co	50%~58%	＜0.1%

The physical properties of ^{60}Co are shown in Table 5. The sorting-out of the physical properties of radionuclides is conducive to understanding the contribution of radionuclides to the field radiation level and finding the measures to avoid the deposition of radionuclides and reduce the activity of the radionuclides.

Table 5 Physical Properties of ^{60}Co

Half-life Period	Decay Energy	Exposure Rate Constant	Existence Form	Particle Diameter
5.27a	1.17/1.32 MeV	$12.94R\cdot cm^2\cdot mCi^{-1}\cdot h^{-1}$	Insoluble Metal Particles	0.2-0.4μm

2.2.1.3 Variation trend of critical nuclide ^{60}Co

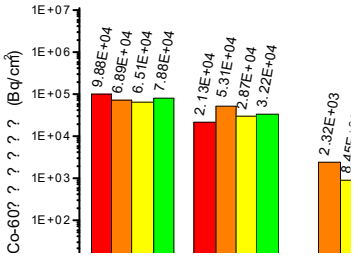

Figure 1 Variations in Surface Activity of ^{60}Co Deposited on Inner Wall of Pipeline

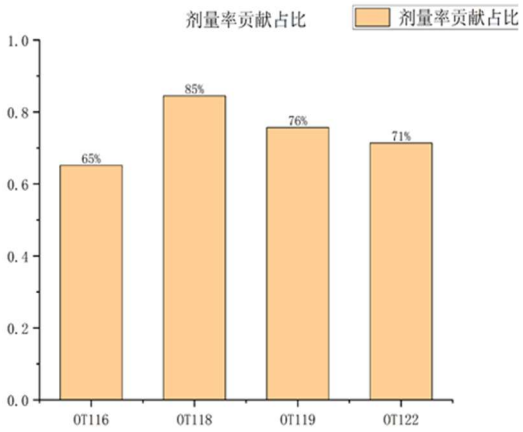

Figure 2 Surface Dose Rate Contribution Proportion of ^{60}Co

1) ^{60}Co has the highest surface activity in the main system, which is maintained basically within the range of 6.0E+04 to 10.0E+4 Bq/cm², with a relatively stable range of fluctuation.

2) Starting from the major overhaul of 116, the pipeline surface activity of ^{60}Co presents a gradually decreasing trend. However, during the major overhaul of 122, it rebounded to certain extent. Among others, the surface activity of ^{60}Co in the main system increases by approximately 20% compared to that during the major overhaul of 119.

3) The dose rate contribution proportion of ^{60}Co in the main system has been decreasing year by year since the major overhaul of OT118.

4) Based on the aforesaid three points, as the main radionuclide of the unit, ^{60}Co sees a decrease in its dose rate contribution proportion despite the increase in its surface activity, indicating that there are other radionuclides deposited abnormally during the major overhaul of 122.

2.2.2 Critical radionuclide ^{58}Co

2.2.2.1 Source and physical properties of ^{58}Co

In pressurized water reactor nuclear power, the target core of ^{58}Co is ^{58}Ni, and its nuclear reaction equation is shown as follow:

$$^{58}_{28}Ni + ^{1}_{0}n \rightarrow ^{58}_{27}Co + ^{1}_{1}H$$

Ni is primarily present in steam generator heat transfer tubes, with an additional portion originating from Ni added to austenitic stainless steel. The physical properties of ^{58}Co are shown in Table 6.

Table 6 Physical Properties of ^{58}Co

Half-life Period	Decay Energy	Exposure Rate Constant	Existence Form	Particle Diameter
70.8d	0.81Mev	5.464R·cm^2·mCi^{-1}·h^{-1}	Insoluble Metal Particles	0.2-0.4μm

2.2.2.3 Variation trend of critical nuclide ^{58}Co

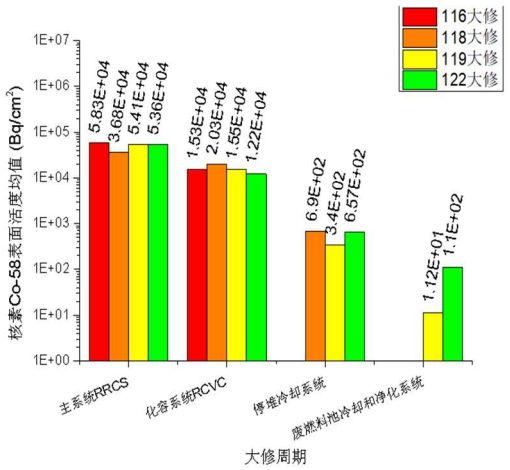

Figure 3 Variations in Surface Activity of ^{58}Co

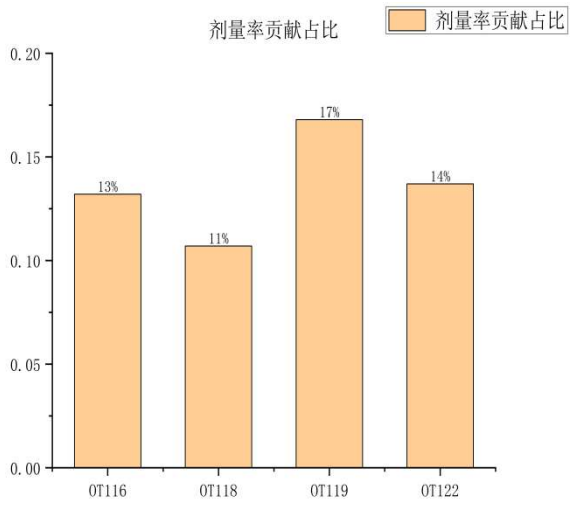

Figure 4 Dose Rate Contribution Proportion of ^{58}Co

1) ^{58}Co has the highest surface activity in the main system, which is maintained basically within the range of 5.0E+04 Bq/cm^2, and tends to become stable in the recent major overhauls, and no abnormal deposition occurred during the major overhaul of 122.

2) The dose rate contribution proportion of ^{58}Co basically ranges from 10% to 15%, which is different from the current phenomenon in the new unit where ^{58}Co is the main contribution nuclide to the dose rate of the unit, mainly due to the balance between the corrosion activation and the relatively short half-life period of ^{58}Co.

2.2.3 Critical Radionuclide ^{124}Sb

2.2.3.1 Source and physical properties of ^{124}Sb

In pressurized water reactor nuclear power, the target nucleus of ^{124}Sb is ^{123}Sb, and its nuclear reaction equation is shown as follows:

$$^{123}_{51}Sb + ^{1}_{0}n \rightarrow ^{124}_{51}Sb + \gamma$$

There are two sources of ^{123}SB [4]:

1) Antimony is added to the bearings of various pumps to guarantee the rigidity of the material. Once wear occurs during the rotation of the pump shaft, a trace amount of antimony will enter the primary circuit system along with the coolant.

2) For the antimony-beryllium secondary neutron source used in the reactor core, once the secondary neutron source is damaged, the radioactive activity of ^{124}Sb will increase to a great extent.

The physical properties of ^{124}Sb are shown in Table 7.

Table 7 Physical Properties of ^{124}Sb

Half-life Period	Decay Energy	Exposure Rate Constant	Existence Form	Particle Diameter
60.2d	0.603MeV	9.5 R·cm2·mCi-1·h-1	Soluble particle	Approximately 0.08μm

2.2.3.3 Variation trend of critical nuclide ^{124}Sb

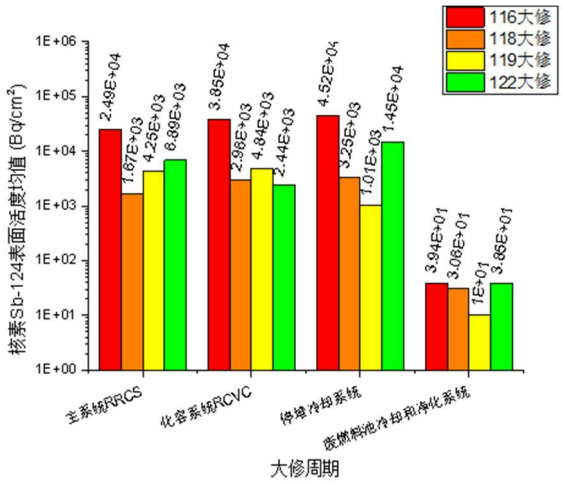

Figure 5 Variations in Surface Activity of ^{124}Sb

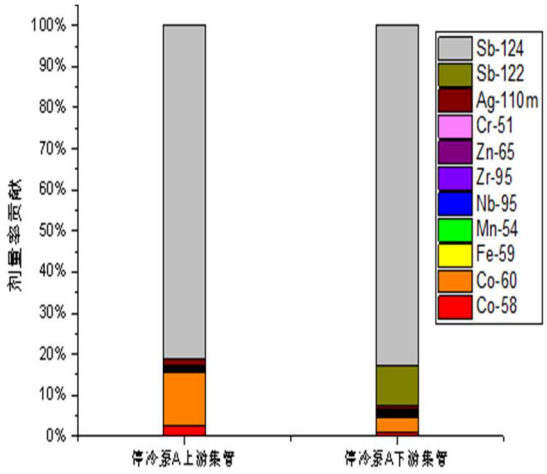

Figure 6 Dose Contribution Proportion of ^{124}Sb

1) ^{124}Sb is mainly deposited in the reactor shutdown cooling system, and its surface activity is twice as high as the mean value of the main system.

2) Since the major overhaul of OT116, the surface activity of ^{124}Sb in the cooling system has been decreasing to a great extent. The surface activity of ^{124}Sb in the cooling system during the major overhaul of 122 increased by an order of magnitude compared to that during the major overhaul of 119, and its dose rate contribution proportion was higher than 80%. It is initially determined that the deposition of the nuclide ^{124}Sb is abnormal.

2.2.4 Impact degree of three nuclides on radiation field

The surface activity of ^{58}Co and ^{60}Co pipes is comparable at the same order of magnitude of 10^4. However, according to the formula $X = \frac{A\Gamma}{R^2}$ (Where: A represents the activity of the radioactive source, R

represents the distance from the radioactive source to a certain point in the air, and Γ represents the exposure rate constant, and X represents the exposure).

The exposure rate constant (Unit: $R \cdot cm^2 \cdot mCi^{-1} \cdot h^{-1}$) of ^{60}Co, ^{58}Co and ^{124}Sb is 12.94, 5.464 and 9.5, respectively. In the condition of consistent radioactive activity, the exposure caused by ^{60}Co at 1m is 2.37 times that of ^{58}Co and 1.36 times that of ^{124}Sb. Meanwhile, in terms of half-life period, ^{60}Co is 5.27 years, ^{58}Co is 71.4 days, and ^{124}Sb is 60.2 days. ^{60}Co has distinct cumulative effect and is not prone to decay and disappearance when deposited in pipeline. ^{58}Co and ^{124}Sb have relatively short half-life period. In the event that the abnormal deposition does not occur continuously, the dissolution-deposition equilibrium can generally be restored within about two cycles.

Furthermore, from the measurement results, it can be seen that ^{60}Co is less evenly deposited on the equipment [5] but rather tends to accumulate in the primary circuit retention area, water supply pipeline, valve and other regions, so as to form radiation hotspots easily and threaten the radiation safety of personnel seriously.

In conclusion, ^{60}Co plays a decisive role in determining the level of radiation at the site of major overhaul and is the key point of source control.

3. Optimization of Radioactive Source Term

3.1 Control the formation of corrosion activated products

3.1.1 Control the entry of valve grinding particles into primary circuit

As analyzed in the previous text, the main target nucleus of ^{60}Co is ^{59}Co added to the Stellite alloy used on the valve sealing surface. During the very low water level period of for the major overhaul, the valve shall be disassembled and ground for open-access maintenance operation of the primary circuit valve. If the cobalt-containing metal particles are not removed during the process of grinding, the metal particles retained on the inner wall of the pipeline will flow into the reactor core along with the upward stage of the coolant unit for activation by neutrons, generating the corrosion activated products. According to the research of EPRI [6], if 40g of cobalt enters the primary circuit system each year, approximately 3200Ci of ^{60}Co will be produced after two cycles. Therefore, strengthening the cleaning control of the valve cavity during the disassembly and maintenance of radioactive valves and reducing the residue of metal particles are of great significance for the control of radioactive source term. At present, the major overhaul of 122 at the First Qinshan Plant has taken notice of this issue, and the corresponding measures are shown as follows.

1) Adjust the pre-maintenance workload of the radioactive valve. At present, the technical team is leading the optimization of the PM project for the maintenance of the radioactive valves at very low water level during the major overhaul at the First Qinshan Plant. By adjusting the PM cycle and reducing the number of radioactive valves to be disassembled, the workload of valve grinding can be reduced, and the possibility of entry of cobalt-containing impurities into the primary circuit can be reduced. In the major overhaul of 122, the number of valves maintained has been reduced from more than 500 to 328.

2) Clean the valve cavity with the vacuum cleaning pump. QC points are established in the maintenance specification, requiring that the valve cavity shall be cleaned with the vacuum cleaning pump after grinding to reduce the entry of grinding particles into the primary circuit system for activation. This operation was implemented by reference during the major overhaul of 122.

3.1.2 Replacement with antimony-containing materials

For First Qinshan Plant, the most important way to reduce the dose rate contribution of ^{124}Sb is to decrease the application of the antimony-containing materials. Due to the short half-life period of 124Sb, by reducing the application of antimony-containing materials from the source, it is possible to lower the radiation field of the reactor building during the next major overhaul. As analyzed above, the main sources of antimony include the wearing of the pump shaft and the damage of the secondary neutron source.

During the R8 period, the First Qinshan Plant replaced the turbine guide bearing of the main pump with antimony-free materials. As a result, the antimony activity of the coolant decreased by 50% during the C9 period, as shown in Figure 7.

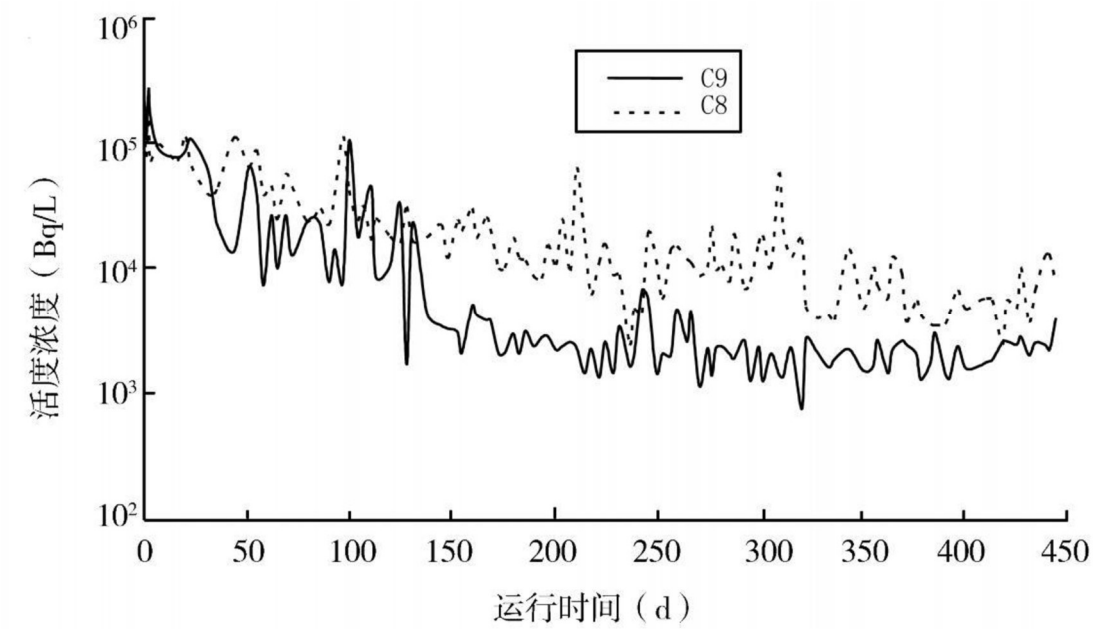

Figure 7 Variations in Radioactivity of ^{124}Sb in C8 and C9 Cycle

For instance, the rotating ring of the rotor component of the cooling pump at the First Qinshan Plant is made of antimony-doped graphite. Antimony-doped graphite is a self-lubricating sealing anti-wear material and produced by impregnating carbon graphite material with molten antimony metal. It is mainly used in mechanical sealing rings and thrust bearings of pumps in nuclear power plants. Although such materials have good mechanical properties, the impurities of the added antimony (Sb) enter the coolant after wearing and are activated to generate radioactive ^{124}Sb and ^{122}Sb.

3.2 Strengthen the purification of corrosion activated products

3.2.1 Oxidation operation

The main purpose of oxidation operation is to take advantage of the characteristic that the solubility of the corrosion activated products varies with temperature. In case of the cold shutdown of the reactor at the temperature of 80ºC (with the maximum solubility), the oxidant [7] is injected to dissolve the corrosion activated products on the coolant and the inner wall of the reactor core equipment rapidly. At this time, the discharge flow of the chemical and volume control system is increased to thoroughly purify and filter the main system in order to reduce the deposition of the corrosion activated products.

3.2.1.1 Extend the shutdown time of the main pump

During the oxidation operation, due to the operation of the main pump, the corrosion activated products flow at high speed to be mixed with the primary circuit coolant thoroughly, so as to reduce the deposition rate of the corrosion activated products. From the perspectives of power plant practice and theoretical calculation, it is possible to well demonstrate the significance of appropriate extension of the main pump operation time for the oxidation purification effect.

1. Practice in oxidation operation in major overhaul

In Figure 9, the data on the radiochemical levels of the main system during the oxidation operation in the last three major overhauls are presented. For oxidation purification in the major overhaul of 120, the main pump operated for 13 hours, and the total radioactive γ activity in the primary circuit decreased by 90%. In contrast, in the major overhaul of 122, the main pump operated for 13 hours, and the total γ activity of the primary circuit decreased by 60%. Thus, it can be seen that the longer the main pump operates, the more thorough the purification of total γ is.

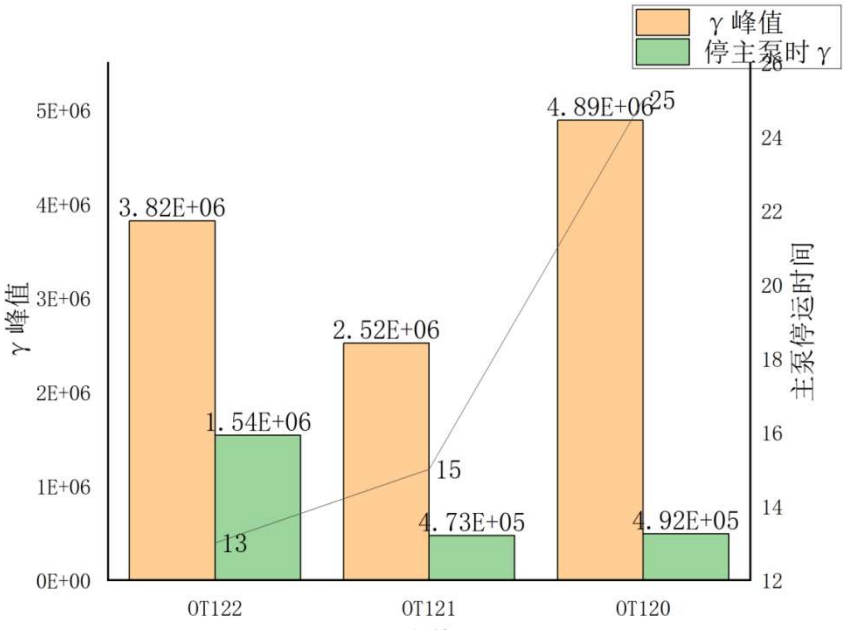

Figure 9 Total γ Activity of Primary Circuit and Operation Time of Main Pump

2. Calculation of theoretical purification capacity

It is known that the water loading capacity of the primary circuit at First Qinshan Plant is m_0, and m_0=165 tons. When $t=t_0$, the total activity in the medium is A, and the specific activity in the medium is c=c(t), c(0)=A/ m_0. Suppose the purification efficiency of the filtration unit is α, and the purification flow rate is m, with m=19t/h.

Consider that within a tiny time Δt, the change in the specific activity is:

$$[c(t+\Delta t)-c(t)]\ m0=-\alpha \cdot m \cdot \Delta t$$

Divide both sides by Δt simultaneously and let Δt→0]

$$\frac{dc}{dt} \cdot m_0 = -\alpha \cdot c \cdot m$$

$$c(0) = \frac{A}{m_0}$$

So, solving this calculus equation gives us:

$$C_1 = \frac{A}{m_0} \cdot e^{-\alpha \frac{m}{m_0} \cdot t}$$

Under the conditions that m_0=165t, the purification efficiency α is 90% and 99% respectively, and the purification flow rate is m=19 and 15t/h, Figure 10 is plotted. It can be seen that under the conditions of the purification efficiency of 99% and the purification flow rate of 19t/h, it takes nearly 20 hours to purify the primary circuit coolant to 10% of its initial activity, which is basically in line with the actual situation of oxidation operation in the major overhaul of 120.

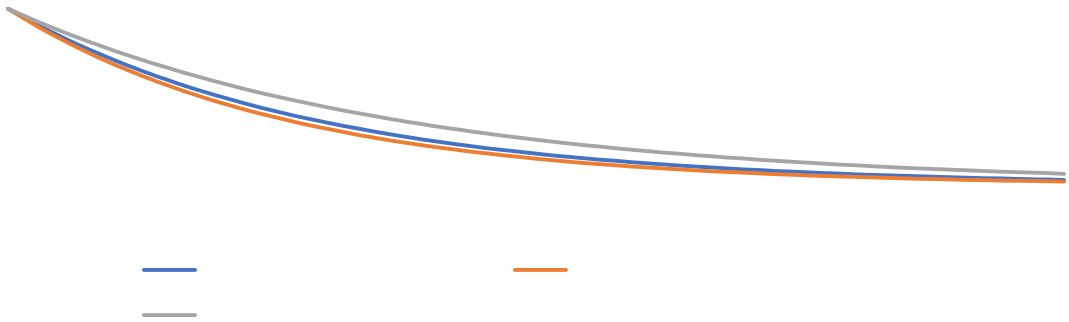

Figure 10 Tendency Chart of Oxidation Purification at First Qinshan Plant

3.2.2 Optimize the filter pore size

The pre-filter S02-19 of the chemical and volume control bed serves as the sole purification channel during the oxidation operation and plays a role in intercepting and removing the corrosion activated products. The pore size of the pre-filter of the chemical and volume control bed at the First Qinshan Plant is 1μm. However, as analyzed above, the particle diameters of ^{60}Co and ^{124}Sb are generally 0.08-0.4μm. The filter capacity for such two radioactive nuclides shall be improved. It can be seen from the comparison in Table 8, the pore size of the filters in domestic power plants has basically been optimized to below 0.45μm at the design stage or through modification and transformation.

Table 8 Comparison of Pore Size of Pre-Filters of Chemical and Volume Control Bed

Pore Sizes of Filters of Some Nuclear Power Units in China Unit: μm							
Power Plant	Daya Bay	Ningde	Fuqing	Hainan	Tianwan	First Qinshan Plant	Fangjiashan
pore size	0.1	0.1	0.45	0.45	0.1	1	0.1

At present, the units at First Qinshan Plant shall continue to promote the work of changing the pore size of the pre-filter of the chemical and volume control bed. Without changing the glass fiber material of the filter, the pore size shall be reduced to enhance the oxidation purification effect.

3.2.3 Extend the opening time of the double-discharge orifice plates after reaching the critical point

First, based on lateral comparison, the designed purification capacity of the units at the First Qinshan Plant is relatively lower than those of CNP650, AP1000 and other units, with a lower purification rate per hour, as shown in Table 9. Therefore, measures shall be taken to enhance the purification of radioactive source term by the unit.

Table 9 Comparison of Purification Units in the Units

Type of Reactor	Water Inventory of Primary Circuit (m^3)	Purification Flow Rate (m^3/h)	Purification Rate/Hour
WWER	300	30	10.0%
AP1000	227	19.5	8.6%
CNP600	165	13.6	8.2%
Hualong No.1	354	25	7.1%
First Qinshan Plant	165	11.2	6.8%

After the major overhaul of the unit reaches the critical point, the opening time of the double discharge orifice plates can be extended appropriately to enhance the purification capacity. At present, after the unit reaches the critical point, only one discharge orifice plate is generally put into use, and the normal drainage flow rate is 11.2t/h. However, due to the fact that the unit has undergone an open maintenance operation for a major overhaul, fine grinding particles may inevitably remain in the primary circuit pipeline. On the other hand, the corrosion activated products that peel off during the oxidation operation may have just adhered to the inner wall of the pipeline. At this time, it is advisable to put two discharge orifice plates (the system flow chart is shown in Figure 11), adopt the high-flow purification mode, and increase the drainage flow to 19t/h to enhance the purification capacity of the unit.

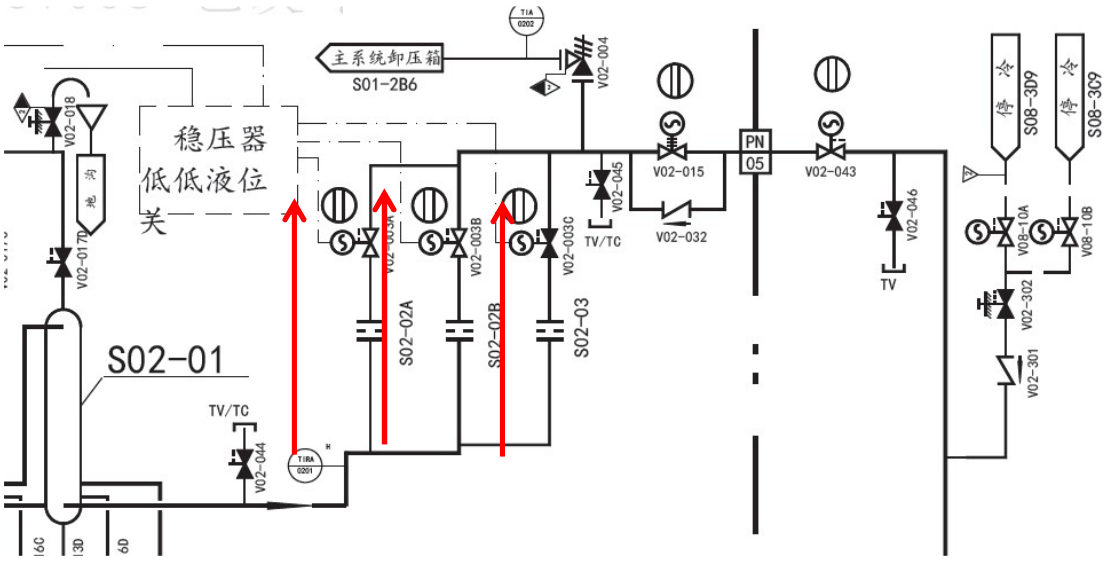

Figure 11 Flow Chart of Chemical and Volume Control System

3.3 Eliminate the impact of corrosion products

3.3.1 Hotspot flushing

Flush the radiation hotspots deposited in the pipeline with the system drainage and demineralized water to remove the deposited radioactive source term effectively. The flushing practice for some hotspots at First Qinshan Plant is shown in Table 10.

1. During the operation, three hotspots of isolation valves in Room 03#105 are flushed

Table 10 Practice for Hotspot Flushing

Location of Hotspot	Exposure Dose Rate μSv/h	Dose Rate at 1m μSv/h	Exposure Dose Rate after Flushing μSv/h	Dose rate at 1m after Flushing μSv/h
V07-42A	2410	112	41	8
V07-46	27300	356	27	11
V07-100	13800	73	95	3

1) Causes of hotspots: The boric acid solution in the refueling tank and the fuel transportation channel in the waste fuel cooling and purification system has high radioactivity and hot particles. When the fuel transfer channel is flushed and decontaminated or the refueling tank is sampled in a circulation manner, the hot particles will deposit at the relevant positions, generating radioactive hotspots.

2) Flushing scheme:

Table 11 Hotspot Flushing Scheme

Location of Hotspot	Flushing Window	Flushing Scheme
V07-42A	System replenishing water (waste fuel pool, refueling tank, etc.)	The radioactive hotspots are flushed by using system replenishing water, demineralized water or boric acid solution flowing through valves and pipelines
V07-46	System recirculation (before chemical sampling)	By recirculating the system, the solution of refueling tank flow through the system to flush the radioactive hotspots in valves and pipelines
V07-100	The refueling tank is full of water or partially filled with water	By using the high-water level in the refueling tank, water is poured into the fuel transportation channel to flush the radioactive hotspots in valves and pipelines.

2. Flushing of new hotspots occurring during major overhaul

The new radioactive hotspots occurring during the major overhaul of 122 were removed by means of high-pressure water gun and demineralized water, which are summarized in Table 12.

Table 12 Comparison Data for Flushing of Hotspots

Location of Hotspot	Exposure Dose Rate mSv/h	Post-treatment Exposure Dose Rate mSv/h	Environmental Dose Rate (mSv/h)	Post-treatment Environmental Dose Rate (mSv/h)
Fuel transfer carriage	120	15	1~4	0.5
01#210 Discharge pipeline	55	6	/	/

(1) Hotspots on the fuel transfer carriage. Upon learning that the stop block of the fuel transfer carriage used for major overhaul of Q1-122 should be replaced, the Radiation Protection suggested flushing this area immediately. The maximum dose rate measured at the hotspot on the carriage was 120mSv/h, and the ambient environmental dose rate was 1 to 4mSv/h. The method was changed from flushing with small high-pressure water gun to extension rod and adhesive tape covering, and then to wiping after connecting long rod with small high-pressure water gun for flushing, but the decontamination effect was still not obvious. Finally, based on discussion, the RP personnel located the hotspots in the inner hole at the bottom of sleeve precisely with the long rod. Then, the nuclear cleaning personnel flushed to remove the dirt with the large high-pressure water gun. Eventually, the hotspot was reduced to 15mSv/h, and the environmental dose rate was reduced to below 1mSv/h.
(2) Hotspots on the discharge pipeline 01#210. The water in the discharge pipeline mainly comes from the residual water in the refueling tank after decontamination. During the regular major overhaul, the water in the lower crossover is discharged only once. After refueling, the residual water from higher crossover decontamination and the hot particles with high dose rate will first be discharged into the lower crossover together and then discharged into the sewage pit through this valve during the contamination of lower crossover. Due to the horizontal arrangement of the discharge pipeline at 01#210, highly radioactive hot particles deposit inside the pipeline, creating the hotspots. At the end of decontamination process in lower crossover, the demineralized water is poured from the floor drain in the lower crossover to flush the pipeline repeatedly under the action of gravity, ultimately reducing the radiation level in this area.

3.3.2 Hotspot shielding

The flexible metal materials with large atomic numbers such as lead and tungsten are used to shield the radiation hotspots, and the field radiation level is reduced effectively through the interaction between rays and substances, so as to minimize the exposure of the deposition source term to the personnel. For instance, during the major overhaul, there are multiple hotspots in the cooling pump room, especially in the S08-01 shutdown cooling pipeline; if only the lead sheets are hanged up for shielding, there are problems such as insufficient lead equivalent and inadequate coverage area.

The multi-layer shielding structure was used for shielding of the shutdown cooling pump room during the major overhaul of 122 at the First Qinshan Plant, and a total of 78 lead sheets, 40 rolls of tungsten rubber, and 14 pieces of lead arch bridges were used, achieving the shielding efficiency of approximately 60%, as shown in Table 13. Among them, for the horizontally arranged cooling pipelines, the lead equivalent of shielding was improved significantly by wrapping with the tungsten rubber and fastening the shutdown cooling pipeline with the lead arch bridge, so as to reduce the amount of scaffolding erected, and lower the dose cost of such erection work.

Table 13 Erection of Shielding for Shutdown Cooling Pump Room

Shielding Object	Shielding Method	Shielding Amount	Shielding Efficiency
Hotspots in Room 02-146	Linear shielding – Lead arch bridge	7 pieces	67%
	Linear shielding – Tungsten rubber	20 rolls	
	Surface shielding – Lead sheet	44 pieces	
Hotspots in Room 02-14	Linear shielding – Lead arch bridge	7 pieces	63%
	Linear shielding – Tungsten rubber	20 rolls	
	Surface shielding – Lead sheet	34 pieces	

4. Conclusions

Based on the above-mentioned analysis and discussion, the following conclusions are drawn in the present paper:

1) For pressurized water reactor nuclear power, the corrosion activated products are the main radioactive source term.

2) The corrosion activated products migrate into the coolant, causing the total radioactive activity of the primary circuit to increase. In case of any change in the physical and chemical properties of the coolant such as temperature and PH, the corrosion activated products deposit on the pipeline to form the deposition source term, thereby affecting the radiation level of the unit. The peeling-off of the corrosion products is not the key point. The focus of source term control lies in prevention of deposition.

3) The main deposition source terms at the First Qinshan Plant include ^{60}Co, ^{58}Co and ^{124}Sb. ^{60}Co is a key factor affecting the radiation level of the unit, with its dose rate contribution accounting for at least 70%. The surface activity of ^{58}Co tends to become stable after the recent major overhauls without obvious fluctuation. The abnormal deposition of ^{124}Sb in the shutdown cooling system during the major overhaul of 122 has become the main contribution to the dose rate of this system.

4) By controlling the entry of cobalt-containing particles into the primary circuit and replacing with antimony-containing materials, the source of the main radioactive nuclides in the unit can be controlled, thereby curbing their formation pathways from the mechanism of their formation. The purification capacity for corrosion activated products is enhanced by optimizing the oxidation operation, reducing the filter pore size, extending the operation of double discharge orifice plate, and other means. The impact of the deposited corrosion term on the radiation level of the unit is eliminated by means of hotspot flushing and shielding. With the above mentioned three directions for reducing the source term, it is possible to control the radiation level of the unit effectively and reduce the field environmental dose rate during the major overhaul.

5) Main follow-up work: On the one hand, further attention shall be paid to the variation trends of ^{60}Co activation and deposition, and various forms of fixed shielding shall be implemented for the deposited radioactive source term; on the other hand, the research shall be conducted on the abnormal deposition of ^{124}Sb in the reactor shutdown cooling system, and the application of the antimony-doped graphite material in the primary circuit and the related quality defect list shall be sorted out to avoid the recurrence of such problems during the subsequent major overhauls.

SESSION 4. Changes in Ionizing Radiation Field During the First Cycle after Zinc Injection into the Primary Circuit of Operating Nuclear Power Units

Haiju Shen

CNNP Nuclear Power Operations Management Co., Ltd., China

Abstract: The Fangjiashan Nuclear Power Unit initiated zinc injection into the primary circuit from its eighth fuel cycle, becoming the first operating nuclear power unit in China to implement such a project. It has now successfully completed the first zinc injection cycle. To investigate the variation patterns of radiation field during the first cycle after zinc injection into the primary circuit of the operating PWR (Pressurized Water Reactor) unit, this paper analyzes and evaluates the impact of zinc addition on radiation field. The analysis is based on monitoring data from the radiation monitoring system, operation of filtration equipment, and changes in radiation field on surfaces of key piping and equipment within primary systems. This involved regular monitoring of radiation levels on filters and piping equipment in the Chemical and Volume Control System (CVCS) during routine operation, combined with tracked radiation level measurements on critical piping and equipment within the reactor building during refueling outage.

The results indicate that:

1. The radioactive source term levels in the primary coolant gradually increased and were significantly higher compared to previous fuel cycles.

2. The growth rate of radiation levels on surfaces of primary system piping and equipment slowed.

3. The rapid upward trend of ambient radiation levels on site was suppressed.

The analysis concludes that, zinc injection accelerated the release of corrosion-activated products which were subsequently filtered and purified by the CVCS, reducing the radioactive source term within the primary systems. Zinc injection played a positive role in radiation field control, leading to an improvement in the previously observed rapid increase of ambient radiation levels within primary system areas.

The zinc injection technology demonstrated significant effectiveness in radiation field control even in the first application cycle, providing crucial practical evidence for radiation protection optimization in operating nuclear power units.

SESSION 4. Source Term Control Technologies for Key Radionuclides in Nuclear Power Plants

Yaru Fu

Shanghai Nuclear Engineering Research & Design Institute, Shanghai, China

Abstract: During nuclear power plant operation, neutron irradiation in the reactor core inevitably generates activation products and corrosion activation products. In the event of fuel rod failure, key fission-product nuclides, such as noble gases and iodine, are also released into the coolant. These radionuclides pose challenges for occupational dose management and radioactive waste processing. Controlling radioactivity at its source is the most economical and effective approach to optimizing radiation protection and minimizing waste. With the fission product source term now relatively low in modern plants, 80%–90% of occupational exposure typically arises from corrosion activation products, predominantly Co-58 and Co-60. Advanced control strategies for corrosion product source terms include initiating zinc injection during hot functional testing, stringent control of cobalt content in materials, the application of advanced water-chemistry techniques during startup and shutdown, and surface treatment technologies. These measures have lowered Co-58 and Co-60 inventories to relatively low levels, enabling reduced collective doses. However, nuclides such as ^{110m}Ag in corrosion products can present significant difficulties: owing to the complex speciation of ^{110m}Ag, conventional processes struggle to have it being removed. If present in primary loop, ^{110m}Ag can prolong outage processing and decontamination time and increase collective dose; its presence should therefore be rigorously prevented through plant design and operational controls. In most light water reactors, dose contributions from internal exposure are already relatively low, mostly thanks to effective control of nuclides such as tritium that dominate internal dose. This is achieved primarily by reducing the tritium inventory in open water systems and ensuring that, by the end of a fuel cycle, the vast majority of tritium in the primary coolant has been discharged to the environment under controlled conditions.

SESSION 4. Investigation For Radioactive Deposition Source Terms Of Ap1000 Units

Quanlu Gou[1], Pengzhen Liu[1], Jiannian Zhang[1], Xiaodong Yu[1]

[1] Shandong Nuclear Power Company Ltd., Haiyang, Shandong, China

Abstract: This paper introduces the formation mechanism, investigation method for deposition source terms at Haiyang Nuclear Power Plant and analyzes the obtained deposition source term data of the AP1000 unit. By comparing the general level of the deposited source term in the reactor cooling system (RCS) at AP1000 units with M310 units, the reason for the difference in the deposition of three nuclides (Co-58, Cr-51, and Ag-110m) in the RCS systems of the two types of units are analyzed from the perspective of the equipment material composition of each type unit. At the same time, the special investigation regarding the problem for having high Ag-110m nuclide content in the RCS systems, and the replacement modification for gaskets on the tube side of the RNS system heat exchange are also introduced. Through this modification, the problem of high Ag-110m nuclide content in the radioactive liquid effluent of the units was solved.

Keywords: Investigation, Deposition source terms, In situ gamma spectrometry technology.

1 Introduction

For radiation protection professionals of NPP, one of the main tasks is to keep the occupational radiation occupational exposures as low as reasonably achievable (ALARA). Throughout the world, Occupational radiation exposure at NPP has steadily decreased since the early 1990s. This downward trend is attributed to effective ALARA management, new technologies, plant design modifications, improved water chemistry and operational ALARA awareness, as well as senior plant management support of a strong ALARA culture and global exchange of ALARA experiences. However, with the continued ageing and life extension of NPPs worldwide, ongoing economic pressures, regulatory, social and political revolutions, along with the new units built, the task for ensuring that occupational exposures are ALARA continues to present challenges to radiation protection professionals, in particular when considering operational costs and social factors.

In normal operation of pressurized water reactors (PWRs), the activated corrosion products (ACPs) may deposit on the inner surface of the primary circuit equipment, such as pipeline, valves, and other equipment, forming deposition source terms（DSTs）, are the main source terms in the primary circuit. Some research show that about 80%–95% of occupational radiation exposure comes from DSTs during refueling outage [1–4]. Therefore, it is of great significance to investigate DSTs. Through the investigation and analysis of DSTs, we can find the the origins and variation trends, formation mechanism, types and amounts of nuclides deposited on the inner surface of equipment, their contribution to the radiation field, which can provide guidance for the decision making for source term control measures at nuclear power plants.

This work investigated the DSTs at Haiyang Nuclear Power Plant, and analyzed the obtained DSTs data from the four operation AP1000 units, also compared with M310 units, analyzed the reason for the difference in the deposition of three nuclides (Co-58, Cr-51, and Ag-110m) in the RCS systems of the two types of units are analyzed, the problem of high Ag-110m nuclide content have been analyzed, the main origins and mitigation measurement are introduced.

2 Introduction for Formation Mechanism of Deposition Source Terms

In normal operation conditions of PWR, Corrosion products are formed by the release of metal-oxide ions, colloids, and particles generated from the general corrosion of materials in contact with the coolant water. Corrosion products are typically comprised of iron and nickel oxides with small amounts of manganese, chromium, and traces of cobalt. Some of these corrosion products are released and are transported by the coolant and redeposit throughout the primary system. At the same time, some of them will be activated under neutron irradiation to form activated corrosion products (ACPs) (the main radionuclide is 58-Co, 60-Co, 51-Cr, 54-Mn, 59-Fe, etc.). ACPs then redeposit on ex-core components forming DSTs, which directly result in increased radiation fields and the collective occupational radiation dose during refueling outage [5]. The main transport processes that lead to corrosion product activation in PWRs showed in fig. 1[6].

Because the primary coolant cleanup systems in LWRs are relatively ineffective for removing activity compared to the decay of corrosion products on out-of-core surfaces. Radiation fields tend to build up over a few years before an equilibrium level is reached following initial startup, chemistry regime changes, or system/component decontamination. Out-of-core surfaces in contact with reactor coolant will pick up particles, colloids and ions. These will be incorporated in the growing film which exists on these surfaces as shown in Fig. 2[6].

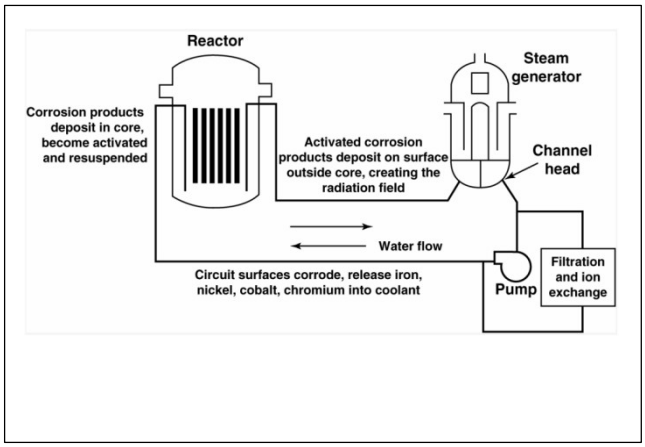

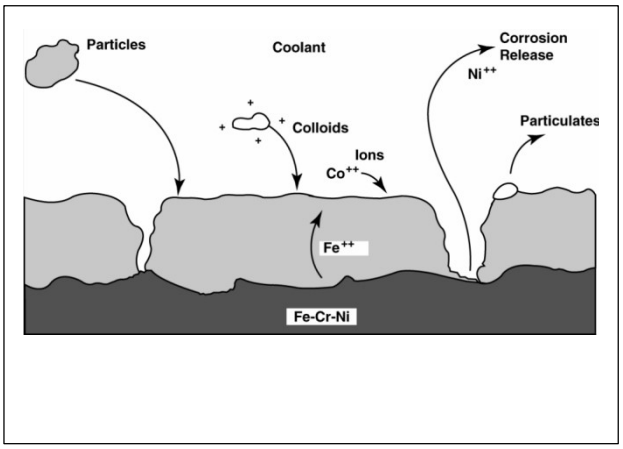

3 Methods for Investigating the DSTs

3.1 Measurement Method for DSTs in Pipeline

During the refueling outage at Haiyang Nuclear Power Plant, the DSTs on the inner surface of pipelines and equipment in the Reactor Coolant System (RCS), Chemical and Volume Control System (CVS), Passive Core Cooling System (PXS), and Residual Heat Removal System (RNS) have been investigated. Because it is difficult to measure the DSTs on the inner surface of the pipelines using traditional sampling measurement methods, in situ gamma spectrometry technology has been used. For this technology, the high-purity Germanium (HPGe) gamma spectrometer are setup directly outside the measured pipeline, and obtain the gamma spectrum, then the type of nuclides and activity in DSTs on the inner surface of the pipeline can be obtained through gamma-ray spectroscopy analysis, using software Genie-2000 of Canberra. As shown in Fig. 3, during measuring the DSTs, the gamma detector is placed outside the measured pipeline to obtain the in-situ gamma spectrum. The spectrum is then analyzed to obtain the full-energy peak net count rate of gamma rays with different energies.

After the measurement conditions are determined, such as parameters of the measured pipeline, parameters of the detector, relative geometric parameters of the detector and the measured pipeline, etc., the surface activity of the different nuclides can be obtained based on the source less efficient calibration and activity calculation. The calculation method for the surface activity of a specific nuclide is expressed in formula (1) [7,8]:

$$A_S = \frac{n_E}{\varepsilon_E \times S \times p_E} \qquad (1)$$

Where:

A_S = surface activity of the nuclide, Bq/m^2

n_E = full-energy peak net count rate of gamma rays, **s^{-1}**

ε_E = full-energy peak detection efficiency of gamma rays

S = effective internal surface area of the pipeline, **cm^2**

p_E = branching ratio of gamma rays.

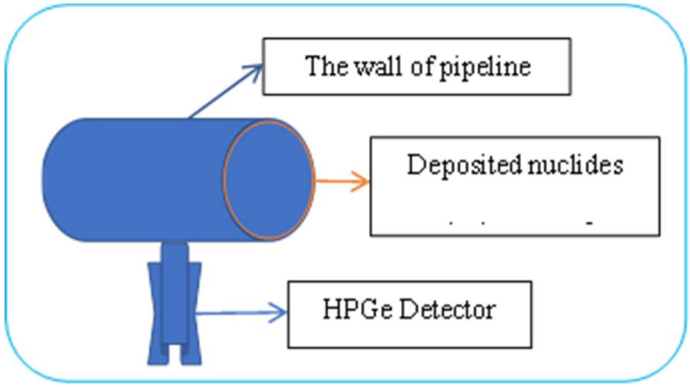

Fig.3 Layout Diagram of in situ High-purity Germanium (HPGe) Gamma Spectrum Measurement

Based on above the surface activity of DSTs, the dose rate generated by the deposited nuclides on the outer surface of the pipeline can be obtained through dose rate calculation, and the reliability of the deposition source term measurement results can be verified by comparing with the actual measured values [9]. The investigation method and process showed in Fig.4.

3.2 Measuring Equipment

The measurement equipment used in this work is in-situ high-purity germanium gamma source term measurement system, as showed in Fig.5. It mainly consists of a high-purity germanium detector, collimator, multi-channel analyzer, mobile trolley, etc. Its measurable height range is 0.35m - 2m, with a mass of 35kg, and the folded volume is 100cm × 50cm × 30cm, making it convenient for in situ use. The high-purity germanium detector has the advantages of high measurement efficiency and good energy resolution. The measurable energy range of the detector is 50keV - 2.2MeV, which can cover the gamma-ray energy of most corrosion activation products in nuclear power plants (generally 300keV - 2.0MeV). When using a high-purity germanium detector to measure the gamma energy spectrum of the deposition source term, the dead time should generally be less than 10%, and the full-energy peak count should be more than 10,000 counts.

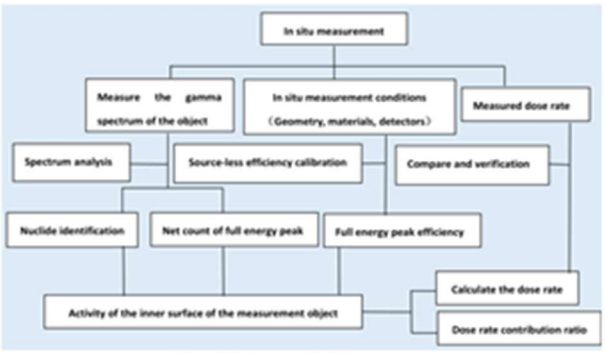

Fig. 4 Schematic Diagram of Deposition Source Term Investigation Method

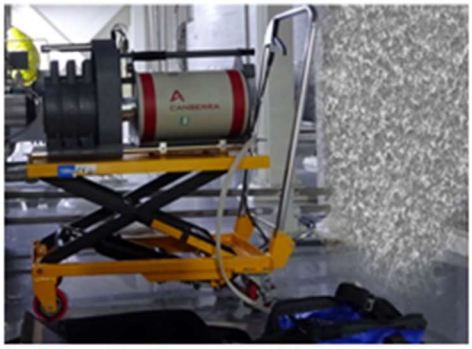

Fig. 5 Deposition Source Term Measuring Equipment

3.3 Selection of the Measuring Points

Because of the rationality of measurement points directly impact the result of source term investigation, the selection of points should follow the following principles as much as possible:

1) The space around the system pipeline to be investigated should be as large as possible, to minimize the influence of scattered radiation on the measurement results.
2) Other radiation hotspots should be avoided as much as possible around the measurement pipeline, to reduce the additional count of the full-energy peaks in the measurement spectrum caused by radioactive nuclides in other pipelines.
3) The structure of the measured pipeline should be as simple as possible. Pipelines with complex geometric structures are prone to factors such as fluid velocity changes and eddy currents that may lead to uneven nuclide deposition, making the measurement results unable to represent the average level of the measured pipeline. At the same time, the complexity of the pipeline structure also affects the accuracy of subsequent calculation work.

According to NB/T 20490-2018 Monitoring requirements for activated corrosion product deposition source items during shutdown and maintenance of pressurized water reactor nuclear power plants [10], combined with the system equipment layout of AP1000 units, some pipelines with high level of radiation dose rate in systems such as RCS, CVS, RNS and PXS are selected as the measuring objects, and the experience of radiation source term investigation in other nuclear power plants are also considered. Based on the above considerations, 12 measurement points were seleced, and their positions listed in table 1.

Table 1 Deposition Source Term Investigation Measurement Points

serial number	system	measurement point	serial number	system	measurement point
1	RCS System	Loop 1 Hot Leg	7	CVS System	Purification Return Pipeline
2	RCS System	Loop 1 Cold Leg	8	RNS System	RNS Header Inlet Pipeline
3	RCS System	Loop 2 Hot Leg	9	RNS System	RNS Header Outlet Pipeline
4	RCS System	Loop 2 Cold Leg	10	RNS System	RNS Heat Exchanger A Inlet Pipeline
5	RCS System	PZR Surge Line	11	PXS System	DVI B Pipeline
6	CVS System	Purification Outlet Pipeline	12	PXS System	PXS PRHR Inlet Pipeline

4 Investigation Results

4.1 Reactor Coolant System (RCS)

The surface activity of radioactive nuclides deposited on the inner walls of the five-section selected pipelines of the RCS system list in table 2. It can be seen that the deposited nuclides in the RCS system include Co-58, Co-60, Fe-59, Mn-54, Nb-95, Zr-95, Zn-65, Cr-51, Ag-110m, and Sb-124, etc.

Table 2 Surface Activity of Main Nuclides Deposited on the Inner Wall of Measured Pipelines of RCS System

investigation point	surface activity of main nuclides deposited on the inner wall of the pipeline (Bq/cm²)									
	Co-58	Co-60	Fe-59	Mn-54	Nb-95	Zr-95	Zn-65	Cr-51	Ag-110m	Sb-124
Loop 1 Hot Leg	6.56E+04	1.43E+05	6.15E+04	5.82E+03	4.26E+03	2.27E+03	7.40E+03	3.92E+07	1.57E+03	2.01E+03
Loop 1 Cold Leg	3.02E+05	4.99E+04	3.18E+04	4.52E+03	5.43E+03	1.57E+03	2.12E+03	2.35E+06	4.48E+03	8.38E+02
Loop 2 Hot Leg	1.08E+05	1.56E+05	7.06E+04	1.30E+04	7.30E+04	4.51E+04	1.85E+04	2.96E+07	7.83E+03	6.14E+03
Loop 2 Cold Leg	1.62E+05	5.25E+04	1.47E+04	2.81E+03	6.36E+03	1.44E+03	1.33E+03	4.03E+06	6.50E+03	5.14E+02
PZR Surge Line	2.80E+04	6.50E+03	6.55E+02	8.25E+02	1.13E+03	1.94E+02	2.23E+02	9.29E+02	3.04E+02	4.54E+01
Average	1.33E+05	8.16E+04	3.59E+04	5.39E+03	1.80E+04	1.01E+04	5.91E+03	1.50E+07	4.14E+03	1.91E+03

From this table, it can be seen that the surface activity of Cr-51 deposited on the inner walls of various pipelines of the RCS system is relatively high. Except for the pressurizer surge line, the activity of Cr-51 in other pipelines of the RCS system ranges from 10^6 to 10^7 Bq/cm². the surface activity of Co-58 is in the order of 10^4 to 10^5 Bq/cm², with an average of 1.33×10^5 Bq/cm². the average surface activities of Co-60, Fe-59, Nb-95, and Zr-95 are above 10^4 Bq/cm². the surface activities of the remaining deposited nuclides range from 10 to 10^4 Bq/cm².

4.2 Chemical and Volume Control System (CVS)

The surface activity of nuclides deposited on the inner walls of the two-section selected pipelines of the CVS system list in table 3. It can be seen that the deposited nuclides on the inner walls of measured pipelines of the CVS system include Co-58, Co-60, Fe-59, Mn-54, Nb-95, Zr-95, Zn-65, Cr-51, Ag-110m, Sb-124, etc. The surface activity of Co-58 in measured pipelines of the system is relatively high, with an average of 4.43×10^4 Bq/cm², followed by Ag-110m, Nb-95, Cr-51, Co-60, and Zr-95, with average surface activities in the order of 10^3 Bq/cm². the average surface activities of other nuclides range from 10-10^2 Bq/cm².

Table 3 Surface Activity of Main Nuclides Deposited on the Inner Walls of Measured Pipelines of CVS System

investigation point	surface activity of main nuclides deposited on the inner wall of the pipeline (Bq/cm²)									
	Co-58	Co-60	Fe-59	Mn-54	Nb-95	Zr-95	Zn-65	Cr-51	Ag-110m	Sb-124
Purification Outlet Pipeline	7.51E+04	1.03E+04	9.68E+02	9.26E+02	1.31E+04	5.42E+03	6.61E+02	1.14E+04	1.60E+04	4.29E+02
Purification Return Pipeline	1.35E+04	1.68E+03	1.60E+02	2.13E+02	1.29E+03	5.74E+02	1.18E+02	1.38E+03	1.69E+03	8.02E+01
Average	4.43E+04	6.01E+03	5.64E+02	5.69E+02	7.22E+03	3.00E+03	3.90E+02	6.40E+03	8.84E+03	2.55E+02

4.3 Residual Heat Removal System (RNS)

The surface activity of the deposition source term on the inner walls of the three-section pipelines of the RNS system list in table 4. It can be seen that the nuclides deposited on the inner walls of measured pipelines of the RNS system include Co-58, Co-60, Fe-59, Mn-54, Nb-95, Zr-95, Zn-65, Cr-51, Ag-110m, Sb-124, etc. In the RNS system, the surface activities of Cr-51, Fe-59, Co-58, Co-60, and Nb-95 deposited on the inner walls of measured pipelines are relatively high, with average values in the order of 10^3 to 10^4 Bq/cm², and the average surface activities of other deposited nuclides range from 10 to 10^2 Bq/cm².

Table 4 Surface Activity of Deposited Nuclides on the Inner Walls of Measured Pipelines of the RNS System

investigation Point	surface activity of main deposited nuclides on the inner wall of the pipeline (Bq/cm²)									
	Co-58	Co-60	Fe-59	Mn-54	Nb-95	Zr-95	Zn-65	Cr-51	Ag-110m	Sb-124
RNS Header Inlet Pipeline	8.88E+03	1.57E+03	7.57E+03	1.72E+02	2.37E+03	1.22E+03	3.67E+01	1.80E+04	7.62E+02	5.05E+02
RNS Header Outlet Pipeline	1.13E+04	1.18E+03	1.52E+04	6.71E+01	1.16E+03	2.43E+02	1.01E+02	3.34E+03	1.71E+03	1.27E+02
RNS HX Inlet Pipeline	2.98E+03	8.97E+02	3.23E+03	7.25E+01	8.08E+02	3.51E+02	1.80E+01	9.42E+03	2.55E+02	1.60E+02
Average	7.73E+03	1.22E+03	8.68E+03	1.04E+02	1.45E+03	6.05E+02	5.19E+01	1.02E+04	9.09E+02	2.64E+02

4.4 Passive Core Cooling System (PXS)

The surface activity of nuclides deposited on the inner walls of 2 measured pipelines of the PXS system list in table 5. It can be seen that the deposited nuclides on the inner walls of measured pipelines of the PXS system include Co-58, Co-60, Fe-59, Mn-54, Nb-95, Zr-95, Zn-65, Cr-51, Ag-110m, Sb-124, etc. The surface activities of Co-58, Co-60, and Cr-51 in various pipelines of the system are relatively high, with average values of approximately 6.42×10^4 Bq/cm², 1.57×10^4 Bq/cm², and 6.73×10^4 Bq/cm² respectively; the average surface activities of other deposited nuclides are in the order of 10^2 to 10^3 Bq/cm².

Table 5 Surface Activity of Main Deposited Nuclides on the Inner Walls of Various Pipelines in the PXS System

investigation point	surface activity of main deposited nuclides on the inner wall of pipeline (Bq/cm²)									
	Co-58	Co-60	Fe-59	Mn-54	Nb-95	Zr-95	Zn-65	Cr-51	Ag-110m	Sb-124
DVI B Pipeline	3.76E+04	1.34E+04	9.95E+03	1.89E+02	2.06E+03	8.93E+02	3.86E+02	1.34E+05	3.18E+03	2.04E+02
PRHR Inlet Pipeline	9.08E+04	1.79E+04	5.76E+02	1.59E+03	7.19E+02	1.79E+02	1.46E+03	9.47E+02	1.96E+03	6.19E+01
Average	6.42E+04	1.57E+04	5.26E+03	8.90E+02	1.39E+03	5.36E+02	9.21E+02	6.73E+04	2.57E+03	1.33E+02

4.5 Comparison of Calculated and Measured Surface Contact Dose Rates of Pipelines

Using the Monte Carlo method, the in-situ γ spectrum measurement conditions are simulated to obtain the detection efficiency of the HPGe measurement system under specific scenarios. This allows for the calculation of the activity of the deposited source terms on the inner walls of the pipes and the sum of the surface dose rates produced by each radionuclide on the outer surface of the pipes (i.e., the calculated surface dose rate of the pipes). During the in-situ γ spectrum measurement, the surface dose rate of the measured pipes is also measured. By comparing the relative deviation between the calculated and measured surface dose rates, the accuracy of the radiation source term measurements can be preliminarily verified. Table 6 presents the relative deviations between the calculated and measured surface dose rates for the investigated pipes during the HY102 refueling outage.

Table 6 Comparison of Calculated and Measured Surface Contact Dose Rates of Pipelines

Related system	Investigation point	Calculated dose rate (μSv/h)	Measured dose rate (μSv/h)	Relative deviation
RCS	Loop1 hot leg	114.03	99.85	14.20%
	Loop1 cold leg	134.99	120.88	11.68%
	Loop2 hot leg	117.03	100.92	15.96%
	Loop2 cold leg	104.43	97.20	7.44%
	PZR surge pipeline	49.43	32.48	47.79%
CVS	Purification outlet pipeline	348.96	285.96	22.03%
	Purification return pipeline	79.47	61.60	29.01%
RNS	RNS Header Inlet Pipeline	59.07	59.04	0.05%
	RNS Header outlet Pipeline	101.74	85.00	19.70%
	RNS HX A inlet pipeline	63.43	46.09	37.63%
PXS	DVI B pipeline	191.25	165.66	15.45%
	PRHR inlet pipeline	145.10	94.20	54.04%
SFS	SFS heat exchanger A outlet pipeline	11.61	9.47	22.55%

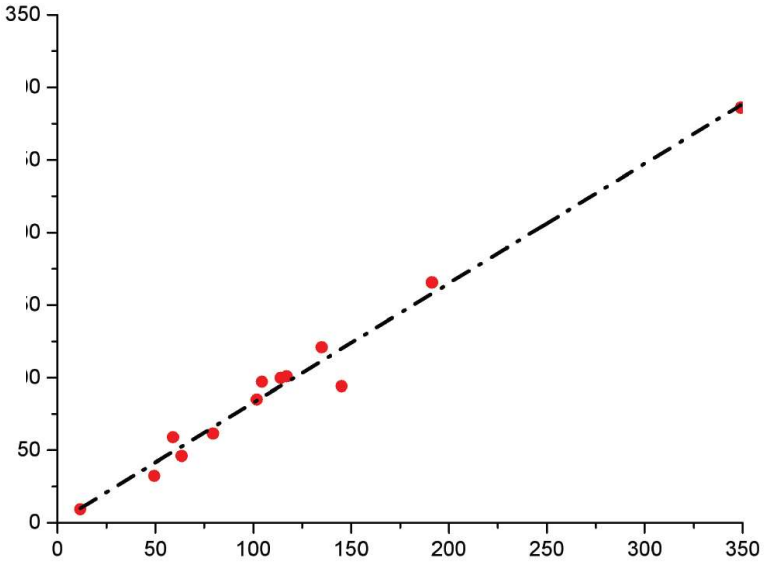

Fig. 6 Scatter plot and linear fitting curve

Statistical analysis of the data in the table shows that the average relative deviation between the calculated and measured surface dose rates at the 12 measurement points in this source term investigation is 22.89%, and the standard deviation of the relative deviation is 14.99%. Overall, from a statistical perspective, the results of this source term investigation are credible. The scatter plot with the calculated dose rate on the X-axis and the measured dose rate on the Y-axis are showed in Fig.6. It can be seen that there is a good linear relationship between the scatter points. After linear fitting, the correlation coefficient is 0.98. Overall, the calculated and measured surface dose rates are consistent.

5 General Level Analysis for Average Surface Activity of Deposition Nuclides

In order to analyze the general level of the DSTs of different types of nuclear power units, this study select 8 nuclear power units, among which 4 units are AP1000 unit, and 4 units are M310 unit. The average surface activity of the deposited nuclides on the inner walls of the RCS system pipes of each type of units are taken to represent the average DSTs of that type of nuclear power unit for comparison.

Compared with M310 nuclear power units, the overall level of Co-58 surface activity deposited on the inner walls of RCS system pipelines in AP1000 units is lower comparable to those in M310 nuclear power units, but the overall levels of surface activities of Cr-51 and Ag-110m are higher. The surface activities of nuclides Co-58, Cr-51, and Ag-110m in the deposition layer on the RCS pipelines of different type units are shown in Fig. 7.

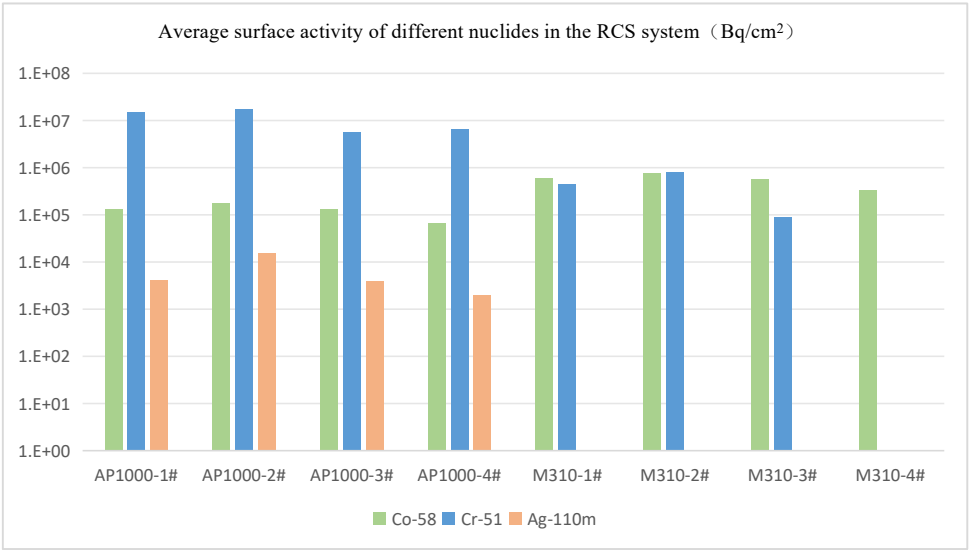

Fig. 7 Surface Activity of Main Deposited Nuclides in RCS Pipelines of Different Units

5.1 Analysis for Co-58 Nuclide Deposition

From Fig. 7, it can be seen that the surface activity of Co-58 nuclides deposition in the RCS system pipelines of the four AP1000 units is between with 1.3×10^5 - 1.7×10^5 Bq/cm², and that of the four M310 units is between with 3.3×10^5 - 7.6×10^5 Bq/cm². The surface deposition activity amount of Co-58 in the RCS system of AP1000 units is lower than that of M310 units. Co-58 is a major source term of radioactive corrosion products in the primary circuit of nuclear power plants and is also one of the nuclides that contribute the most to the collective dose of the plant. Co-58 nuclides in the primary circuit are mainly generated by the (n,p) reaction of Ni-58. The stable nuclide Ni-58 (isotopic abundance 68.077%) is the main component of the nickel-based alloy used as the main material for steam generator heat transfer tubes.

The main reasons why the surface deposition amount of Co-58 in the RCS system of AP1000 units is lower than that of M310 units are as follows:

1) The steam generator heat transfer tubes of AP1000 units use Inconel 690 nickel-based alloy, while those of M310 units use Inconel 600 nickel-based alloy. As shown in Table 7, the nickel content in Inconel 690 is more than 58%, and that in Inconel 600 is 72%. Under the same contact area with the primary loop, the Co-58 nuclides caused by nickel corrosion activation products in the SG heat transfer tubes of M310 units are higher than those of AP1000 units.
2) In terms of design, the system, equipment and layout of the primary circuit at A1000 unit are optimized and reduced the use of radioactive equipment and components. Compared with other pressurized water reactor nuclear power plants, the number of valves has been reduced by 50%, pumps by 65%, and pipelines by 20% [11], which reduces the generation of corrosion activation products.
3) In terms of operation, the technology of zinc injections to the primary circuit are adopted from beginning of the hot functional tests to operation stage for AP1000 units. After the primary circuit is saturated with zinc, the anti-corrosion property of the oxide film on the inner surface of the equipment was enhanced, which alleviated the corrosion and release of system materials, and reduced the source term of corrosion products. [12]

Table 7 Alloy Composition of Primary Loop Materials

alloy	proportion of contact area with primary loop	alloy composition（%）							
		Fe	Cr	Ni	Zr	O	Sn	Mn	Co
Zr-4 or Zr (fuel rod cladding)	0.24	0.2	0.1	-	98.5	0.12	1.40	-	0.002
Inconel 600 (SG heat transfer tube)	0.69	8	9	72	-	-	-	-	0.45
Inconel 690 (SG heat transfer tube)		9	29	58	-	-	-	0.5	0.15
Inconel 718	Low proportion	17	19	52.5	-	-	-	0.35	0.04
304 SS low Co	0.02	70	19	9	-	-	-	2	0.05
304 SS unlimited Co	0.05	70	19	9	-	-	-	2	0.15
Stellite（hard facing）	Low proportion	1	24.5	1	-	-	-	-	57

5.2 Analysis of Cr-51 Nuclide Deposition

From Fig.7, it can be seen that the surface activity of Cr-51 nuclide deposition in the RCS system pipelines of the three AP1000 units is between with 6.0×10^{6} - 1.7×10^{7} Bq/cm², and that of the four M310 units is between with 8.0×10^{4} - 7.9×10^{5} Bq/cm². The surface deposition activity amount of Cr-51 in the RCS system of AP1000 units is much higher than that of M310 units (more than an order of magnitude).

Cr-51 is a major source term of radioactive corrosion products in the primary circuit of nuclear power plants. Due to its gamma-ray energy of 320keV [13], the low ray energy makes it difficult to penetrate the pipeline wall thickness. Therefore, the Cr-51 nuclides deposited on the inner wall of the pipeline contribute little to the radiation exposure of workers and the collective dose of the nuclear power plant. Cr-51 nuclides in the primary circuit are mainly generated by the (n,γ) reaction of Cr-50. Cr-50 mainly comes from the corrosion of stainless steel and nickel alloys.

The main reasons why the surface deposition amount of Cr-51 in the RCS system of AP1000 units is much higher than that of M310 units are as follows:

1) As shown in Table 7, the Cr content in Inconel 690 nickel-based alloy used for the steam generator heat transfer tubes of AP1000 units (29%) is higher than that in Inconel 600 nickel-based alloy of M310 units (9%);
2) The outer surface of the control rod cladding of AP1000 units adopts Cr plating technology, and the control rods are irradiated by high neutron flux in the core for a long time during the entire power

operation period, so Cr-50 has a higher probability of being activated into Cr-51.

5.3 Analysis of Ag-110m Nuclide Deposition

Ag-110m radionuclides in the primary circuit are mainly generated by the (n,γ) reaction of Ag-109. It is one of the major source terms of radioactive corrosion products in the primary circuit of Haiyang Nuclear Power Plant, and also one of the raidonuclides that contribute the most to the collective dose of the plant. From Fig.6, it can be seen that Ag-110m nuclide deposition occurs in the RCS system pipelines of the three AP1000 units, with surface activities is between with 4.0×10^{3} - 1.5×10^{4} Bq/cm². All the surface activities of Ag-110m in the DSTs of RCS pipelines of the four M310 units are below the detection limit. Compared with M310 units, AP1000 units have higher Ag-110m nuclide deposition.

So, more attention is paid to the problem of high Ag-110m content at Haiyang Nuclear Power Plant. The special investigation targeting the equipment, and components with silver-containing material that result in high activity of Ag-10m in the primary circuit have been conducted and confirmed that the silver-containing gaskets on the tube side of the RNS heat exchanger are the main source of nuclide Ag-110m in the system. Nuclide Ag-109 in the silver-containing gaskets on the tube side of the RNS heat exchanger dissolves into the coolant and is activated in the core to become Ag-110m. Based on the above study conclusion, modification to replace the tube side gaskets of the RNS system of Unit 1 with silver-free gaskets are conducted. During the oxidation operation in the fourth refueling outage of Unit 1, the maximum Ag concentration decreased from 77ppb before replacement to 6ppb and finally dropped below the detection limit (4ppb) with the continuous operation of oxidation purification. Later, based on the experience feedback from Unit 1, the replacement work for the tube side gaskets of the RNS system of Unit 2 was also carried out. Through this modification, the problem of high Ag-110m nuclide content in the radioactive liquid effluent of the units was solved.

6 Conclusion

1) The results of the investigation for AP1000 units show that the overall level of Co-58 surface activity deposited on the inner walls of RCS system pipelines in AP1000 units is lower,comparable to those in M310 nuclear power units, and the overall levels of surface activities of Cr-51 and Ag-110m are higher.
2) The main reasons why the surface activity of Co-58 nuclide in the deposition source term of AP1000 units is lower than that of M310 units are the lower nickel content in Inconel 690, fewer primary loop equipment in AP1000 units, and the adoption of zinc addition technology.
3) The main reasons for the high Cr-51 nuclide in the deposition source term of AP1000 units are the high chromium content in Inconel 690 and the adoption of chromium plating technology for the control rods of AP1000 units.
4) The main reason for the high Ag-110m nuclide in the deposition source term of AP1000 units is that the silver in the silver-containing gaskets on the tube side of the RNS heat exchanger enters the core with the coolant, is activated, and is deposited in other systems with the coolant. Haiyang Nuclear Power has replaced all the silver-containing gaskets of the RNS heat exchangers in both units with silver-free gaskets, fundamentally solving the problem of Ag-110m in AP1000 units.

References

[1]. M. YANG and D. CHEN, “Proactive and Experience of Occupational Exposure Control in the Outages of Daya Bay Nuclear Power Plant,” Radiat. Prot., 24, 3–4, 144 (2004).

[2]. F. LI et al., “Simulation of Coolant Radiolysis Products in Operating Conditions During the Shutdown of PWRs,” Nucl. Power Eng., 44, 3, 202 (2023).

[3]. Y. SUN et al., “Study on the Formation Mechanism and Preparation of 110mAg Colloid in the Primary Circuit of PWR Nuclear Power Plant,” Radiat. Prot., 44, 3, 248 (2024).

[4]. P. LI et al., “Influence of pH on Source Term of Activated Corrosion Product in Reactor,” At. Energy Sci. Technol., 12, 2498 (2022).

[5] Deshon, J.: PWRAxial Offset Anomaly (AOA) Guidelines. EPRI Technical Report, 1008102

(2004)

[6]. Riess, R.: Chemistry Experience in the Primary Heat Transfer Circuit of Kraftwerk Union

Pressurized Water Reactors. Nuclear Technology, Taylor & Francis Group, pp. 153–159

(2017)

[7] L. LIU et al., “In-Situ Gamma-Spectrometry Measurement of Radiological Source Term for Primary System of NPPs Based on HPGe Detector,” Radiat. Proti. 35, 5, 257 (2015). 15.

[8] S. XIA et al., “On-Site Monitoring the Activity Concentration of Nuclide 58 Co in Coolant During PWR Oxygenation Shutdown,” Nucl. Tech., 41, 12, 120603 (2018).

[9] Liu Liye. In-situ Gamma Spectrum Measurement of Radiation Source Term in Primary Loop System of Nuclear Power Plant Based on High-Purity Germanium Detector [J]. Radiation Protection, 2015, 35(5): 257-260.

[10] NB/T 20490-2018 Monitoring requirements for activated corrosion product deposition source items during shutdown and maintenance of pressurized water reactor nuclear power plants[S]. Beijing: Nuclear Industry Standardization Institute Press, 2018.

[11] Wan Dengwei. Optimization of Radiation Protection in AP1000 Nuclear Power Plant Design [J]. Radiation Protection Communication, 2013, 33(5): 22-26.

[12] Que Liangsheng. Research on Application of Zinc Addition in Newly Built Nuclear Power Plants [J]. Progress Report of China's Nuclear Science and Technology (Volume IV), 2015, Nuclear Chemistry and Radiochemistry Volume: 8-13.

[13] Zhao Zhixiang. Handbook of Nuclide Data [M]. Beijing: Atomic Energy Press, 2004, 35.

Author Introduction: Gou Quanlu (1966 -), male, from Gansu, Gansu Province, senior engineer of radiation protection, currently engaged in the radiation protection management at nuclear power plants.

SESSION 5. Preliminary Comparison Study on the Dosimetric Characteristics of Personal Neutron Dosimeters in a Nuclear Power Plant

Lizhi Zhang[1], Ceming Yang[1], Shan He[1], Haoyuan Xue[1], Zhijiang Wang[2], Xueyuan Song[3]

[1]State Nuclear Power Demonstration Plant Co., Ltd., Rongcheng, Shandong, China

[2]China Institute for Radiation Protection, Taiyuan, Shanxi, China

[3]State Power Investment Corporation (Shandong) Nuclear Environmental Protection Co., Ltd., Haiyang, Shandong, China

Abstract: Electronic personal dosimeters (EPDs) and thermos luminescent dosimeters (TLDs) are essential tools for monitoring occupational exposure and evaluating the effectiveness of radiation protection measures. However, in practical nuclear power plant (NPP) environments, neutron radiation fields often exhibit complex energy spectra and varying incident angles, which significantly affect the dosimetric response of neutron personal dosimeters.

In this study, a comparative analysis was conducted involving a domestic EPD, the Thermo Fisher EPD-N2, and TLD-600/700 dosimeters. Measurements were performed under both a ^{252}Cf neutron source field and actual reactor hall neutron radiation fields. The aim was to evaluate the response characteristics of each dosimeter under different neutron energy spectrum conditions.

Experimental results indicate that the domestic EPD may overestimate dose by a factor of 5–8 in thermal- and intermediate-neutron dominated fields, while underestimating dose by a factor of 3–6 in fast neutron fields. The TLD system also showed dose overestimation in thermal/intermediate neutron fields, likely due to design characteristics.

Further analysis was carried out from the perspectives of detector material composition, neutron moderation path design, signal processing mechanisms, and algorithmic response. Based on these findings, several preliminary recommendations are proposed to improve the accuracy of neutron dosimetry in complex radiation environments. This study provides practical insights for the performance evaluation and potential optimization of personal neutron dosimeters in NPP operations.

SESSION 5. Investigation on Weakly Penetrating Radiation and Personal Dose Monitoring for VVER Units

Bingjun Hou

Jiangsu Nuclear Power Corporation (JNPC), Lianyungang, Jiangsu Province, China

Abstract: During the refueling outage of Tianwan Nuclear Power Plant, a survey on weak-penetrating radiation was conducted for VVER units. The main work included radiation dose rate monitoring in areas with potential high risks of weak-penetrating radiation, monitoring of weak-penetrating radiation doses received by some representative workers and testing of the protective effect of protective equipment. Based on the weak-penetrating radiation measurement results, it is recommended to carry out eye lens dose and skin dose monitoring for maintenance personnel engaged in special maintenance tasks such as maintenance of extractable components of main pumps, cleaning of reactor pools, maintenance of pumps and valves in the KBA system, and sorting of radioactive waste. In recent years, VVER units have focused on special continuous monitoring, and both the skin dose Hp (0.07) and eye lens dose Hp (3) are far below the national standard's individual dose limit of 500 mSv/a and the new IAEA limit of 20 mSv/a, respectively.

SESSION 5. Research and Development of Online Monitoring System for Nuclear Power Plant Radioactive Sources under 5G Environment

Bo Sun, Xiuchuan Li, Bing Qu

Liaoning Hongyanhe Nuclear Power Co., Ltd., Dalian, Liaoning Province, China

Abstract: The developed composite positioning and online monitoring system for radioactive sources in nuclear power plants integrates radioactive source management with Ultra-Wide Band (UWB) and BeiDou positioning technologies, achieving seamless high-precision tracking both indoors and outdoors. For outdoor positioning, the system employs Dilution of Precision (DOP) evaluation and Kalman filtering to enhance data reliability. For indoor positioning, it innovatively applies Time Division Multiplexing Access (TDMA) technology to the UWB Time Difference of Arrival (TDOA) positioning system, maximizing system concurrency capacity while achieving high-precision positioning with an accuracy of ±10 cm, meeting the demand for precise monitoring of minute movements of radioactive sources. Leveraging the nuclear power plant's dedicated 5G network for real-time data transmission, the system successfully enables intelligent and digitalized end-to-end management, ensuring the safety of radioactive sources during storage, transportation, and use. It can promptly identify potential safety hazards in the storage and usage of radioactive sources, reduce the risk of unplanned exposure caused by radioactive sources, prevent loss and uncontrolled handling of radioactive sources, and improve emergency response efficiency in case of radioactive source incidents or accidents. This system provides a novel approach to the safety supervision of radioactive sources in nuclear power plants.

Keyword: Radioactive sources、Internet of Things、Positioning、3D

SESSION 5. In-situ Gamma Spectroscopy Measurement of Activated Corrosion Products in Nuclear Power Plants and Its Applications

Liye Liu[1,2,3], Ruiwen Liu[1,2,3], Qinjian Cao[1,2,3], Hua Li[1,2,3], Yuan Zhao[1,2,3], Peitao Song[1,2,3]

[1]China Institute for Radiation Protection, Taiyuan, China.

[2]Shanxi Key Laboratory for Radiation Safety and Protection, Taiyuan, China.

[3]CNNC Key Laboratory for Radiation Protection Technology, Taiyuan, China.

Occupational collective dose is a critical performance indicator in the peer review process conducted by the World Association of Nuclear Operators (WANO). It directly reflects the level of radiation protection in nuclear power plants and the effectiveness of measures implemented to achieve the ALARA (as low as reasonably achievable) principle in radiation protection optimization. Reducing occupational collective dose has long been a persistent goal for nuclear power plant operators and relevant research institutions.

Operational experience from nuclear power plants both in China and abroad indicates that approximately 80% of the collective dose in pressurized water reactor (PWR) plants is generated during maintenance activities in outage periods. The primary radiation source contributing to such exposures is activated corrosion products (ACPs) present in pipeline components such as pipes and valves. Due to the extensive pipeline networks and high maintenance workload, ACPs have become the main source of occupational exposure during outage periods at nuclear power plants.

To address ACPs deposited on the inner walls of pipelines in the primary loop of nuclear power plants, research on in-situ gamma spectroscopy measurement technology was carried out. In-situ gamma spectroscopy measurement systems were developed based on High-Purity Germanium (HPGe) detectors and Cadmium Zinc Telluride (CZT) detectors, respectively. Source-less efficiency calibration was performed using the Monte Carlo method, and laboratory validation was conducted to verify the feasibility and accuracy of the in-situ gamma spectroscopy measurement technology.

Since 2005, over 80 measurements have been conducted at nuclear power plants in China. The measurement points covered key pipelines in major radioactive systems, including the reactor coolant system, chemical and volume control system, and residual heat removal system. These measurements provided data on the surface activity of ACPs. Furthermore, key findings were summarized, such as the identification of key nuclides and their variation patterns during plant operational cycles, as well as the effects of water chemistry measures (e.g., zinc addition and oxidative operation) on the surface activity of deposited ACPs in both the primary loop and auxiliary systems.

SESSION 5. Implementation and Verification of a free-moving 3-D Compton Imaging System for γ source Term Monitoring in Nuclear Power Plants

Chongyang Wang[1, 2, 3], Liye Liu[1, 2, 3, *], Huaizhong Gao[1, 2, 3, 4, 5], Yongfu Cheng[1, 2, 3], Sanqiang Xia[1, 2, 3], Hua Li[1, 2, 3], Hengguan Yi[1, 2, 3], Hui Li[1, 2, 3], Xiaolong Wang[1, 2, 3], Ming Zeng[4, 5]

[1]China Institute for radiation proctection , Taiyuan, Shanxi, China；[2]Shanxi Provincial Key Laboratory for Radiation Safety and Protection, Taiyuan, Shanxi, China；[3]CNNC Key Laboratory for Radiation Protection Technology, Taiyuan, Shanxi, China；[4]Key Laboratory of Particle and Radiation Imaging, Ministry of Education, Tsinghua University, Beijing, China；[5]Department of Engineering Physics, Tsinghua University, Beijing, China

Abstract: Following the advances in information technology, the nuclear power plants (NPPs) in China are also making digital transformations and applying the information technology to all aspects of operation. One vital part of such transformation is radiation protection and management, which is an essential task to ensure personnel safety. Such transition necessitates the real-time display of the radiation distribution within the NPP facilities, which is mostly γ-radiation with complex and diffused spatial distributions within areas that possess intricate internal structures such as the piping system. This demands on the on-site source term monitoring devices to perform rapid radiation measurements via free-moving inspections and producing data constrained with the internal structures of the facilities. The development of technologies including Compton cameras and simultaneous localization and mapping (SLAM) in the recent years has inspired a new type of radiation measurement device, namely the free-moving Compton cameras. This type of device can perform effective γ-ray imaging within the energy range from a few hundreds of keV to a few MeV, which covers most of the common radioactive sources that exist in the NPPs, with a field of view of 4π. Combined with SLAM and scene data fusion (SDF) techniques, such device is capable of directly reconstructing the 3-dimensional radiation distribution through free-moving measurements. However, the existing equipment still has the drawback in the applicability to scenes with intricate internal structures such as the NPP facilities. These methods, implemented based on the Maximum Likelihood-Expectation Maximization (ML-EM) algorithm, can be heavily affected by the corner-like features that are commonly found in the NPP-like scenes due to the intrinsic property of the ML-EM algorithm, thus leading to artifacts (“corner artifacts”) that significantly impact the correctness of the derived radiation distribution.

In this paper, we present the implementation and verification of a novel free-moving 3-D radiation mapping system. It is developed based on as previously produced Compton camera that adopts a detector system with spherical configuration. The camera has an angular resolution of 15 ° and an intrinsic detection efficiency of 91.32 cps/(μSv/h) at 662 keV. Furthermore, the excellent uniformity in angular response (≥ 90 % at 662 keV) makes it fairly suitable for applications involving free-moving measurements of source terms with complex spatial distributions, which demands the complete and uniform coverage of incident γ-ray photons from numerous directions. A SLAM system is integrated with the camera to form the prototype 3-D radiation mapping system. Along with the hardware implementation, a new algorithm tailored for the application in scenes with intricate internal structures is proposed. It is developed based on the Origin Ensemble (OE) algorithm that does not produce corner artifacts. Further improvement to the algorithm is implemented to tackle with the issues brought by the characteristics of the scene-constrained radiation dataset collected via free-moving measurements. Multiple representative point sampling is introduced to the subset-driven origin ensemble algorithm with resolution recovery (SD-OE-RR) to overcome the limitations in precision due to the reduced number of events acquired with free-moving imaging. A rapid intersection search along the surface of the Compton

cones based on breadth first search (BFS) algorithm is implemented within the voxelized 3-D space containing the point cloud obtained with the SLAM system to speed up the initialization process of the image reconstruction. Field testing of the developed 3-D radiation mapping system is performed within the Qinshan Phase II NPP by measuring the radiation distribution in several rooms with intricate internals structures that contain γ-ray hotspots. The developed system is capable of accurately localizing the hotspots for all obtained data with no artifacts, thus proving the effectiveness of the system for source-term monitoring in NPPs. With further improvements applied, this system can offer a more intelligent and convenient approach for on-site source term monitoring and a powerful tool as the data input of future radiation protection and management systems.

Key words: Compton camera, Free-moving imaging, Scene data fusion, Origin Ensemble, Source term monitoring

SESSION 6. An Engineering Approach of Building Effective 3D Radiation Map with Low Cost

Ming Han

Huaneng Shandong Shidao Bay Nuclear Power Co., Ltd., Rongcheng, China

Abstract: This paper aims to propose an engineering approach of building effective 3D radiation map with low cost,by using experienced digital practice in other industries.This paper introduces three methods to build this map.One is a data processing center,while the other two is 5G internet highway binded with radiation detectors and smart robots.Through building this 3D radiation map,employees can easily get precise radiation level in the plant so as to protect themselves better.

Key Words:3D radiation map,low cost,data center,5G internet,smart robots

Introduction:

The CPC Central Committee and the State Council on 11 August officially released "on accelerating the economic and social development of the overall green transformation of the views", "the views" pointed out to "accelerate the Northwest wind power photovoltaic, Southwest hydropower, offshore wind power, coastal nuclear power and other clean energy base construction. This is the first time that the national top-level document clearly indicates that it will accelerate the construction of coastal nuclear power clean energy base. Nuclear power plant with its high-power density, safe and stable operation, green and pollution-free and favoured by governments. Many foreign nuclear power countries to speed up the construction of nuclear power recovery, but China is particularly rapid. Nuclear power plants on the one hand benefit mankind at the same time, but also because of the potential radioactive contamination and people's attention, especially for the power plant staff, in the power plant to carry out internal operation or maintenance processing, may face the risk of accidental radiation exposure and health injuries, in order to protect the nuclear power plant staff from invisible and intangible rays of the harm brought about by the use of modern information technology to build a characterisation of power plantIn order to protect the staff of the nuclear power plant from unseen rays, it is necessary to use modern information technology to construct a visual map characterising the radiation level of the power plant, i.e. three-dimensional radiation field map. So that the staff can work before the work intuitively understand the work area will go to the radiation level information, so as to do a good job of protective measures; in the work area in real time to receive the surrounding radiation dose information, in a timely manner to avoid radiation hotspots; in the completion of the work can be completed to obtain a complete personal whole-body dose information, in order to facilitate the assessment of health damage or not.

Main article:

In order to establish a three-dimensional radiation map of a nuclear power plant, it is necessary to make use of modern information technology, which mainly includes the construction of a three-dimensional digital model of the plant, the visualisation of radiation data embedded in the three-dimensional model of the plant to form a data processing centre, the use of the 5G Internet highway to ensure that the personnel are connected from time to time, and the use of intelligent robots to assist in the completion of the collection of radiation data from the key areas. The discussion will be carried out in the following chapters.

1 Constructing a three-dimensional digital model of the power plant

This engineering method adopts the Smart 3D 3D mapping software widely used in the industry, and the map construction personnel complete the spatial 3D conversion by entering the construction drawing data of each area of each plant into the editing interface of the software, so as to realise the construction of the 3D framework of the power plant, and then carry out the supplementation of the details, i.e., the 3D dimension information of each equipment will be entered into the editing interface of the area in which the plant is located, so as to generate a refined 3D power plantdigital model of the power plant. It should be noted that the 3D model of the power plant constructed at this time is based on the 3D model of the engineering drawings, the subsequent use of the real power plant engineering transformation of the data need to be entered into the software in a timely manner, in order to update the 3D model to ensure that the model of the authenticity of the data. Note that the model will be built into the Data Processing Centre described in the next section.

2 Data Processing Centre

The centre is actually a visual data processing and monitoring centre, where the environmental dose data and surface contamination dose data obtained from various sources are converted into data according to the units of radiation zoning limits, in order to obtain the radiation zoning indications that should be rendered by the environmental dose data and surface contamination dose data of different regions, and the colour rendering function of the software is used to convert different regions into white, green, yellow, orange, and yellow in accordance with the radiation zoning indications that have been formed after the conversion.Formation of white, green, yellow, orange, red five colours, corresponding to radiation supervision area, radiation green area, radiation yellow area, radiation orange area and radiation red area, so as to obtain intuitive information display. While receiving the transmitted radiation data, the Data Processing Centre automatically obtains the 3D coordinates of the detector and the 3D coordinates of the detected area and then embeds the coordinate information and the rendered zone colours into the 3D digital model of the power plant in the previous section. The following functionality will be achieved: when clicking on an area of the 3D model in the monitoring interface, the radiation dose and the rendered zonal colours of the area will be displayed in real time, together with an indication of the recommended protective measures to be applied. It is important to note that the monitoring interface is updated in real time, as the radiation dose data from various sources is fed into the data processing centre, which is also connected to the plant staff at all times via the 5G Internet highway. The internet highway is described in the next section.

The Data Processing Centre also has the function of automatically generating complete personal whole body dose information, minus personal protective shielding, and pushing it to the staff's PDA (Personal Data Terminal) after they have completed their work, in order to assess whether or not the staff's health has been compromised.

3 5G Internet Highway

This engineering method makes full use of Internet technology to achieve high-speed interconnection and intercommunication of 3D radiation maps by adopting the 5G private network built by the power plant. The method of implementation is as follows: the data processing centre swallows dose data obtained by various means from time to time and generates a visual radiation three-dimensional map through the server computing platform. The three-dimensional map is output through the 5G Internet, and the personnel holding the networked PDA (personal data terminal) can consult the three-dimensional radiation field data information transmitted by the Data Processing Centre in the area of concern to the personnel and take good personal protection measures with the help of the protective measures suggested by the system. And in the work, the personnel can always view the surrounding

environment dose and surface contamination information, the data centre also has the surrounding dose exceeds the threshold of the emergency alarm function, prompting the staff to evacuate as soon as possible.

This 5G Internet highway receives radiation data uploaded by networked fixed radiation detectors and radiation protection personnel's mobile radiation patrol instruments (including gamma cameras), and the above radiation data are processed in the Data Processing Centre in order to generate real-time updated visualised three-dimensional radiation field maps.

If funds permit, a 3D positioning module can be installed outside the staff PDA to realise the real-time display of the staff's area on the 3D radiation field map, which is convenient for the company's radiation protection engineers/radiation protection contractors to check the dose information of the environment in which the staff of the plant are located at any time to ensure that the staff do not mistakenly enter the high-risk area and to assess the collective dose of the staff and whether the protective measures adopted are appropriate.etc.

4 Intelligent Robots

Along with the rapid advancement of AI, robots have shown broader application prospects in nuclear power plants, as they can work more tolerantly in high-radiation areas, and can enter narrow, oxygen-deprived areas that cannot be easily accessed by personnel. Intelligent robots can master basic walking routes and detection work steps through deep learning, while the highly developed Chinese robotics cluster can achieve the low-cost advantage of high-mobility robot parts. This engineering approach proposes to use intelligent robots to realise radiation detection in areas inaccessible to personnel and routine regional radiation dose patrol, surface contamination sampling and detection, in order to liberate radiation workers. The intelligent robot adopts a highly reliable multifunctional radiation detection sensor networked with the data platform to measure multiple radiation parameters, and the robot has a built-in data discrimination function that automatically rejects invalid data and transmits the detection data to the data processing centre.

The robot is fully covered with radiation shielding, has variable tracked wheels for all-terrain travel, and uses an automotive-grade rechargeable lithium-ion battery pack to ensure operational endurance.

5 Wireless Positioning Electronic Dosimeter

Personnel engaged in radiation work in operating nuclear power plants must wear epd (personal electronic dosimeters) for monitoring personal irradiated dose. For the construction and updating of three-dimensional radiation field maps, it is possible to make use of infrastructure such as the 5g private network covering the plant and epd with wireless transmission and remote positioning function to measure the cumulative irradiated dose of the staff in real time and the ambient dose rate of their location, and transmit the information of personal irradiated dose, ambient dose rate of the location and location information in real time to the backstage terminals and transfer the ambient dose data of each location in the plant to the data processing centre for transformation and data display.The environmental dose data of each location of the plant is transferred to the data processing centre for transformation and data display, thus realizing the construction and updating of the three-dimensional radiation field map. The environmental dose data of each location of the plant is transferred to the data processing centre for transformation and data display, thus realizing the dynamic update of the three-dimensional radiation field map. The traditional solution is to use mobile phones and Bluetooth beacons as intermediaries for data transmission and positioning. However, too many transmission links means more chance of failure, but users are not willing to bring their personal mobile phones into the control area (and the control area does not allow personal mobile phones to be brought in), the application leads to high power

consumption of mobile phones, running traffic and other problems. This thesis proposes to adopt the second scheme, i.e., EPD embedded EPD mobile signal communication module, which will transmit the personal dose information directly to the backend server via wireless network, due to the traditional network bandwidth factor, which leads to high power consumption of the device, the scheme is proposed to adopt NB-iot (narrowband IoT based on cellular network), the construction of NB network is based on the existing cellular data base station. Its advantages are low power consumption, wide coverage and small bandwidth occupation. By embedding the wireless transmission and remote positioning chip in the conventional epd equipment, it is connected to the 5g dedicated network of the plant and interconnected with the personal dose control system in the radiation control area on the backend server, and at the same time, it has the features of anti-interference and long endurance, which can satisfy the demand of long-time use in the nuclear island plant. The wireless positioning electronic dosimeter adopts automatic dispensing cabinet for authorisation management, which also solves the problem of power management. Wireless positioning electronic dosimeter real-time personal dose information and location information of the holder is transmitted to the background server, compared with the staff handheld pda, wireless positioning electronic dosimeter use time and coverage is wider, its real-time transmission of data can be complemented with the handheld pda, to ensure that the three-dimensional radiation field maps are more accurate and updated. Therefore, it is the monitoring equipment that must be worn by all staff entering the radiation control area.

6 Conclusion

The engineering method of constructing three-dimensional radiation field maps of nuclear power plants fully adopts mature engineering practices, with high construction efficiency, high reliability, accurate real-time data updating, easy-to-read and easy-to-operate interfaces, and low engineering costs; at the same time, the application of the three-dimensional radiation maps can better safeguard the staff of the power plants from excessive radiation exposure, which is of practical significance in eliminating the fear of radiation hazards. It is of practical significance for eliminating the fear of radiation hazards. It has the value of popularisation and application.

SESSION 6. Nuclear Power Plant Radiation Protection Digital Transformation Implementation Path and Application Effect — A Case Study of Taishan Nuclear Power Plant

Weihua He

Taishan Nuclear Power Joint Venture Company Limited, Taishan, China

Abstract: In the context of the intelligent development trend, the digital transformation of radiation protection in nuclear power plants has become a key approach to enhance safety levels and management efficiency. This paper takes Taishan Nuclear Power Plant as a typical case to systematically study its implementation path and application effects of radiation protection digital transformation. By constructing a "data-driven - model-supported - scenario-implementation" transformation path, Taishan Nuclear Power Plant introduced wireless transmission, big data, and artificial intelligence technologies, achieving digital upgrading of radiation protection management and addressing pain points and challenges in radiation protection practices. Specific implementation paths include the construction of a digital monitoring network, the development of an intelligent decision support system, the establishment of a digital emergency response system, and the optimization of radiation protection through data-driven approaches. The application results demonstrate that digital transformation has significantly improved management efficiency, enhanced safety, improved decision-making capabilities, and reduced collective doses for staff. The research conclusion indicates that digital transformation, with technology integration and business restructuring as its core, can achieve dual enhancements in safety and efficiency for nuclear power plant radiation protection. Future development directions will focus on "predictive protection" and "zero-intervention management," further improving radiation safety management efficiency.

Keywords: nuclear power plant; radiation protection; digital transformation; safety management; intelligent decision-making

SESSION 6. Real-time Primary Coolant Isotopic Trending using 3-D Pixelated CZT Spectrometers

Weiyi Wang, PhD [1 *]; David R. Nestle, CHP [1, 3]; Brian Eick [2]

[1] H3D, Inc., Ann Arbor, Michigan, USA

[2] NextEra Energy, Point Beach Nuclear Plant, Two Rivers, Wisconsin, USA

[3] Palisades Nuclear Plant, Covert, Michigan, USA

Developments in pixelated cadmium-zinc-telluride (CZT) detector technology allow for the collection of continuous, real-time, nuclide-specific data on radionuclide transport through plant systems and components. Deployment of these devices has provided significant learnings regarding the presence and transport of silver isotope contamination (Ag-110m) in the source term of some nuclear power plants. In addition, these detectors provide a powerful tool to monitor impacts to plant source term from physical and chemical changes to plant systems, such as reactor coolant temperature, pressure, pH, and chemical additions. Recently, this technology has been used at multiple facilities to precisely trend xenon concentrations resulting from fuel defects during operating cycles.

For example, measurements taken at the Palisades Power Plant demonstrate how CZT detector technology was used to inform the plant's source-term-reduction strategy, and how the impacts of those changes were successfully monitored. CZT spectrometers placed in strategic locations along the primary system purification loop allowed for better recognition of Ag-110m during changes in primary system chemistry and differences in the behavior of Ag-110m to other primary radionuclides impacting workers' equivalent dose (Co-58 and Co-60).

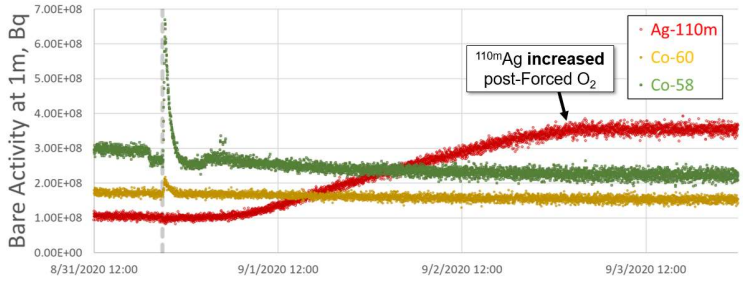

Figure 1: Qualitative trends of three primary radionuclides following injection of hydrogen peroxide to the primary system at Palisades

Data from the first outage period were impactful to developing several changes to the plant's source-term-reduction strategy, including improved availability of plant demineralizers and efforts to support solubility of silver to improve transport to demineralizers. Revisions to strategies for end-of-cycle boron, improved zinc injection at end of cycle and longer acid-reducing periods were also implemented to improve cobalt clean-up. Continued monitoring over multiple outages provided for ready assessment of the impact of those changes on the silver and cobalt concentrations in the primary systems.

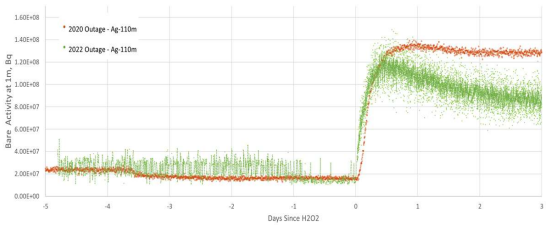

Figure 2: Comparison of Ag-110m at Palisades over two outage periods

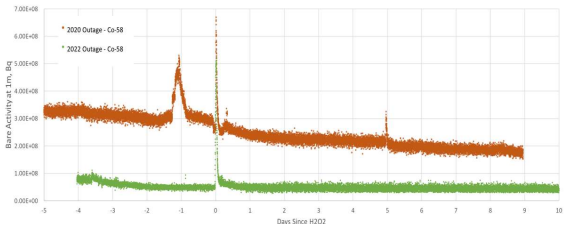

Figure 3: Comparison of Co-58 trends at Palisades over two outage period

SESSION 6. Study On Digital Refined Management of Radiation Protection in Nuclear Power Plants Based on Wireless Positioning EPD

Yangxing Hu[1], Yuanwei Wang[1], Xiyu Liu[1], Gangxue Wang[1],
Yunong Liu[1], Zijing Fang[1], Zeqi Liu[1], Huishan Su[1], Zikui Tang[1], Zhuo Wang[1]

[1] Huaneng Hainan Changjiang Nuclear Power Co., Ltd, Hainan, China

Abstract: The realization of digital radiation protection in nuclear power plants has its core in establishing a collaborative management system for personnel dose and position through wireless positioning electronic personnel dosimeters (EPD) and supporting systems, thereby achieving refined control of occupational exposure. Relying on existing EPD technology, it integrates such technologies as 5G network, high-precision positioning base stations, and digital modules for displaying personal dose and position information: Wireless positioning EPD, by embedding positioning and communication modules, enables synchronized collection and real-time upload of "dose-position-time" three-dimensional data, with positioning accuracy reaching the sub-meter level (RMS error better than 1m); The 5G private network ensures high-speed data transmission in complex nuclear island environments, with delay controlled within 1 second; The digital display module visualizes radiation data and personnel trajectories, supporting path planning in high-radiation areas and traceability of historical data; The supplementary deployment of high-precision positioning base stations enhances positioning stability in complex environments. This scheme has realized the upgrade from simple dose measurement with traditional EPD to "positioning-dose-management" integrated digital protection. Through the technical advantages of real-time performance and accuracy, it supports the full-process management covering pre-operation planning, in-operation monitoring, and post-operation evaluation. It features low cost (based on the transformation of existing equipment), high reliability (adapting to the nuclear island environment), and ease of promotion, providing a feasible path for the digital transformation of radiation protection in nuclear power plants.

Keywords: Nuclear power plant; Digital radiation protection; Wireless positioning EPD; Refined management; Integrated scheme

SESSION 7. Indoor 3D Gamma Radiation Mapping Based on VSLAM and Its Preliminary Application in Digital Systems

Hui Li[1,2], Hua Li[1], Liye Liu[1], Qing Fan[1], Mingmin Wang[1], Faguo Chen[1], Zhi Chen[2]

[1]China Institute for Radiation Protection, Taiyuan, China

[2]University of Science and Technology of China, Hefei, China

Nuclear facilities—whether during operation, maintenance, or decommissioning—demand precise and comprehensive radiation data to ensure safety and optimize processes. Traditional radiation measurement methods are often slow, labor-intensive, and poorly suited to dynamic environments, such as those encountered during decommissioning, where radiation fields may change hourly. With the growing emphasis on digitalization, there is a pressing need for near-real-time, automated solutions that integrate seamlessly with digital platforms.

Our research tackles these challenges by leveraging Visual Simultaneous Localization and Mapping(VSLAM) to revolutionize how we measure 3D gamma dose rate fields. Our method combines VSLAM with a gamma dose detection module. The VSLAM system uses an RGBD camera to generate a 3D point cloud of the environment while tracking the device's trajectory with high precision. For gamma dose measurement, we designed a hot-pluggable Geiger-Müller tube, capable of detecting doses from 0.01 μSv/h to 10 mSv/h with a response time under 3 seconds. To fuse the spatial and radiation data, we synchronized timestamps and applied an integral path midpoint method, ensuring seamless integration of the two datasets. This approach allows us to map radiation fields in three dimensions as the device moves through the environment.

Compared to traditional methods involving 3D laser scanners, total stations, and separate dosimeters, our approach improves data acquisition efficiency by a factor of 26.8. While conventional methods took 3–5 minutes per scan and 30 seconds per sampling point, our VSLAM device allowed a single operator to collect data at 3 seconds per point while freely walking through the site. In terms of accuracy, over 80% of our scene point cloud matched the reference cloud within a 0.2-meter nearest neighbor distance. Trajectory localization achieved an average error of just 4.2 centimeters, with a standard deviation of 0.4 centimeters. For dose measurements, the relative error stayed below ±5% across the tested range, demonstrating the reliability of our gamma detection module. One of the standout features of our system is its integration with digital platforms. By combining VSLAM data with dose measurements, we achieved 3D spatial interpolation of radiation fields, enabling detailed visualization of radiation distribution. The localization error for a single gamma source was less than 0.2 meters, which is impressive for real-time applications. This digital compatibility allows operators to visualize radiation hotspots, plan safe interventions, and make data-driven decisions—critical advancements for nuclear safety and protection.

This technology has broad applications in nuclear safety, from routine monitoring to decommissioning and emergency response scenarios. We're exploring enhancements like more sensitive sensors, an expanded dose range, and even autonomous operation using drones or robots. These advancements could further reduce human exposure and increase measurement flexibility in hazardous environments.

Figure 1 Instrument developed for VSLAM radiation based dose rate mapping

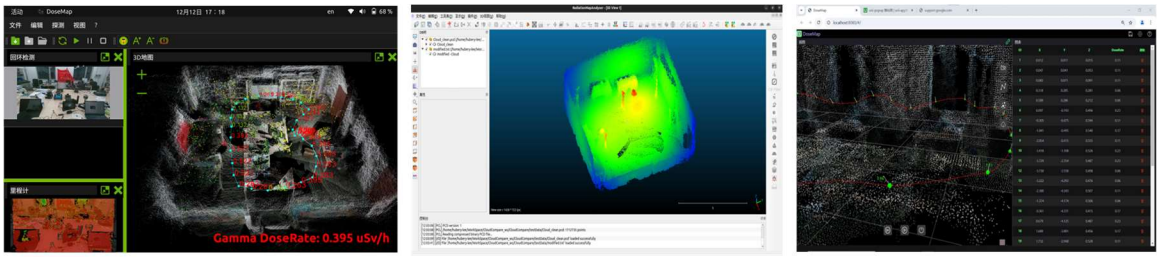

DoseMap RadiationMapAnalyser DoseMap-Web

Figure 2 Softwares developed for VSLAM radiation based dose rate mapping

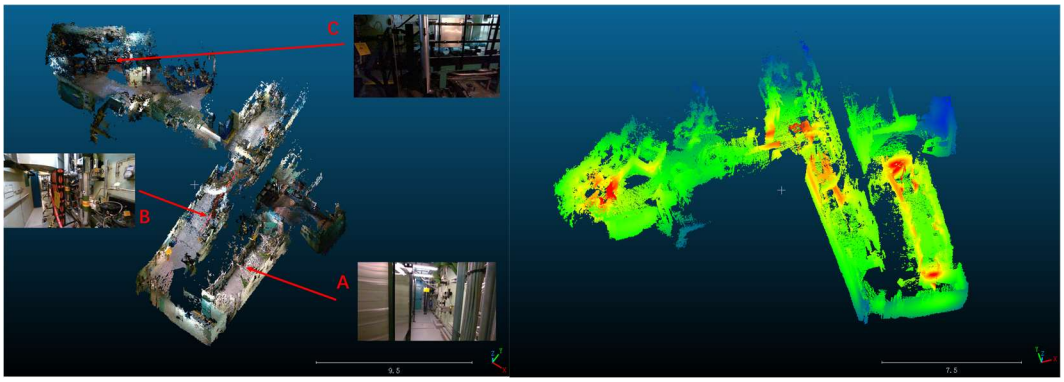

Figure 3 Measurement test and radiation hotspot localization in nuclear facilities

SESSION 7. A New Solution for Occupational Exposure Management at Nuclear Facilities Using SMARP System

Liye Liu[1,2,3], Chuan Wang[4], Yuan Zhao[1,2,3], Qinjian Cao[1,2,3], Hua Li[1,2,3],

Peitao Song[1,2,3], Ji Ma[1,2,3]

[1]China Institute for Radiation Protection, Taiyuan, China.

[2]Shanxi Key Laboratory for Radiation Safety and Protection, Taiyuan, China.

[3]CNNC Key Laboratory for Radiation Protection Technology, Taiyuan, China.

[4]Nuclear Power Operations Research Institute, Shanghai, China

Occupational exposure management is an important segment for the safe operation of nuclear facilities and plays a crucial role in the safe development of the nuclear industry. With the development of nuclear technology applications, radiation protection management is gradually becoming more precise and efficient. Traditional monitoring and management methods of radiation protection are no longer meet the above needs. Introducing digital technology into monitoring and management can be an effective solution.

In this context, China Institute for Radiation Protection (CIRP) has proposed a development plan for digital radiation protection and developed the SMart Alara system for Radiation Protection (SMARP). This system includes digital radiation monitoring equipment, radiation protection simulation technology and advanced human-computer interaction functions.

For the aspect of radiation monitoring, SMARP upgrade the existing radiation monitoring equipment by combining facial recognition, wireless communication and indoor high-precision positioning technologies. As a result, this system supports the digital collection of data on whole body contamination, ambient dose rates, and personnel dose associated with location information.

In terms of dose simulation, the collected radiation information and three-dimensional scene models are be used, then the three-dimensional radiation field reconstruction can be achieved by employing algorithms such as the Point-Kernel or Kriging interpolation. Utilizing a dynamically updated and visualized 3D radiation field, this system allows for simulation of high radiation risk operations and pre-assessment of external exposure doses.

SMARP also provides digital management functions such as visualization of radiation scenarios, equipment query, positioning and navigation, and management of radiation work permits (RWP). It offers advanced digital radiation protection support to different users.

SMARP V1.0 now has been successfully verified and validated and will be fully deployed across all 23 operational nuclear power plants of China National Nuclear Corporation (CNNC) by the end of 2026. In the future, updated versions of SMARP using digital twin, artificial intelligence technologies will be gradually released, and provide more effective solutions for occupational exposure management at nuclear facilities.

SESSION 7. Development of Small and Medium-Sized Robotic Platform System for Nuclear Emergencies and High-Radiation Scenarios

Yanan Hong, Yang Liu, Jianhua Wu, Xiaoyu Shi, Miao Pan, Yuan He

China Institute of Atomic Energy, Beijing, China

Abstract: In response to the urgent need for emergency response in extreme radiation environments such as nuclear accidents, this study has developed a small and medium-sized robot platform system that can perform surveys, monitoring, and disposal, and has high radiation resistance. This robot system can be stably controlled in a strong radiation field (dose rate ≥500 Gy/h, cumulative dose ≥1.0 ×104 Gy), has strong environmental adaptability, and has a certain ability to pass through complex terrain after a nuclear accident. This study uses a multi-level radiation-resistant design strategy, from the device, circuit, system level, etc., through device screening, chip reinforcement, circuit design, elaborate shielding and other measures to achieve a breakthrough in the robot's radiation-resistant reinforcement technology and miniaturizes and lightweights the robot system. Based on the irradiation test of more than 200 kinds of electronic components, a radiation-resistant device library was constructed, and key components with a total dose tolerance of ≥1.0×104 Gy were screened out; radiation-resistant data transmission chips were independently developed, and the ring-gate MOS design was adopted to significantly improve the radiation resistance of key components; the robot drive circuit and control circuit were designed, and the radiation field simulation and measured data were combined, and the weak parts were elaboratly shielded using shielding material, so that the system's cumulative dose tolerance was increased to 1.0×104Gy. The system has two lightweight chassis, wheeled and tracked, with reserved power supply and communication interfaces. It can carry radiation detectors, radiation-resistant cameras, and operating terminals driven by DC motors or hydraulics. Among them, the wheeled chassis has a size of 0.4m×0.4m, able to climb over 6cm high obstacles, a deadweight of less than 15kg, and a load capacity of 20kg; the tracked chassis has a size of 0.7m×0.65m, able to climb over 20cm high obstacles, a deadweight of 30kg, and a load capacity of 40kg. This robot system has been used in a Stuck Source Malfunction. The average dose rate in the operating site environment reaches 1000Gy/h, and the highest dose rate reaches 2000Gy/h. It finally takes 8 hours to solve the Stuck Source Malfunction. The total dose of a single robot with radiation resistance reaches 8000Gy, it should be emphasized that the drive circuit and control circuit of robots were not replaced during the operation. Research results and practical applications show that the robot system can carry cameras and disposal tools to complete the disposal tasks in nuclear emergency and strong radiation scenarios such as Stuck Source Accident, providing key technical support for the in-depth defense system of nuclear accidents.

Keywords：Nuclear emergency; Radiation-resistant robot; Total dose; Elaborate shielding.

Figure 1 Device irradiation test

Figure 2 Small and Medium-Sized Robotic Platform System for Nuclear Emergencies and High-Radiation Scenarios

TOPICAL SESSION 1. Optimization Of Radioactive Sources and Radiographic Inspection Management in Nuclear Power Plant Engineering Area

Yangxing Hu[1], Yuanwei Wang[1], Xiyu Liu[1], Gangxue Wang[1],
Yunong Liu[1], Zijing Fang[1], Zeqi Liu[1], Huishan Su[1], Zikui Tang[1], Zhuo Wang[1]

[1] Huaneng Hainan Changjiang nuclear power Co., Ltd, Hainan, China

Abstract: As an industrial non-destructive testing technology widely used in nuclear grade equipment and pipeline welding quality inspection, radiographic inspection has ionizing radiation risk compared with other monitoring means, which brings great challenges to the supervision and management of operation safety. At present, Huaneng Changjiang No. 3 and No. 4 nuclear power units are in the peak period of civil construction and equipment installation. On-site radiographic inspection operations are frequent, and site personnel are complex, and potential radiation risks are high. In order to strengthen radiation safety management in engineering area, improve supervision efficiency, Huaneng Changjiang Company optimize the supervisory and regulatory mechanism that established a joint radiation safety investigation team. Huaneng Changjiang Company are directed against for radioactive sources management and radiographic inspection conduct the identification of risk factors as well as the analysis of risk, compiled standardized safety inspection lists for radiographic inspection and radiographic source management, established a high-standard supervision and management system, and achieved remarkable results. Compared with the peer power plant Huaneng Changjiang Company, the supervision frequency and control of radiographic inspection operations in the project area were stronger. The radiation safety of the workers and the public in the construction stage is effectively guaranteed.

Keywords: Radioactive Source, Radiographic Inspection, Nuclear Power Plants, Safety Supervision, Management Optimization.

TOPICAL SESSION 1. Practical Experience of Limiting Radiation Field in a Nuclear Power Plant

Pingwei Li, Zhigang Zhao, Wen Wang, Xiaolong Qiang, Shun Lu

Yangjiang Nuclear Power Co., Ltd., Yangjiang, Guangdong, China

Abstract: Collective dose is a performance indicator of nuclear power units, which is used to promote the reduction of occupational exposure of workers in power plants. By decreasing the radiation field, reduction of collective dose can be achieved. The formation of radiation field from corrosion products contains several steps, including generation and release, deposition on fuel element and activated, transport and deposition on the surfaces out of the core. However，the operation of the unit plays an important role. Through trace the history of radiation field changes，and identify its difference in the operation，this paper summarized the operation experience that suitable for this unit，which succeed to limit the radiation field in the following up operation.

TOPICAL SESSION 2. Research on Mitigation of Radioactive Contamination

Shen Fu[1], Tao Ma, Yang Liu

China Institute for Radiation Protection, Taiyuan, Shanxi, China,

Abstract: Operation with radioactivity in sealed spaces is critical technology for nuclear power plant and etc. facilities processing radioactive materials. The quality of ventilation within these sealed spaces is paramount to controlling and reducing radioactive contamination. Existing research lacks sufficient experimental support, particularly regarding the reduction of radiation levels. This study employs a systematic experimental approach to investigate the influence of ventilation location and air exchange rates on the concentration of radioactive substances within sealed spaces. Radioactive simulants were introduced into the sealed space, and concentrations were quantitatively analyzed under different ventilation configurations. Experiments identified optimal air exchange rates and exhaust port positions for minimizing radioactive concentrations, providing data support for reducing radiation hazards and offering practical guidance for the design and optimization of ventilation systems in sealed spaces handling radioactive materials.

Keywords: Radioactivity, Contamination Reduction, Sealed Space, Simulation, Radiation Protection

TOPICAL SESSION 3. Experimental Study on Graphite Dust Deposition in Pipelines under Simulated HTGR Conditions

Shulong Huang, Lixiao Guo, Yuhang Zhang

China Institute for Radiation Protection, Taiyuan, Shanxi, China

Abstract: The high-temperature gas-cooled reactor (HTGR), particularly in pebble-bed configurations exemplified by China's HTR-PM, offers significant advantages in safety, energy efficiency, and long-term operational stability. However, the generation and transport of radioactive graphite dust during extended operation present serious challenges in terms of safety and maintenance. This study presents a systematic experimental investigation on graphite dust deposition and resuspension within a straight pipeline, under varying flow velocities, temperatures, and carrier gases including air and helium. Deposition was quantitatively analyzed at upstream, midstream, and downstream positions. The results show that higher flow velocity significantly reduces dust deposition. Compared to the condition at 1.5 m/s, deposition decreased by 97.6%t at 6 m/s, and was nearly negligible at 9 m/s. The axial distribution followed a consistent trend, with the front section accounting for 22%-28% of the total mass, the middle section 17%-20%, and the rear section 16%-18%. Increasing the temperature from 25 to 300℃ resulted in deposition reductions of 35% at the front, 33% at the middle, and 18% at the rear, while also improving distribution uniformity along the pipeline. In helium environments, the overall deposition was lower than in air, which is attributed to helium's higher viscosity and lower density that reduce particle inertia and promote better flow conformity. Resuspension experiments showed that wind speeds above 9 m/s enhanced particle detachment, but complete resuspension was not observed even at the maximum tested speed of 28 m/s. This suggests that strong adhesion forces, possibly including electrostatic effects and surface interactions, may play a role in preventing full resuspension. These findings provide valuable experimental benchmarks for computational fluid dynamics validation and offer guidance for designing effective graphite dust mitigation strategies to support the safe and efficient operation of HTGR systems.

TOPICAL SESSION 3. Analysis of The Current Status of Research on Neutron Shielding Materials

Caixia Miao[1], Xiaohui Du [1], Hailei Lv[1], Hongchen Han[1]

Department of Nuclear Safety and Environmental Engineering Technology, China Institute of Atomic Energy, Beijing, China

Abstract： With the extensive application of nuclear technology in industries such as industry, agriculture, and medicine, the safety issues associated with neutron radiation have become increasingly prominent. Due to their high penetrability and strong ionization effect, neutrons can cause serious health risks by directly damaging DNA or inducing secondary γ radiation, the neutron radiation protection become a core challenge in radiation protection. To ensure the safe development of nuclear technology, neutron shielding materials are indispensable and is the core technical foundation of radiation protection. This paper reviews the theory of neutron radiation protection and the research progress of neutron shielding materials, focusing on analyzing the current application status and existing problems of neutron shielding materials, and looking forward to the future development trends, aiming to provide theoretical support and technical references for the safe application and development of nuclear technology.

Keywords: Nuclear safety; neutron; radiation protection; shielding material.

TOPICAL SESSION 3. Development of a Novel Neutron Spectrometer for Application in Boron Neutron Capture Therapy (BNCT)

Zhenglin Huang[a,b,c], Zhihui Tang[a,b,c*], Yingjing Wei[a,b,c,d], Jiayu Duan[a,b,c], Bowen Sun[a,b,c]

a. China Institute for Radiation Protection (CIRP), CNNC, Taiyuan, China

b. Shanxi Key Laboratory of Radiation Safety and Protection, Taiyuan, China
c. CNNC Key Laboratory of Radiation Protection Technology, Taiyuan, China

Abstract: A single-moderator directional neutron beam spectrometer (SNBS) was designed by integrating multiple SiC semiconductor detectors (coated with LiF) and charge-sensitive preamplifiers into a cylindrical moderator. Online measurement was achieved through dedicated digital circuits, communication modules and user software. Calibration was performed using an isotopic neutron source (^{252}Cf) at the Metrology Station of the China Institute for Radiation Protection, yielding detection efficiency calibration coefficients for each detector. The measured results of the SNBS at various distances from the beam port of a BNCT neutron radiation field—based on the Compact Pulsed Hadron Source (CPHS) at Tsinghua University—were corrected using these calibration factors. The overall deviation between the corrected count rates of each detector and the standard count rates (calculated from the reference spectrum) under different measurement conditions was computed, with a maximum deviation of 9.64%. Finally, the proportions of thermal, epithermal, and fast neutrons were analyzed. The measurement results showed good agreement with calculations overall. The SNBS developed in this work can be applied to neutron spectrum measurements in various high-flux directional neutron radiation environments.

Key words: Neutron energy spectrum measurement, Single sphere neutron spectrometer, BNCT neutron radiation field

Introduction

Neutron spectrum measurement is a critical experimental technique with significant importance in fields such as the study of nuclear material properties, investigation of nuclear reaction mechanisms, and calculation of neutron radiation doses. Shortly after James Chadwick's discovery of the neutron in 1932, neutron energy measurement was initially performed using the principle of neutron scattering in hydrogen or nitrogen [1]. It was not until the 1960s that various methods were developed, including time-of-flight spectrometers, recoil proton spectrometers, Bonner sphere neutron spectrometers, threshold detector methods, and other types of detectors such as silicon spectrometers, diamond spectrometers, and germanium spectrometers [2]. Each of these methods has its own advantages and limitations, making them suitable for different measurement conditions.

Multisphere neutron spectrometers [3–6] are widely used in various research institutions and neutron measurement facilities due to their broad energy measurement range, cost-effectiveness, isotropic response, ease of operation, and simplicity in measurement [7, 8].

With the advancement of nuclear technology, efforts have been made to simplify the operation of neutron spectrometers and improve their portability. Neutron spectrometers have evolved from multiple moderators to single-moderator designs, with most of the latter being spherical or cylindrical in shape. Among them, spherical single-sphere neutron spectrometers exhibit superior isotropic performance. For instance, the SP2 designed by R. Bedogni et al. [9] and a TLD-600-based single-sphere neutron spectrometer proposed by M. Lis et al. Both demonstrated excellent angular response characteristics [10].

With the rapid development of Boron Neutron Capture Therapy (BNCT) facilities, there is a growing demand for directional neutron spectrum measurements. As a result, cylindrical neutron spectrometers have gained increasing attention due to their advantages in such applications. In 2015, R. Bedogni et al. developed a directional neutron spectrometer named CYSP (CYLINDRICAL

SPectrometer), which was experimentally evaluated in monoenergetic reference neutron fields ranging from 144 keV to 16.5 MeV as well as in a ^{252}Cf radiation field [11]. Three years later, they upgraded the CYSP to CYSP-HS for low-flux neutron field measurements, such as in cosmic radiation environments [12]. The CYSP-HS primarily employs large-area ^{6}LiF-coated silicon diodes, resulting in a sensitivity approximately one order of magnitude higher than that of the original CYSP. For high-flux accelerator neutron radiation field measurements, they further designed a directional neutron spectrometer named CYSP-BEAM in 2019 [13].

The design of a single-moderator multi-detector system serves as the foundation for enabling online measurement. Furthermore, the neutron radiation field in BNCT facilities covers an energy range from thermal neutrons up to 20 MeV, with a neutron flux that can reach 1×10^{9} n·cm^{-2}·s^{-1} and is accompanied by intense gamma radiation. This study proposes the design of an online neutron spectrum measurement system (SNBS) capable of n/γ discrimination, suitable for high-flux neutron environments, which covers a broad energy measurement range.

Materials and Methods

In this work, a cylindrical moderator based on high-density polyethylene (HDPE) and boron-doped polyethylene was employed, and a SiC detector coated with a LiF layer was selected to capture thermal neutrons. A geometric model of the probe was established using the FLUKA software according to the specific probe structure, and the corresponding response matrix was calculated. The operational status of the SNBS was verified and its detection efficiency was calibrated using a standard ^{252}Cf radiation source. The unfolding of the neutron energy spectrum is performed based on the measured data and the calculated response matrix, a process implemented in this work using the GRAVEL program.

1.1 Experimental Setup

1.1.1 Standard Radiation Field for SNBS Calibration

The China Institute for Radiation Protection (CIRP) hosts a leading national standard radiation field for isotopic neutron sources. This facility is equipped with five isotopic neutron sources: ^{241}Am-Be and ^{252}Cf neutron sources. The neutron fluence rate of this standard device is traceable to the Chinese national standard, with a measurable range of (10–10^{4}) cm^{-2}·s^{-1}.

The Department of Engineering Physics at Tsinghua University has designed and constructed a BNCT-terminus mock-up on the CPHS accelerator platform. The CPHS facility delivers 13 MeV protons with a maximum current of 30 mA; the proton-beam pulse width is adjustable from 5 μs to 200 μs, the pulse-repetition frequency can be varied between 1 Hz and 10 Hz, and the overall accelerator power lies in the range 50–830 W. A schematic diagram of the CPHS is presented in Figure 1.

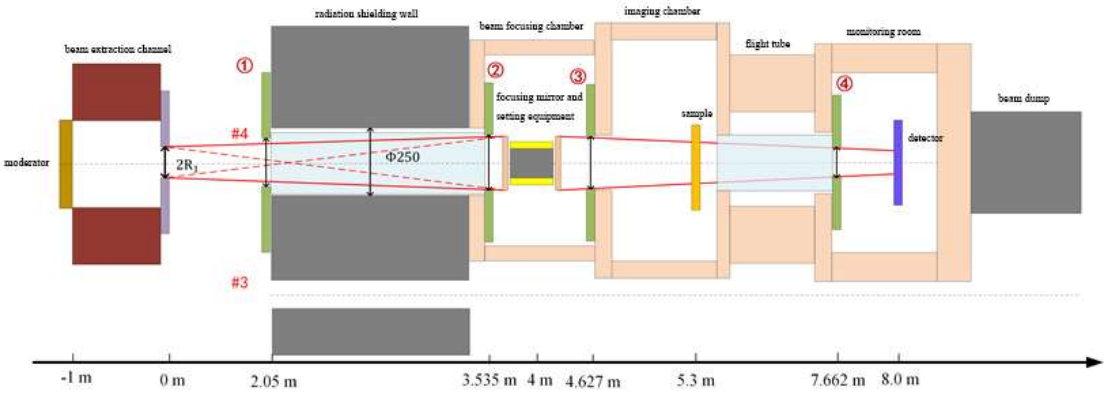

Fig.1. Schematic Diagram of the Tsinghua University CPHS Accelerator Structure

1.1.2 SNBS

The SNBS consists of a cylindrical probe, a signal processing module, and user software. Its hardware includes both the probe unit and the signal processing module. The probe comprises six thermal neutron detectors, preamplifiers, and a moderator. The signal processing module mainly includes a main amplifier, gate signal processing circuit, pulse discriminator, FPGA counting circuit, and a multichannel analyzer. Corresponding hardware design involves the selection of thermal neutron detectors, the dimension and structural design of the moderator, the circuit design of the preamplifier, the circuit design of the signal processing module, and the interconnection among these components.

(1) Given the high neutron flux ($\geq 10^9$ n·cm^{-2}·s^{-1}) and strong accompanying gamma radiation in BNCT radiation fields, this study selected compact semiconductor detectors with minimal gamma response—fabricated by coating LiF onto a SiC substrate. The moderator was constructed using polyethylene and borated polyethylene. Its dimensions were optimized through Monte Carlo simulation software to maximize the effective energy coverage of the response matrix for each detector while providing shielding against lateral thermal neutrons. The final design adopted a three-layer coaxial cylindrical structure, with the intermediate shielding layer made of borated polyethylene (15 wt% B_4C). The overall dimensions of the moderator are Φ20 × 30 cm.

Fig.2. Schematic Diagram of the SNBS Moderator Structure (white part: polyethylene; black part: boron-doped polyethylene)

(2) The signal processing module mainly consists of a charge-sensitive preamplifier, a pole-zero cancellation circuit, a signal conditioning circuit, an FPGA-based multi-channel pulse processing circuit, and a power supply circuit. Its overall structure is shown in Figure 3. In this work, the detector and the charge-sensitive preamplifier were directly soldered together to ensure the preamplifier output signal has a good signal-to-noise ratio. The SiC detector is located in the very center of the PCB. A shield made of German silver (0.2 mm thick) was designed to cover both sides of the PCB, further reducing external electromagnetic interference. Figure 4 shows details of the preamplifier and the output pulse shape.

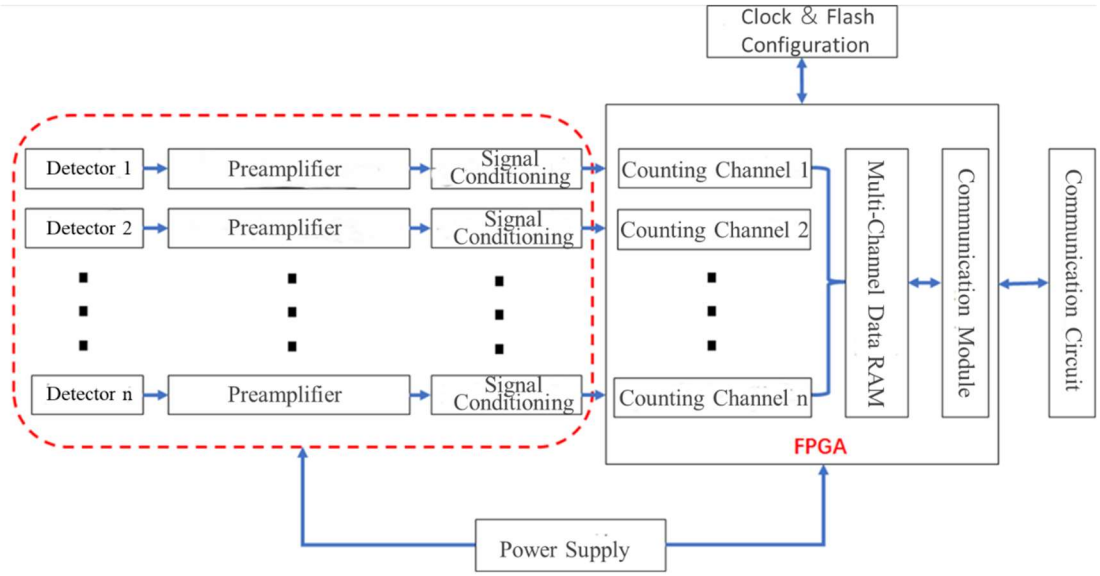

Fig.3. Design Diagram of the SNBS Electronics Section

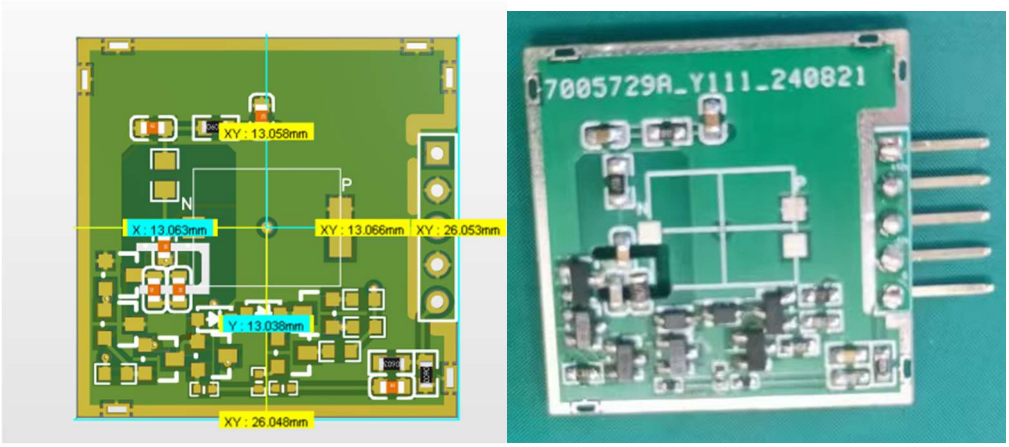

(a) (b)

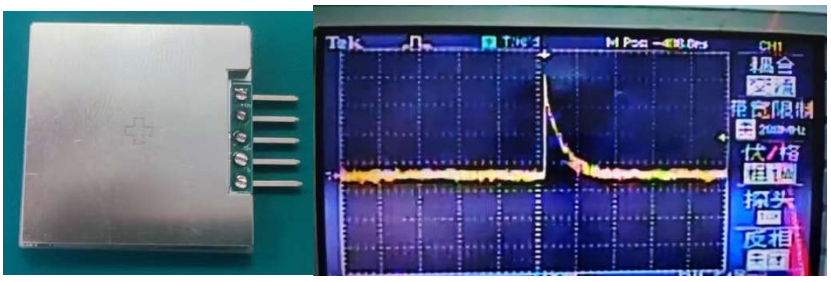

(a) (d)

Fig.4. Charge-Sensitive Preamplifier and Test (a: PCB design; b: physical object; c: physical object with shielding shell; d: measured neutron pulse)

The SNBS incorporates six SiC neutron detectors arranged coaxially at different spacings. To facilitate accurate detector positioning and lossless output of pulse signals, a PCB-based detector array board was designed. Using probes to fix the detectors onto this PCB array board greatly simplifies the internal wiring within the moderator.

The neutron signals amplified by the preamplifier require filtering and shaping. The signal conditioning circuit primarily converts the decaying exponential pulse from the probe output into a quasi-Gaussian pulse with a larger amplitude. This signal is then processed by a comparator and a monostable circuit to generate a square wave signal of standard width. The monostable circuit converts the square wave into one with a fixed pulse width, suitable for acquisition and processing by the FPGA. The probe signals are connected to the signal processing unit via a multi-core shielded cable.

The FPGA-based multi-channel signal acquisition circuit is primarily responsible for counting pulse data from six channels, processing pulse energy spectra, and handling data communication. Owing to the pipelined parallel processing architecture of the FPGA, the counting processes for each channel operate independently without mutual interference. Within the FPGA, the pulse counting module increments the current count by one upon detecting a valid rising edge of a pulse. Once the measurement period concludes, the total data for each channel is transferred to an 8-channel data RAM module, after which the counters are reset. Finally, the RAM module transmits all data to the host computer software via Ethernet. The overall logical framework is illustrated in Figure 5.

The energy spectrum processing module performs pulse shaping, threshold denoising, pile-up rejection, and amplitude extraction on each pulse signal to derive the corresponding energy spectrum data. The data communication module transmits the respective counting information, energy spectrum data, or raw pulse data to the host computer software in accordance with communication protocol commands.

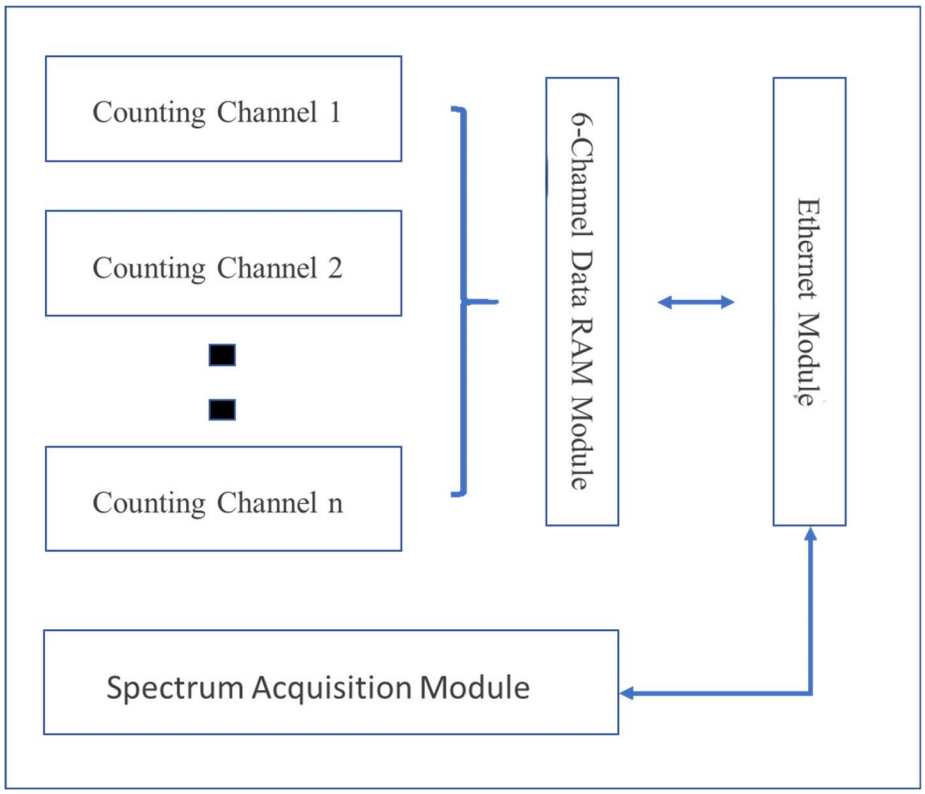

Fig.5. Logical Architecture of the FPGA Internal Program

(3) Building upon the above, this works also developed host computer software interfacing with the signal processing system. This software serves to control the operational status and mode of the signal processing module, as well as to manage the execution of the neutron spectrum unfolding

program (based on the maximum entropy principal Gravel algorithm), thereby streamlining its operation. The entire control software is divided into the following modules: main interface, historical data module, neutron counting module, spectrum normalization module, raw data module, and charged particle spectrum display module.

Additionally, an aluminum alloy enclosure was designed for the system, with a wall thickness of 1.5 mm on the sides and 1 mm on the bottom. This housing provides effective shielding against electromagnetic interference and also helps protect the moderator assembly from physical damage.

1.2 Calibration and Experiments

1.2.1 Calibration of the SNBS

Based on the work of J.M. Gómez-Ros et al. (2011) [14], the SNBS was calibrated at the standard neutron fluence assembly of the Metrology Station at the China Institute for Radiation Protection (see Fig. 6). A ^{252}Cf radioactive source was used as the standard neutron source for calibration, employing a shadow cone to subtract the contribution of scattered neutrons. Throughout the calibration procedure, the distance between the front surface of the probe and the neutron source was maintained at 135 cm. The reference count rates for the six detectors were derived by multiplying the response matrix with the standard ^{252}Cf spectrum provided by ISO. The calculation is expressed as follows:

$$N_i = \sum_j R_{ij}(E_j)\Phi_j(E_j) \cdot S \cdot \varphi_{std} \cdot \frac{1}{\varepsilon} \quad (1)$$

Where N_i is the count rate of the i*i*-th detector, $R_{ij}(E_j)$ is the response sensitivity of the *i*-th detector to neutrons in the *j*-th energy group, E_j denotes the neutron energy of the *j*-th group, $\Phi_j(E_j)$ is the flux density (i.e., neutron energy spectrum) corresponding to neutrons of energy E_jEj, S is the frontal surface area of the broad-energy neutron spectrum detection system, φ_{std} is the true fluence rate at 135 cm in the ^{252}Cf standard radiation field of the CIRP Metrology Station, and ε is the geometric efficiency of the broad-energy neutron spectrum detection system at a distance of 135 cm from the point source.

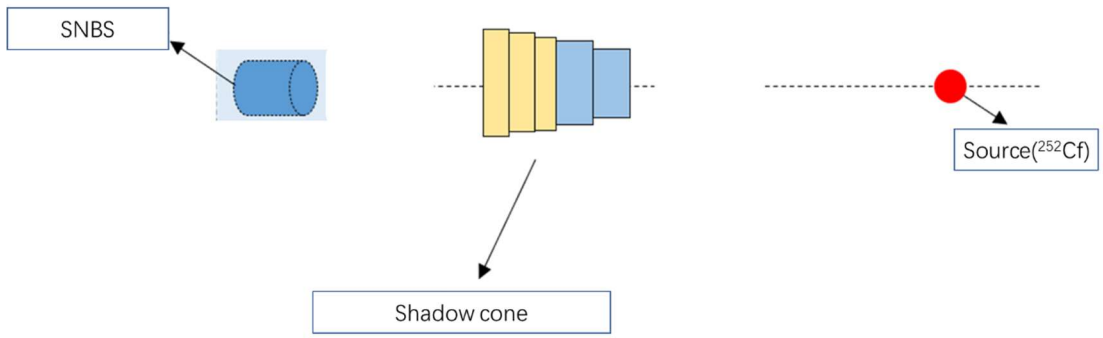

Fig.6. SNBS Calibration

By combining the experimental results obtained in the ^{252}Cf radiation field with the standard calculated values, the calibration coefficient for each detector can be determined as follows:

$$C_i = \frac{N_i^{cal}}{N_i^{exp}} \quad (2)$$

where C_i is the calibration coefficient for each detector, N_i^{cal} is the detector response value obtained from matrix calculation, and N_i^{exp} is the experimentally measured detector count rate. The raw data acquired in the ^{252}Cf standard radiation field and the corresponding standard count rates derived from the calculation are presented in Table 1.

Table 1 calibration results of SNBS

Detector identification numbers	Experimental counts	Calculated counts	Calibration coefficients
1	3338	19044	5.705
2	5539	26370	4.761
3	6295	34714	5.514
4	9338	37227	3.986
5	5747	26176	4.554
6	2562	11356	4.432
Time(s)	77440	77440	/
Distance（cm）	135	135	135

1.2.2 Performance Testing

The energy spectrum detection accuracy of the SNBS was tested on the CPHS accelerator platform at Tsinghua University, as illustrated in Fig.7. During the test, a sliding rail platform and an aluminum support were used to adjust the vertical height of the probe and the horizontal distance between the front surface of the probe and the beam port of the BSA. A laser alignment system was employed to ensure that the axis of the detector remained coincident with the center of the beam port. Under these conditions, neutron spectra were measured at distances of 1 cm, 11 cm, 31 cm, and 51 cm between the front surface of the probe and the beam port.

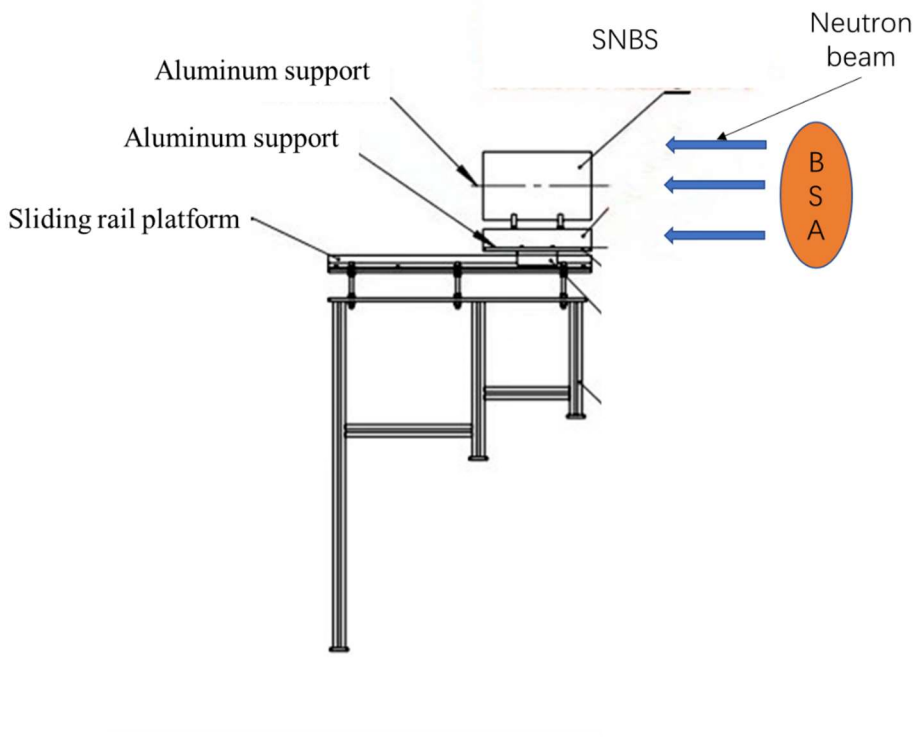

Fig.7. SNBS Testing on the CPHS Platform

2 Experimental Results and Analysis

The neutron spectra were unfolded using the Gravel code based on the calibrated measurement results. Figure 8 shows a comparison between the measured neutron spectra and the reference spectra at different measurement distances. It can be observed from the figure that the measured neutron spectra are generally consistent with the reference spectra. To more intuitively illustrate the degree of discrepancy between the two, the relative deviations between the reference and measured spectra at various distances were calculated. The root mean square of the relative errors between the experimental and theoretical values was used to evaluate the overall deviation. This error calculation method refers to the work of Gómez-Ros et al. (2010) [15].

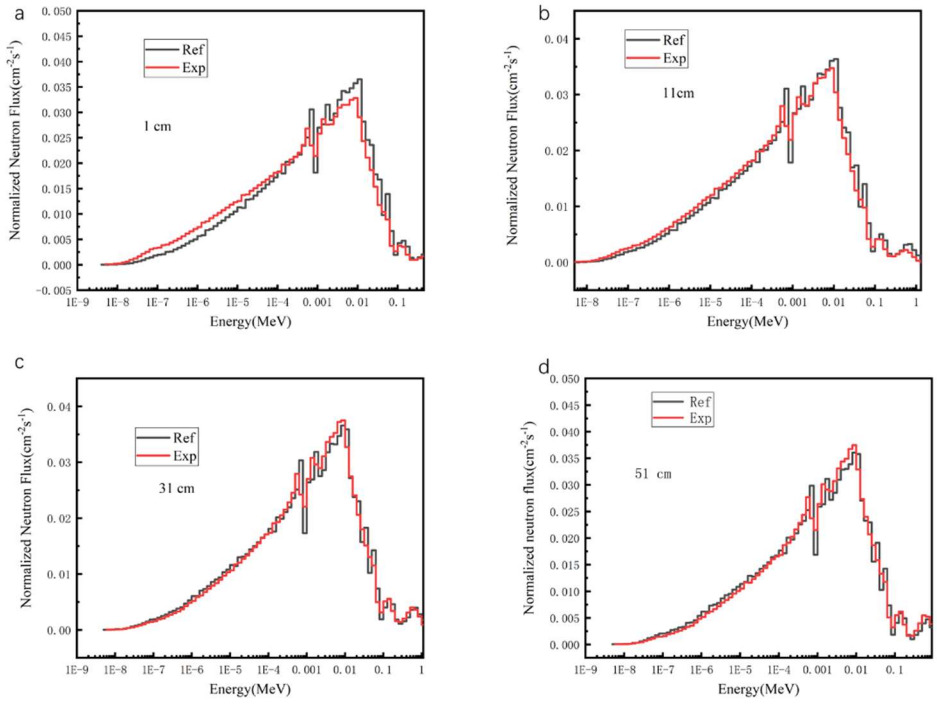

Fig.8. Unfolded Neutron Energy Spectra at Different Measurement Distances (a: result at 1 cm; b: result at 11 cm; c: result at 31 cm; d: result at 51 cm)

The calculated neutron energy spectrum measurement errors and the relative deviations between the count rates of each thermal neutron detector and the calculated values at different distances are summarized in Table 2. A decrease in measurement distance can amplify the impact of geometric deviations introduced during the alignment process.

Table 2 Neutron energy spectrum measurement errors at different distances

Detector identification numbers		*L*=1 cm	*L*=11 cm	*L*=31 cm	*L*=51 cm
1		12.62%	5.79%	0.15%	2.14%
2		1.66%	0.24%	3.67%	5.04%
3	relative	1.46%	3.42%	5.65%	6.36%
4	deviation	3.38%	1.77%	1.53%	1.40%
5		3.34%	4.30%	3.54%	2.58%
6		19.27%	16.2%	5.91%	3.73%
Energy spectrum measurement error		9.64%	7.39%	3.98%	3.94%

The proportion of epithermal neutrons in BNCT facilities is of paramount importance. Based on the measured neutron spectra, this study calculated the proportions of thermal, epithermal, and fast neutrons at different distances and determined the relative deviations between the measured results and the reference spectrum in the corresponding energy regions. Detailed results are presented in Table 3. The deviation between measured and calculated values in the epithermal neutron energy region was less than 10%, and the results in the fast neutron region were also relatively consistent. Due to the low proportion of thermal neutrons, even minor deviations in the epithermal and fast

neutron ranges can lead to significant relative changes in the thermal neutron proportion. However, since the dose conversion coefficient for thermal neutrons is much lower than that for fast neutrons, the impact of this deviation on the overall dose calculation is minimal.

Table 3 relative deviation in the proportion of epithermal neutrons between the measured spectrum and the reference spectrum

Distance	Energy range	≤0.5 eV	0.5 eV~10 keV	≥10 keV	relative deviation
1 cm	Exp (%)	4.56	81.5	14.0	6.3%
	Ref (%)	2.69	76.7	20.7	
11 cm	Exp (%)	4.14	78.3	17.6	1.8%
	Ref (%)	2.68	76.9	20.7	
31 cm	Exp (%)	2.71	76.9	11.7	0.7%
	Ref (%)	2.74	76.4	12.1	
51 cm	Exp (%)	2.53	79.0	18.4	4.4%
	Ref (%)	2.93	75.7	21.4	

3 Summary and Conclusions

This study presents the design of a cylindrical single-moderator neutron spectrometer (SNBS) for neutron spectrum measurement in boron neutron capture therapy (BNCT). After detector calibration was completed using the isotopic neutron radiation field at the Metrology Station of the China Institute of Radiation Protection, the experimental data obtained from the Compact Pulsed Hadron Source (CPHS) platform at the Department of Engineering Physics, Tsinghua University, were corrected using the calibration coefficients. The neutron spectrum was unfolded using the Gravel software based on the corrected results and the response matrix derived from Monte Carlo calculations. The measured spectra showed good agreement with the reference spectrum provided by Tsinghua University, with a maximum measurement error of less than 10%. Statistical analysis indicated that the epithermal neutron fraction at different measurement positions was consistent with the reference spectrum, exhibiting a maximum deviation of 6.3%.

4. Acknowledgments

The authors are deeply grateful to the Department of Engineering Physics at Tsinghua University for providing the opportunity to conduct experiments with the SNBS at the Compact Pulsed Hadron Source (CPHS), which was instrumental to this work.

Reference

[1] J. CHADWICK, “The Existence of a Neutron,” Proc. of the Royal Society A: Mathematical, Physical and Engineering Sciences, pp. 692−708 (1932).

[2] F. D. BROOKS and H. KLEIN, “Nuclear Instruments & Methods in Physics Research Section A—Accelerators, Spectrometers, Detectors, and Associated Equipment,” Neutron Spectrometry, 476, 1 (2002).

[3] Bramblett, L R, Ewing, I R, Bonner, W T. 1960. A NEW TYPE OF NEUTRON SPECTROMETER[J]. Nuclear Instruments & Methods, 9(1): 1-12.

[4] Bricka M, et al. 1973. Proceedings of a Symposium on Neutron Monitoring for Radiation Protection Purposes, IAEA, Vienna: 279.

[5] Dubeau J, Witharana S S H, Atanackovic J, Yonkeu A, Matysiak W, Waker A J, Ibrahim A, Archambault J P. 2012. A field portable neutron spectrometer based on the Bonner Sphere Principles[J].

[6] Buonomo B. 2012. Designing an extended energy range single-sphere multi-detector neutron spectrometer[J]. Nuclear Inst & Methods in Physics Research A, 677(677): 4-9.

[7] Chernyaev A, Gaponov I, Kazennov A. 2004. Direct methods for radionuclides measurement in water environment[J]. Journal of Environmental Radioactivity, 72(1): 187-194.

[8] Li T, Fang D, Li H. 2007. A Monte Carlo design of a neutron dose-equivalent survey meter based on a set of He-3 proportional counters[J]. RADIATION MEASUREMENTS, 42(1): 49-54.

[9] Bedogni R, Bortot D, Buonomo B, et al.First test of SP2: A novel active neutron spectrometer condensing the functionality of Bonner spheres in a single moderator[J]. Nuclear Inst & Methods in Physics Research A, 2014, 767(dec.11): 159-162.DOI: 10.1016/j.nima.2014.08.004.

[10] Lis M, Gomez-Ros J M, Bedogni R, et al.Design and feasibility of a multi-detector neutron spectrometer for radiation protection applications based on thermoluminescent 6LiF: Ti,Mg (TLD-600) detectors[J]. NUCLEAR INSTRUMENTS AND METHODS IN PHYSICS RESEARCH SECTION A, 2008, 584(1): 196-203.DOI: 10.1016/j.nima.2007.10.009.

[11] Bedogni R, J. Gómez-Ros, Pola A, et al.Experimental test of a newly developed single-moderator, multi-detector, directional neutron spectrometer in reference monochromatic fields from 144keV to 16.5MeV[J]. Nuclear Instruments & Methods in Physics Research Section A-accelerators Spectrometers Detectors and Associated Equipment, 2015, 782: 35-39.DOI: 10.1016/J.NIMA.2015.02.008.

[12] Bedogni R, Gómez-Ros, J.M, Pola A, et al.CYSP-HS: A new version of the CYSP directional neutron spectrometer with increased sensitivity[J]. Applied Radiation and Isotopes, 2018, 142: 38-41.DOI: 10.1016/j.apradiso.2018.09.018.

[13] A R B, J.M. Gómez-Ros a b, C K A A, et al.CYSP-BEAM: A multi-detector directional spectrometer for in-beam neutron spectrometry[J]. Nuclear Instruments and Methods in Physics Research Section A: Accelerators, Spectrometers, Detectors and Associated Equipment, 2019, 927: 151-154.DOI: 10.1016/j.nima.2019.02.031.

[14] J.M. Gómez-Ros, et al. Design and validation of a photon insensitive multidetector neutron spectrometer based on Dysprosium activation foils[J]. Radiation Measurements, 2011, 46(12): 1712-1715.DOI: 10.1016/j.radmeas.2011.06.037.

[15] José María Gómez-Ros, Bedogni R, Moraleda M, et al. Design and validation of a single sphere multi-detector neutron spectrometer based on LiF: Mg,Cu,P thermoluminescent dosemeters[J]. RadiationMeasurements,2010,45(10): 12201223.DOI: 10.1016/j.radmeas.2010.05.016.

TOPICAL SESSION 4. Envisioned Automation of Thermoluminescent Measurement System

Haijiang Shi, Xiaohui Du, Lili Chu, Hongchen Han, Hailei Lv,

Caixia Miao, Chenyu Wang, Qi Sun, Bokang Long

China Institute of Atomic Energy, Beijing, China

Abstract: Thermoluminescent Dosimeters (TLDs) are critical devices in the field of radiation protection and dose monitoring, widely used in radiotherapy, the nuclear industry, environmental radiation detection, aerospace, and other scenarios. Currently, TLD measurement systems face several issues, such as the need to correlate detection reports with dosimeter calibration parameters, environmental conditions (e.g., temperature and humidity), historical dose data of subjects, and other multi-source information. Manual integration is error-prone and lacks logical validation, while the single template for measurement reports fails to meet diverse requirements. This paper proposes the use of NFC technology to achieve contactless reading of device identity information and personnel data, establishing a tripartite correlation mechanism among "commissioned testing information, personnel information, and personal dose detection data". It also proposes the use of the doctemplater template engine to construct a visual report generation system, which automatically maps detection data to a predefined report framework. By setting data thresholds, intelligent judgment of abnormal data is achieved, simultaneously triggering differentiated generation logic for normal detection reports and abnormal warning reports. Additionally, a multi-user permission control mechanism is proposed to achieve hierarchical sharing and secure flow of detection data. The integrated framework of "data collection-intelligent analysis-report generation-permission control" provides a reusable technical pathway for informatization research in the field of radiation protection.

Keywords: Thermoluminescent measurement; NFC technology; Report generation; Permission control

TOPICAL SESSION 4. Domestic Commercial VDMOS as a High Radiation Doses Sensor

Zhiji Pan[1], Xiaofeng Wei[1,2,3], Yuan Zhao*[1,2,3]

[1].China Institute for Radiation Protection, Taiyuan, China; [2]Shanxi Key Laboratory of Radiation Safety and Protection, Taiyuan, China; [3]CNNC Key Laboratory of Radiation Protection Technology, Taiyuan, China

Abstract: p-MOSFET dosimeters are widely used for radiation monitoring in various high-dose environments. However, due to the need for special semiconductor manufacturing processes, the cost of p-MOSFET dosimeters is too high. In this paper, an ordinary domestic commercial VDMOS is selected for dosimetry experiments to explore the sensitivity, linearity, range, fading of VDMOS under online and passive measurement scenarios, and study the reuse performance after annealing and dose rate response characteristics. The methods of increasing VDMOS irradiation sensitivity by adding bias voltage and stacked mode are verified. The results show that the VDMOS in the experiment has good linearity in the dose range of 0.05-40Gy. The irradiation sensitivity in online measurement mode is 6.99mV/Gy, and in zero biased passive measurement mode is 2.36mV/Gy. By applying a 10V biased voltage and four-stacked methods, the irradiation sensitivity can be increased to 4.96 times and 4.24 times that of a single VDMOS in zero biased mode, respectively. Besides, the VDMOS shows good performance in reuse and fading. According to these experimental results, domestic commercial VDMOS is an effective low-cost method for measuring high doses.

Key words：domestic；commercial VDMOS；high radiation doses；low-cost

TOPICAL SESSION 4. Research on Screening Method of Heavy Charged Ions in Solid State Nuclear Track Detector

Qi Zhang[1,2,3,4], Xiaofeng Wei[1,2,3], Qinjian Cao[*,1,2,3]

[1]China Institute for Radiation Protection, Taiyuan, China; [2]Shanxi Key Laboratory of Radiation Safety and Protection, Taiyuan, China; [3]CNNC Key Laboratory of Radiation Protection Technology, Taiyuan, China; [4]College of Nuclear Science and Technology, Harbin Engineering University, Harbin, China

Abstract： Distinguishing between alpha particles and protons based on their track characteristics in CR-39 is a crucial step for conducting space radiation dose monitoring. To address this issue, this study employed Geant4 and Track as simulation tools, following a research framework encompassing the simulation of range and linear stopping power for alpha particles and protons in CR-39, simulation of track morphology, determination of optimal etching conditions, and development of particle discrimination methods. Simulation results revealed distinct differences in range, linear stopping power, and track morphology between alpha particles and protons in CR-39. At the same energy, the range of alpha particles was 4.5 to 10.5 times greater than that of protons, while the stopping power differed by a factor of 3.7 to 5.5. Under identical etching conditions, alpha particle tracks appeared as black circular pits without over-etching, whereas proton tracks manifested as gray circular pits with over-etching. Based on these findings, optimal etching conditions were determined, enabling the precise discrimination between alpha particles and protons. This work provides technical support and practical guidance for space radiation dose monitoring.

Keywords: Space radiation; Solid State Nuclear Track Detectors (SSNTDs); CR-39; Geant4 toolkit; TRACK simulation; Track morphology; Alpha particles; Proton

TOPICAL SESSION 4. Design and Validation of a Single-Sphere Neutron Spectrometer with Nearly Isotropic Response for Workplace Spectroscopy

Bowen Sun[1,2,3], Zhihui Tang[1,2,3,4], Jiayu Duan[1,2,3], Zhen Wang[1,2,3], Yingjing Wei[1,2,3]

[1]China Institute for Radiation Protection, Taiyuan, China [2]Shanxi Key Laboratory for Radiation Safety and Protection, Taiyuan, China; [3]CNNC Key Laboratory for Radiation Protection Technology, Taiyuan, China; [4]Department of Engineering Physics, Tsinghua University, Beijing, China

Abstract：Neutron spectrum measurement is a fundamental safeguard for neutron radiation protection. To address the shortcomings commonly encountered in multi-moderator neutron spectrometers, this work adopts a single-moderator & multi-detector approach to develop a single-sphere neutron spectrometer. The proposed design embeds 80 ^{6}LiF detectors within a 15cm-radius polyethylene sphere. The performance of spectrometer is validated through simulation. Results show that the response of spectrometer is nearly isotropic, which suits workplace spectroscopy.

Keywords：single-sphere neutron spectrometer; neutron spectroscopy; neutron detection.

1.Introduction

Neutron radiation and technology are being used widely in the fields of energy, medicine, materials science, and others. In typical applications their energies span a broad range, from thermal neutrons up to MeV and beyond. The interaction mechanisms of neutrons with matter vary markedly with energy. The neutron energy spectrum—the energy distribution of the neutron field—is one of its key characteristic parameters. Accurate measurement of this spectrum is essential for studying nuclear-reactor behavior, calculating neutron-induced secondary ionizing radiation, assessing biological effects of neutrons, and guiding neutron-radiation protection.

Commonly employed neutron-spectrum measurement techniques include the multi-sphere spectrometer method, the time-of-flight method, and the nuclear-recoil method[1]. Among these, the multi-sphere spectrometer stands out for its broad energy range and excellent isotropic response, making it widely used for characterizing workplace neutron fields. Originally devised by Bonner et al.[2], this spectrometer consists of an array of polyethylene moderating spheres of different diameters, each centered on a thermal-neutron detector—typically a ^{3}He proportional counter. Each sphere–detector combination yields a distinct energy response, and by successively interchanging spheres one can obtain the neutron spectrum over an extended energy range.

Traditional multi-sphere spectrometers require a set of physically distinct moderators, which makes the system heavy and the measurement procedure cumbersome. To overcome these shortcomings, a streamlined design has recently been proposed in which many neutron detectors are embedded in a single moderator. Because the detectors are located at different positions inside the sphere, they provide a set of distinct energy responses. A single exposure is therefore sufficient: the counts from all detectors are recorded simultaneously and by spectrum unfolding one can reconstruct the neutron spectrum.

Research groups in Europe and Japan have already pursued this single-sphere concept. J. M. Gómez-Ros (Spain) and R. Bedogni (Italy) developed a passive single-sphere spectrometer[3]. Its moderator is a 25 cm-diameter polyethylene sphere in which 31 dysprosium activation foils are arranged along three orthogonal axes. To enhance the high-energy response, a 1 cm-thick lead shell is embedded within the polyethylene; the moderator assembly is shown in Fig.1. An active version was built by H. Toyokawa et al. in Japan[4]. As depicted in Fig.2, their design places 19 pairs of ^{6}Li–^{7}Li loaded glass scintillators inside a 30 cm polyethylene sphere. Neutrons are distinguished from charged-particle events by ^{6}Li–^{7}Li anticoincidence technique, and the neutron interaction position is determined by the associated electronic read-out. Counting events by position yields response functions that are unfolded to recover the neutron spectrum.

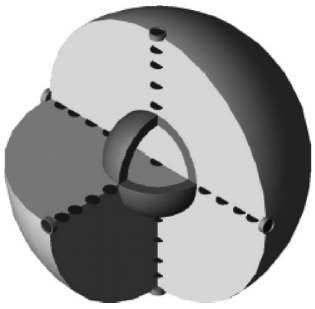

Fig.1 A passive single-sphere neutron spectrometer [3]

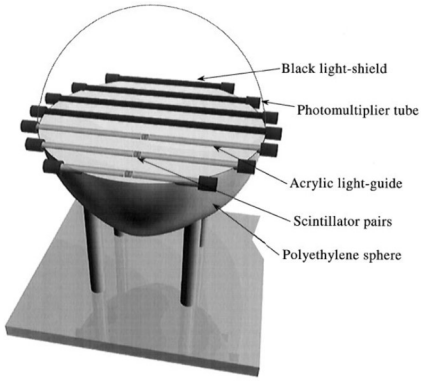

Fig.2 An active single-sphere neutron spectrometer [4]

Compared with the multi-sphere spectrometer, the single-sphere version can obtain the neutron spectrum with only one device in a single measurement, while covering a comparable energy range. It eliminates the multi-sphere drawbacks of non-simultaneous, non-co-located measurements, excessive weight and complicated operation, and is therefore being adopted ever more widely for neutron-spectrometry tasks.

In this paper we present the structural design of a single-sphere spectrometer that contains multiple active ^{6}LiF neutron detectors inside a single polyethylene moderator. The response matrix of the spectrometer is calculated with a Monte-Carlo code, its readings under irradiation from a ^{241}Am–Be source are simulated, and the resulting data are unfolded to reconstruct the spectrum. These results lay the groundwork for the subsequent development of the single-sphere neutron spectrometer.

2 Design

2.1 Detectors and moderator

The single-sphere neutron spectrometer consists of multiple identical thermal-neutron detectors positioned at different locations within one polyethylene moderator. An electronic unit converts the current pulses from each detector into discrete count signals. Because the detectors sit at different positions, each exhibits a distinct energy response; collectively, their count rates encode the neutron energy information. Feeding these counts into an unfolding algorithm yields the neutron spectrum.

The neutron detector inside the single-sphere neutron spectrometer consists of a SiC semiconductor coated with ^{6}LiF. When thermal neutrons are incident on the detector, the energy is deposited through the nuclear reaction ^{6}Li (n, α) T. The secondary charged particles produced in the reaction create electron–hole pairs in the semiconductor, generating a current-pulse signal.

The moderator in the single-sphere neutron spectrometer is polyethylene with a density of 0.93 g/cm³. The moderator has a spherical structure with an outer diameter of 30 cm and contains several internal cavities designed to snugly accommodate the assembly of the detector and its preamplifier circuit.

2.2 Energy Response Calculation

The energy response of detectors located at different positions within the moderator is calculated using the Monte-Carlo method. The schematic of the Monte-Carlo model is shown in Fig.3. The distance between detector and nearest sphere surface is denoted as D, the radius of sphere is denoted as R, and the angle between the incident neutron and +z axis is denoted as θ. Due to the non-centrosymmetric geometry, the energy response varies with the direction of incident neutrons. Therefore, the condition of '4π isotropic incidence' is considered. It refers to the case in which the neutron arrival direction is chosen with equal probability over the entire 4π solid angle. In this paper, the response is obtained with a weighted-average method as shown in (1).

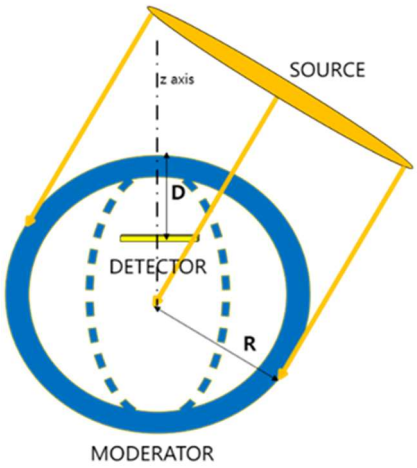

Fig.3 Schematic diagram of the calculation and modeling of the response of single-sphere neutron spectrometer in a single incidence scenario

$$R = \sum_{i=1}^{n} r_i p_i \quad (1)$$

In the equation, r_i refers to the response of detectors in a single incidence scenario with a given θ_i. θ_i is set discretely as 0°, 15°, …, 180°, with an interval of 15 °. p_i refers to the probability that theta falls closest to the angle, which is calculated by (2).

$$p_i = \frac{1}{2}\left(\cos\frac{\theta_{i-1}+\theta_i}{2} - \cos\frac{\theta_i+\theta_{i+1}}{2}\right) \qquad (2)$$

Note：in（2）$\theta_0=0^o$，$\theta_{n+1}=180^o$.

We calculate the response curve for R=15cm and D=1,2, 3, …,10cm, and for R=12,15,20,25cm and D=2,4,6,8,10cm. For each curve we calculate the energy peak region (the energy range over which the response is ≥90 % of the maximum value). Results are shown in Table 1.

Table 1 Energy Peak Region for Response Curve

(a) R=15cm

Depth(cm)	Energy Peak Region (MeV)
1	6.29×10^{-8}~2.45×10^{-6}
2	2.48×10^{-7}~1.63×10^{-4}
3	2.43×10^{-6}~3.15
4	0.43~3.34
5	0.78~3.43
6	1.30~3.33
7	1.55~5.30
8	2.04~5.40
9	2.24~6.07
10	1.81~7.63

(b) R=12~25cm (MeV)

D(cm)	R(cm)			
	12	15	20	25
2	6.37×10^{-7}~1.53×10^{-5}	2.48×10^{-7}~1.63×10^{-4}	6.39×10^{-7}~7.91×10^{-6}	3.57×10^{-7}~8.77×10^{-5}
4	0.44~2.78	0.43~3.34	0.30~2.93	0.20~2.60
8	1.10~3.36	2.04~5.40	1.68~9.70	2.30~8.49
10	1.33~3.39	1.81~7.63	5.35~8.46	5.70~9.12

Simulation result show that the shape of the response curve and its peak region are strongly influenced by the detector depth. As the depth increases, the peak region of the response function shifts toward higher energies. For a 15 cm moderating sphere, the response curves differ significantly in shape and peak region when the detector depth varies from 1 cm to 4 cm; when the depth ranges

from 5 cm to 10 cm, the curves are similar in shape, and their peak regions are nearly the same. The shape of the response function and its peak region are only weakly affected by the radius of the moderating sphere.

2.3 Detector Position within the Moderator

The detector position is specified by two variables: depth and angular (directional) coordinate. By reviewing the 4π-isotropic-incidence responses calculated above, the detector position is designed with the objective of achieving an optimal energy response.

To meet the need for workplace spectroscopy, the spectrometer must cover a wide energy range from thermal neutrons up to 20 MeV, with emphasis on unfolding the fast-neutron region. Consequently, the detectors inside the spectrometer are positioned at eight distinct depths: 2, 3, 4, 5, 7, 8, 9 and 10 cm.

Due to limited space inside the moderator, only a small number of detectors can be accommodated. Two schemes are proposed for arranging detectors within the spectrometer:

A: At each depth, 6 detectors are deployed along the directions (1, 0, 0), (−1, 0, 0), (0, 1, 0), (0, −1, 0), (0, 0, 1), and (0, 0, −1).

B: At each depth, 14 detectors are deployed along the directions (1,0,0) (-1,0,0) (0,1,0) (0,-1,0) (0,0,1) (0,0,-1) (1,1,1) (1,1,-1) (1,-1,1) (1,-1,-1) (-1,1,1) (-1,1,-1) (-1,-1,1) (-1,-1,-1).

A Monte-Carlo model is constructed with the source specified as a ^{241}Am–Be source whose direction is sampled uniformly over the 4π solid angle. For each of the two schemes, the counts registered by every detector inside the spectrometer are computed, and the mean count of all detectors at the same depth is tabulated versus depth. The source direction is then randomly varied 10^4 times, and the entire calculation is repeated, yielding a sample size of 10^4. The variance of the resulting data set divided by its mean gives the angular response of the average count at each depth.

Result are shown in Table 2. For depths of 2–5 cm, the angular response exceeds 2 % under Scheme A but remains below 2 % under Scheme B; for depths of 7–10 cm, both schemes yield an angular response below 2 %. To achieve optimal angular response, for depths of 2–5 cm, 14 detectors per depth are positioned as specified in Scheme B; for depths of 7–10 cm, 6 detectors per depth are arranged as specified in Scheme A. In total, 80 detectors are embedded within a 15 cm-radius polyethylene sphere, the exact positions are detailed in Table 3.

Table 2 Angular response of the average count of all detectors located at the same depth

Depth(cm)	angular variance (%)	
	Scheme A	Scheme B
2	4.63	0.80
3	4.18	0.68
4	3.56	0.59
5	2.81	0.42
7	1.32	0.22
8	1.18	0.18
9	0.71	0.17
10	0.27	0.09

Table 3 Detector Positioning Scheme Inside the Single-Sphere Neutron Spectrometer

Depth(cm)	2	3	4	5	7	8	9	10
dir(1,0,0)	√	√	√	√	√	√	√	√
(-1,0,0)	√	√	√	√	√	√	√	√
(0,1,0)	√	√	√	√	√	√	√	√
(0, -1,0)	√	√	√	√	√	√	√	√
(0,0,1)	√	√	√	√	√	√	√	√
(0,0, -1)	√	√	√	√	√	√	√	√
(1,1,1)	√	√	√	√				
(1,1, -1)	√	√	√	√				
(1, -1,1)	√	√	√	√				
(1, -1, -1)	√	√	√	√				
(-1,1,1)	√	√	√	√				
(-1,1, -1)	√	√	√	√				

(-1, -1,1)	√	√	√	√
(-1, -1, -1)	√	√	√	√

Based on the moderator configuration shown in Table 3, a Monte-Carlo geometrical model of the single-sphere neutron spectrometer was built. Directions were sampled isotropically over the full 4π solid angle, and the response of each detector was calculated. For every radial depth the counts of all detectors located at that depth were averaged. The source direction was then randomized 100 times and the whole procedure was repeated, yielding a statistical sample of 100 independent runs. The mean of these 100 results was taken as the detector energy response of the single-sphere neutron spectrometer under 4π uniform incidence and is plotted in Fig.4.

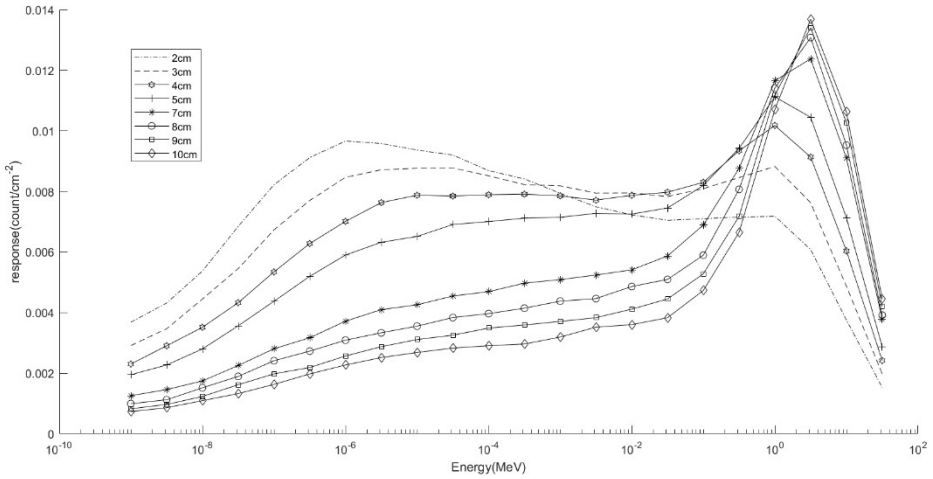

Fig.4 Energy response for each depth of the single-sphere neutron spectrometer under 4π uniform incidence conditions

2.4 Electronics & Unfolding Algorithm

The ^{6}LiF detector emits an analogue current pulse. The goal of electronics is to convert the signal into a discrete count stream that the computer can interpret. The electronic process chain comprises three stages: a pre-amplifier, a CR-RC shaping stage and an FPGA counter. The pre-amplifier is coupled directly to the detector, boosting the current pulse by an order of 10. A metal enclosure shields the assembly from electromagnetic interference, as shown in Fig.5. The CR-RC shaping network filters and de-noises the pulse, improving the signal-to-noise ratio and reshaping the exponential tail into a clean square wave. The FPGA counter employs a multi-channel parallel architecture: each rising edge of the square wave is registered as a count, and the tallies are streamed in real time to the host software via an on-board RAM buffer.

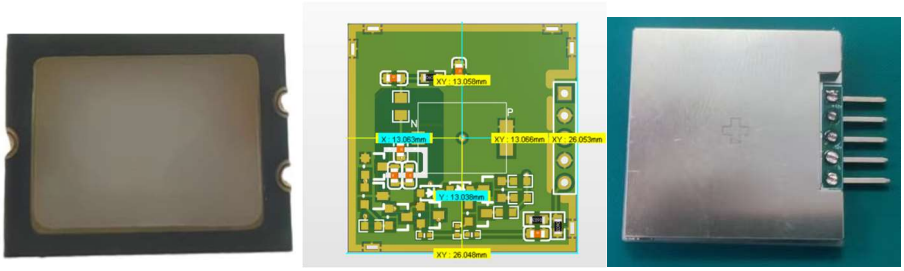

Fig.5 Neutron detector and pre-amplifier circuit. From left to right: thermal-neutron detector, pre-amplifier schematic, fully encapsulated assembly.

In lieu with multi sphere spectrometer, the input of spectrum unfolding is the averaged count of all detectors in each depth. In this study, the neutron spectrum is obtained by the least-squares method, specifically the GRV_FC31 algorithm[5] implemented in the UMG few-channel unfolding package developed by the Physikalisch-Technische Bundesanstalt (PTB). The algorithm requires an initial spectrum and performs iterative calculations according to the following equation:

$$\phi_i^{J+1} = \phi_i^J \exp\{\frac{\sum_k \frac{Re_k^i f_i^J}{\sum_l Re_{kl} f_l^J} \frac{v_k^2}{\sigma_k^2} \log(\frac{v_k}{\sum_l Re_{kl} f_l^J})}{\sum_k W_{ik}^J}\} \quad (3)$$

Here, v_k denotes the measured counts in detector k,σ_k denotes the corresponding counting uncertainty, Re_{kl} represents the energy response. The unfolding algorithm enforces non-negativity of the solution and ensures that the chi-square error decreases monotonically with successive iterations.

3 Validation

3.1 Unfolding of Isotopic-Source Spectra through Simulation

Monte Carlo simulations were used to generate the expected detector counts for the single-sphere spectrometer when exposed to a ^{241}Am-Be source, a bare ^{252}Cf source, and a D_2O moderated ^{252}Cf source. In the calculations the neutron source was treated as a point source located 110 cm from the center of the spectrometer, with its direction sampled uniformly over the full 4π solid angle. The unfolded spectra for D_2O moderated ^{252}Cf source are shown in Fig.6, the corresponding mean energies and fluence-to-dose ratios are listed in Table 4.

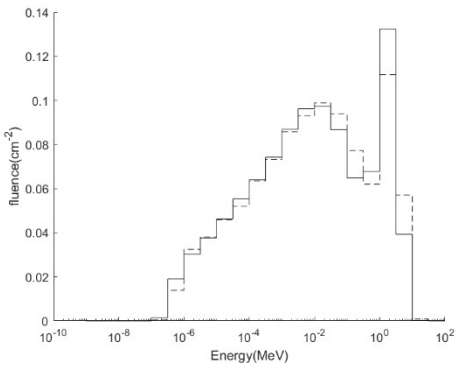

Fig.6 Simulated unfolding results for D_2O moderated ^{252}Cf source with the single-sphere neutron spectrometer

Table 4 Simulated and reference values of mean energy and fluence-to-dose ratio of neutron spectrums

Source Type	mean Energy (MeV)		fluence-to-dose ratio (pSv·cm^2)	
	simulated	reference	simulated	reference
^{241}Am-Be	3.25	4.06	396	387
^{252}Cf	1.81	2.13	390	385
D_2O moderated ^{252}Cf	0.48	0.57	115	114

3.2 Evaluation of Angular-Response via Simulation

The angular response of the single-sphere neutron spectrometer was analyzed via Monte-Carlo methods. The ^{241}Am-Be spectrum was used as reference source; neutron incidence directions were sampled uniformly over the full 4π solid angle. Using the multi-detector geometry model, the Monte-Carlo code computed the counts induced in each detector for every sampled direction. These counts were then fed into the unfolding algorithm to obtain the spectrum reconstructed under that specific incidence direction. A total of 100 calculations were performed; statistical analysis of the unfolded spectra yielded a sample coefficient of variation of approximately 1.56%.

4 Conclusion

The single-moderator, multi-detector neutron dosimeter is a novel instrument concept that determines the neutron spectrum in a single exposure and, from that spectrum, accurately calculates neutron dose. It is now being increasingly adopted for workplace neutron-spectrometry and dosimetry. In this work, Monte-Carlo simulations were used to investigate how the response functions of a single-sphere spectrometer depend on geometry variables. With the dual objectives of optimizing energy response and angular response, a design is proposed in which 80 ^{6}LiF detectors are embedded in a 15 cm-radius polyethylene sphere. Unfolding tests demonstrate that the spectrometer reconstructs spectra such as that of a ^{252}Cf source with good fidelity.

The next step will focus on the realization of the moderation structure of the single-sphere neutron spectrometer, the complete development of the single-sphere neutron spectrometer, and the testing of the single-sphere neutron spectrometer.

Reference

[1] 丁大钊，叶春堂，赵志祥等. 中子物理学（上册）. 北京：原子能出版社，2005
[2] Bramblett R L, Ewing R I, Bonner T W. A new type of neutron spectrometer[J]. Nuclear Instruments & Methods, 1960, 9(1): 1-12.
[3] Bedogni R, J.M. Gómez-Ros, Esposito A, et al.Workplace testing of the new single sphere neutron spectrometer based on Dysprosium activation foils (Dy-SSS) - ScienceDirect[J]. Nuclear Instruments & Methods in Physics Research, 2012, 684(16): 105-108.DOI: 10.1016/j.nima.2012.05.032.
[4] Yamaguchi S, Uritani A, Sakai H, et al.Spherical neutron detector for space neutron measurement[J]. Nuclear Instruments & Methods in Physics Research, 1999, 422(1-3): 600-605.DOI:10.1016/S0168-9002(98)00946-2.
[5] Reginatto, Marcel, et al. "UMG 3.3, Analysis of data measured with spectrometers using unfolding

techniques." (2004).
[6] ISO 8529-1:2021. Reference neutron radiations-Part 1：Characteristics and methods of production[S].
[7] ISO 8529-2:2000(E). Reference neutron radiations—Part 2: calibration fundamentals of radiation protection devices related to the basic quantities characterizing the radiation field[R]. Geneva, CH: International Organization for Standardization, 2000.

TOPICAL SESSION 4. Analysis of Weakly Penetrating Radiation Dose Distribution in Heavy-Ion Therapy Based on GATE Simulation

Yingguo Li [1,2,3], Yuqing Wang[1,2,3], Bowen Sun[1,2,3], Zhigang Li[1,2,3], Zhihui Tang[1,2,3], YingjingWei[1,2,3]

[1]China Institute for Radiation Protection, Taiyuan, China, [2]Shanxi Key Laboratory for Radiation Safety and Protection, Taiyuan, China, [3]CNNC Key Laboratory for Radiation Protection Technology, Taiyuan, China

Abstract: The rising global cancer burden, particularly the high incidence of breast and lung cancers, underscores the critical need for advanced radiotherapy techniques. Compared to conventional photon-based radiotherapy, heavy ion therapy offers superior dose distribution and biological effectiveness due to its inverted depth-dose profile and higher linear energy transfer (LET), enabling precise tumor targeting while sparing surrounding healthy tissues.This study employs the GATE simulation platform to analyze the secondary particle production and dose distribution resulting from carbon-12 ion irradiation in a water phantom. Beam energies ranging from 121 to 363 MeV/u were simulated with a spread of 0.1% and an intensity of 10^7 particles per second. The secondary particles generated include gamma rays, neutrons, electrons, protons, and deuterons, with gamma rays predominating (67.4%) followed by electrons (8.2%). The simulated depth-dose curves exhibit distinct Bragg peaks, consistent with experimental measurements obtained using a MP3-P water tank system at the Wuwei Heavy Ion Center. The Bragg peak positions from simulations show errors of less than 2.9 mm and relative errors below 2.4%, confirming the reliability of the model Further analysis reveals that electron doses are concentrated within 2 mm of the beam entry surface, with peak electron doses reaching 0.03 Gy for a 5 Gy carbon ion dose. This highlights the necessity of electron protection during treatment. Gamma doses, though increasing with beam energy, remain negligible and require no additional shielding. Additionally, the activity of positron-emitting nuclides was analyzed, showing concentrated production at the end of the beam path. Short-lived nuclides dominate during irradiation, while long-lived species contribute post-irradiation. This activity distribution supports the feasibility of in-beam positron emission tomography (PET) for real-time treatment monitoring. In conclusion, the results validate the GATE model for heavy ion therapy simulations, provide insights into secondary particle doses, and emphasize the importance of electron protection and the potential of PET-based treatment verification.

Key words: Weakly Penetrating Radiation; Carbon-12 Ion Radiotherapy; GATE Simulation; Dose Distribution.

Introduction

1.1 Global Burden of Cancer and the Role of Radiotherapy

Cancer remains one of the leading causes of mortality worldwide, imposing severe public health and socioeconomic burdens. According to data released by the International Agency for Research on Cancer (IARC) in 2020, breast cancer and lung cancer accounted for the highest proportions of newly diagnosed cases: breast cancer was the most prevalent among females, while lung cancer dominated among males. Notably, China has become the country with the largest number of cancer patients,

driven by factors such as population aging and lifestyle changes. To address this crisis, researchers globally have intensively explored advanced cancer treatment modalities, among which radiotherapy is a cornerstone—used in over 50% of cancer cases for curative, adjuvant, or palliative purposes. Conventional radiotherapy primarily relies on photon beams, which deposit dose exponentially as they penetrate tissue—resulting in significant dose to normal tissues anterior to the tumor and residual dose posterior to the target. In contrast, particle radiotherapy (protons and heavy ions) offers unparalleled advantages in dose distribution and cellular biology. Heavy ions exhibit an inverted percentage depth dose distribution, known as the Bragg peak: most energy is deposited at a specific depth, with minimal dose to surrounding healthy tissues. Additionally, heavy ions have higher linear energy transfer (LET) and relative biological effectiveness compared to photons: for example, proton beams induce mostly repairable single-strand DNA breaks, while carbon ions—due to their high LET —cause irreparable double-strand DNA breaks, making them more lethal to radioresistant tumors. The clinical adoption of heavy ion radiotherapy has accelerated in recent decades. As of December 2021, 103 proton and heavy ion centers were in operation across 19 countries. Asia leads in regional deployment, with 31 active facilities: 23 in Japan and 2 in South Korea. In China, the field is expanding rapidly, with 5 centers operational, 24 under construction, and 19 planned. This growth underscores the increasing recognition of heavy ions as a transformative therapy for complex cancers.

1.2 Challenge: Weak-Penetrating Radiation from Secondary Particles

Despite its advantages, heavy ion irradiation generates secondary particles—including electrons (beta rays, 60 keV–4 MeV) and low-energy gamma rays (<15 keV)—classified as weak-penetrating radiation. These particles, though less intense than the primary ion beam, can accumulate dose in superficial tissues (e.g., skin, eye lens) and increase the risk of radiation-induced toxicities. The International Commission on Radiological Protection (ICRP) Report No. 118 (2012) highlighted the importance of mitigating weak-penetrating radiation by revising occupational dose limits: the annual equivalent dose limit for the eye lens was reduced from 150 mSv to 20 mSv (5-year average) with a single-year cap of 50 mSv, while the limit for skin and extremities (hands/feet) remained 500 mSv/year. For patients, even low doses of weak-penetrating radiation can cause acute skin reactions or late effects, emphasizing the need for quantitative analysis of electron and gamma ray dose distributions.

To optimize heavy ion therapy and ensure radiation safety, it is critical to characterize the dose profiles of secondary electrons and gamma rays. Experimental measurements of these particles are challenging due to their low energy and short range, making simulation tools indispensable. GATE, an open-source software based on the Geant4 toolkit, is widely used in medical physics for modeling particle transport, dose deposition, and imaging systems. Its ability to accurately simulate nuclear interactions and dose accumulation makes it ideal for studying heavy ion-induced secondary radiation.

This study aimed to: Develop a GATE simulation model for ^{12}C ion irradiation of a water phantom (a standard tissue-equivalent material); Validate the model by comparing simulation results with clinical measurements from the Wuwei Heavy Ion Hospital; Analyze the dose distributions of electrons and gamma rays across a range of ^{12}C energies; Evaluate the potential of positron-emitting nuclides for in-beam PET monitoring. The findings are expected to inform radiation protection strategies and improve the precision of heavy ion therapy.

2. Materials and Methods

2.1 Simulation Setup

GATE (version 9.2) was used as the core simulation platform. Derived from Geant4, a Monte Carlo toolkit for particle transport, GATE is specifically optimized for medical applications—including radiotherapy dose calculation and preclinical imaging. Geant4's physics lists were selected to model high-energy nuclear interactions, ionization, bremsstrahlung, and positron annihilation—processes critical to heavy ion transport and secondary particle generation.

A homogeneous water phantom was modeled as a cube with dimensions 200 mm × 200 mm × 200 mm. Water was chosen because it closely mimics the radiation interaction properties of human soft tissue, making it the gold standard for dose simulation in radiotherapy. The phantom was positioned such that the ^{12}C ion beam was incident along the z-axis, with the beam axis centered on the phantom's front face.

The ^{12}C ion beam was configured to match clinical treatment conditions:

Energy range: 163.95, 203.67, 242.95, 282.69, and 322.04 MeV/u, covering typical energies for treating tumors at depths of 3–19 cm in tissue.

Energy spread: 0.1%, consistent with beam quality from modern heavy ion accelerators.

Beam intensity: 10^7 pulses per second (pps), corresponding to a clinically relevant dose rate.

Cyclic beam pattern: A 8.95 s cycle (7.4 s beam-off, 1.55 s beam-on) was implemented to simulate the pulsed operation of heavy ion accelerators. A total of 100 pulses were irradiated to accumulate sufficient dose for statistical reliability.

GATE's DoseActor module was used to calculate 3D dose distributions in the water phantom. To isolate electron and gamma ray doses from the primary ^{12}C ion dose, Particle Filters were implemented.

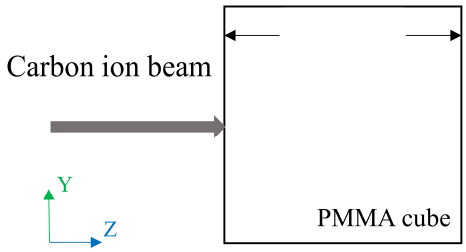

Fig.1 Schematic diagram of carbon ion irradiation of phantom

2.4 Experimental Validation

To validate the GATE model, experimental measurements were conducted at the Wuwei Heavy Ion Hospital, a clinical facility specializing in heavy ion radiotherapy.

2.4.1 Experimental Setup

Irradiation system: A ^{12}C ion beam from a synchrotron accelerator was used to irradiate the same 200 mm × 200 mm × 200 mm water phantom as in the simulation.

Dose measurement: A MP3-P (PTW-Freiburg, Germany) 3D water tank was employed to measure dose-depth profiles. The system has a minimum positioning accuracy of 0.1 mm and uses a 0.125 cm^3 ionization chamber as the detector. Measurement protocol: For each ^{12}C energy 163.95–322.04 MeV/u, dose was measured at 0.1 mm intervals along the beam axis to determine the Bragg peak position.

3. Results

3.1 Secondary Particle Yield from ^{12}C Irradiation

When a single carbon-12 pulse irradiates a water phantom, a ring-shaped scintillator detector is used to measure the number of secondary particles, as shown in the table. These mainly include prompt gamma ray, neutron, electron, proton, and deuteron, with the gamma being the most numerous. They primarily originate from bremsstrahlung, inelastic collisions of ions, and annihilation of positron-electron pairs. Beta rays are mainly due to the ionization and secondary ionization of the target material by the carbon ion beam. Among them, gamma rays account for 67.4%, and beta rays account for 8.2%.

Table 1. Secondary Particle Yields from a Single ^{12}C Pulse Irradiating a Water Phantom

Particle Type	Gamma	Neutron	Electron	Proton	Deuteron
Number	7.8×10^6	2.6×10^6	9.5×10^5	1.0×10^5	1.2×10^4
Percentage (%)	67.4%	23.5%	8.2%	0.8%	0.1%

Gamma rays originated from three key processes: (1) Bremsstrahlung: Electrons decelerate in the electric field of water nuclei, emitting photons; (2) Inelastic collisions: ^{12}C ions excite or ionize water nuclei, which de-excite by emitting gamma rays; (3) Positron-electron annihilation: Positrons collide with electrons, producing two 511 keV gamma rays. Electrons, by contrast, were primarily generated by the ionization of water molecules: ^{12}C ions strip electrons from H_2O, creating primary electrons, which then ionize additional molecules to produce secondary electrons.

3.2 Validation of the GATE Simulation Model

Table 2 compares the Bragg peak positions of ^{12}C ion beams from GATE simulations and experimental measurements using the MP3-P 3D water tank. For all energies, the absolute error in Bragg peak position was <2.9 mm, and the relative error was <2.4%. The smallest relative error was observed at 242.95 MeV/u, while the largest occurred at 163.95 MeV/u. This level of agreement is within the clinical tolerance for heavy ion radiotherapy, confirming the reliability of the GATE model.

Table 2. Comparison of ^{12}C Bragg Peak Positions: Simulation vs. Experiment

Energy（MeV/u）	163.95	203.67	242.95	282.69	322.04
Measured value（mm）	57.6	85.4	116.7	152	189.9
Simulated value（mm）	59	87	117	151	187
Relative error（%）	+2.4	+1.8	+0.3	-0.6	-1.5

To verify the reliability of this GATE software simulation, a comparison was made with the results of carbon-12 ion beam irradiation of a water phantom at the heavy ion radiotherapy center in Wuwei, using the MP3-P (PTW-Freiburg) three-dimensional water tank measurement system to obtain the depth distribution of dose in water, with a minimum positioning accuracy of 0.1mm, as shown in the table 2.

To ensure the reliability of this GATE software simulation, the results were compared with those obtained from irradiating a water phantom with a carbon-12 beam at the Heavy Ion Hospital in Wuwei. In the experiment, a MP3-P three-dimensional water tank measurement system was used to obtain the dose-depth distribution in water, with a minimum positioning accuracy of 0.1mm, and the results are shown in the table.

Table 2 shows that for the five energies, the Bragg peak positions obtained from the GATE simulation have an error less than 2.9mm compared to the actual measurements, with a relative error less than 2.4%. The simulation results are in good agreement with the experimental results, validating the authenticity and reliability of the setup for carbon ion beam irradiation of water phantoms.

3.3 Dose Distribution of Carbon-12

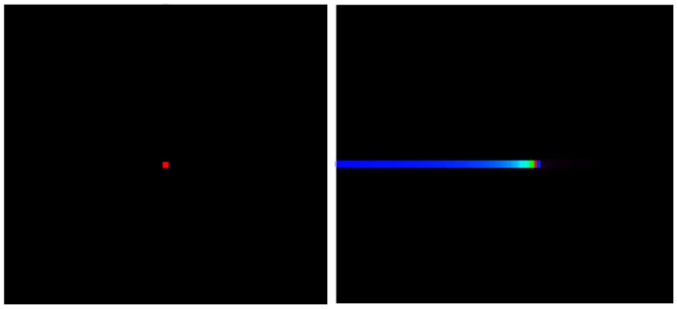

Fig.2 The 2D dose distribution of ^{12}C ions at 242.95 MeV/u of the water phantom.

Taking 242.95 MeV/u as an example, the figure shown is a schematic diagram of the cross-sectional and coronal dose distribution of heavy ions incident on a water target.The two-dimensional dose distribution image of electron entering the scintillation crystal from the irradiation of a 242.95MeV/u heavy ion pencil beam in a water phantom is shown in figure 2. The dose is highly concentrated along the beam axis, with a distinct Bragg peak at z=117.0 mm. Off-axis dose is <10% of the peak dose, demonstrating the excellent lateral dose conformity of ^{12}C ions—critical for sparing adjacent organs at risk.

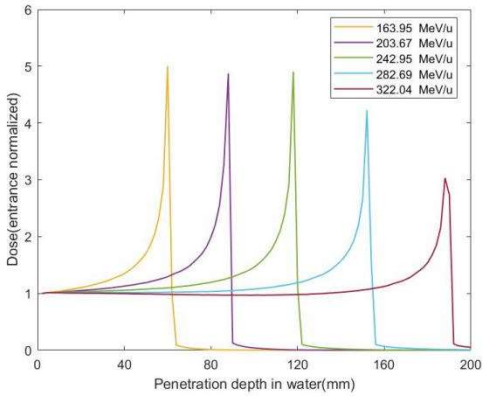

Fig.3 The carbon-12 dose distribution curves of five different energy heavy ions

The dose distribution curves of five different energy heavy ions are plotted as shown in figure 3, and the dose value at the incident point is normalized, with the image shown on the right. Across all five energies, the Bragg peak depth increased linearly with ^{12}C energy: from 35.0 mm (163.95 MeV/u) to 187.0 mm (322.04 MeV/u). The simulation results show that the dose curve of heavy ions agrees well with the theoretical values, exhibiting a distinct Bragg peak, and the dose magnitude shows a trend of decreasing with increasing energy. As the energy of the heavy ion increases, the depth of electron dose in the water phantom also increases accordingly. It is observed that the higher the energy of the heavy ion, the greater the electron dose tends to be. Similarly, using the heavy ion dose normalization coefficient for comparative analysis, it is found that at a heavy ion dose of 5Gy, the peak electron dose is 0.03Gy. Moreover, as the depth increases, the dose drops rapidly, and the peak electron dose produced by heavy ions of different energies is all within 2mm of the beam incidence depth.

3.4 Dose Distribution of Electrons

Figure 4 and 5 displays the curves of electrons dose distribution for five different energies are plotted as depicted, and the profile image displaying the dose distribution with the incident point dose value normalized is also shown. The electron dose is maximized 0.03 Gy within 2 mm of the phantom surface 0–2 mm and decreases rapidly with depth: at z=5 mm, the dose is <0.01 Gy, and at z=10 mm, it is near-zero. This shallow depth profile is attributed to the short range of low-energy electrons, which deposit most of their energy in superficial tissues. For all ^{12}C energies, the electron dose peak increased with ^{12}C energy: from <0.01 Gy to 0.03 Gy at a ^{12}C dose of 5 Gy. This trend arises because higher-energy ^{12}C ions generate more secondary electrons via ionization—due to their higher LET and greater interaction cross-section with water molecules. At a clinical ^{12}C dose of 5 Gy, the electron dose peak reaches 0.03 Gy. While this dose is low, repeated fractions could result in a cumulative electron dose—approaching the threshold for mild skin erythema. Additionally, the electron dose is concentrated in the skin, making it a potential contributor to acute skin toxicity. Thus, protective measuresmay be necessary for patients receiving high-energy ^{12}C therapy

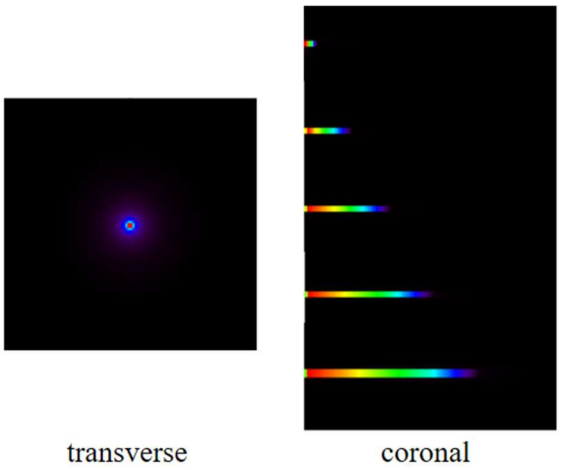

Fig.4 The 2D dose distribution of electrons of the water phantom.

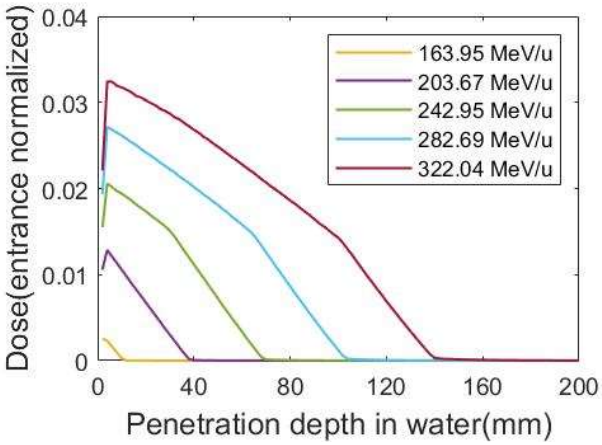

Fig.5 The electrons dose distribution curves of five different energy heavy ions

3.5 Dose Distribution of Gamma Rays

Figure 6 and 7 display the curves of gamma dose distribution for five different energies are plotted as depicted, and the profile image displaying the dose distribution with the incident point dose value normalized is also shown. Across all ^{12}C energies, the gamma ray dose peak increased slightly with ^{12}C energy: from $<0.2\times10^{-6}$ Gy (163.95 MeV/u) to $<0.9\times10^{-6}$ Gy (322.04 MeV/u) at a ^{12}C dose of 5 Gy. Unlike electrons, gamma rays penetrate deeper into the phantom, but their dose is negligible.Even at the highest energy, the gamma dose is four orders of magnitude lower than the electron dose and six orders of magnitude lower than the ^{12}C dose.The negligible gamma ray dose is far below the ICRP's annual dose limits for skin (500 mSv) and eye lenses (50 mSv). Even after 100 fractions, the cumulative gamma dose would be <0.2 mSv—posing no meaningful risk to patients or staff. Thus, no special protection measures are required for gamma rays in ^{12}C ion therapy.

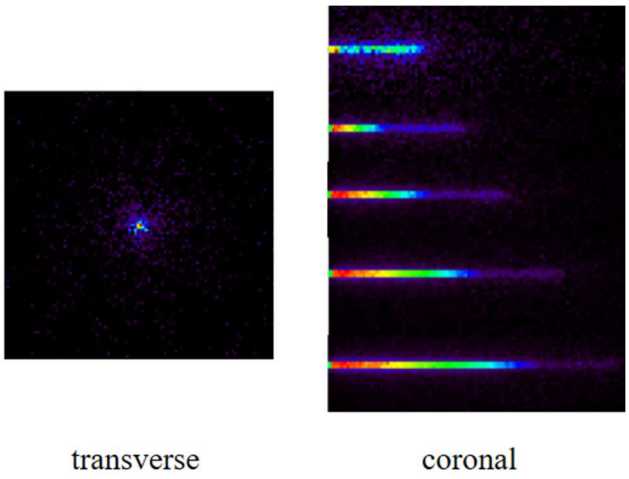

Fig.6 The 2D dose distribution of gamma of the water phantom.

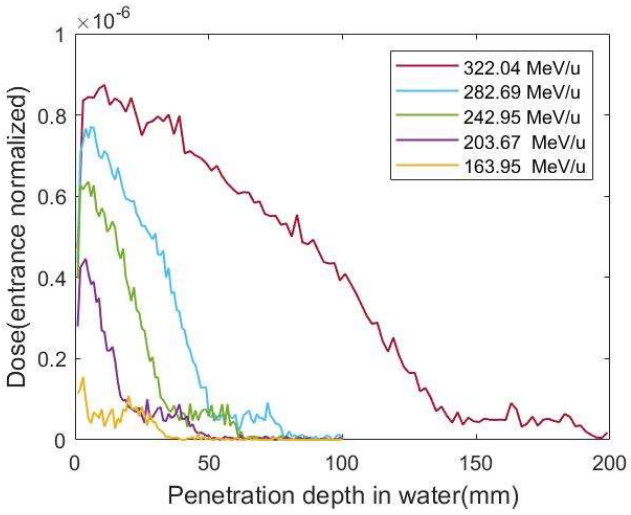

Fig.7 The gamma dose distribution curves of five different energy heavy ions

4. Discussion

4.1 Reliability of the GATE Model

The GATE simulation model exhibited excellent agreement with experimental measurements: Bragg peak position errors <2.9 mm and relative errors <2.4%. This validation is critical, as accurate dose simulation is a prerequisite for optimizing treatment plans and assessing radiation risks. Notably, the largest relative error (2.4%) occurred at the lowest energy (163.95 MeV/u). This may be due to increased stochastic noise in the simulation at lower energies—where ^{12}C ions undergo more frequent collisions, leading to greater variability in dose deposition. Future work could reduce this error by increasing the number of simulated particles to improve statistical precision.

4.2 Clinical Significance of ^{12}C Dose Distribution

The ^{12}C dose profiles confirmed the modality's key advantages for cancer treatment: (1) Sharp Bragg peak: Enables high dose to the tumor while sparing anterior/posterior normal tissues. For example,

a 322.04 MeV/u ^{12}C beam delivers 95% of its dose to a 10 mm interval around the Bragg peak, making it ideal for treating deep-seated tumors. (2) Excellent lateral conformity: Off-axis dose is <10% of the peak dose, reducing the risk of damage to nearby OARs. These characteristics explain why ^{12}C ion therapy is particularly effective for radioresistant and anatomically complex tumors.

4.3 Electron Radiation: A Critical Consideration for Skin Protection

The electron dose distribution revealed a significant risk of superficial dose accumulation: 0.03 Gy per 5 Gy ^{12}C fraction, concentrated in the first 2 mm of skin. While this dose is low per fraction, cumulative doses over 20–30 fractions could cause acute skin reactionsin sensitive patients.

4.4 Gamma Radiation: No Need for Special Protection

The gamma ray dose was negligible, even at the highest ^{12}C energy. This is because: (1) Most gamma rays are low-energy and are absorbed within the phantom before reaching the skin; (2) The yield of gamma rays, while high, is distributed over a large volume, reducing the dose per unit volume. Thus, gamma rays do not contribute meaningfully to patient or staff dose, and no special protection measures are required—consistent with findings from other heavy ion simulation studies.

Conclusion

This study used GATE software to systematically simulate the dose distributions of ^{12}C ions, electrons, and gamma rays in a water phantom—validating the model against clinical measurements and providing critical insights into weak-penetrating radiation in heavy ion therapy. Key findings included:

The GATE model is reliable, with Bragg peak position errors <2.9 mm and relative errors <2.4% compared to experimental data. ^{12}C ions exhibit a sharp Bragg peak and excellent lateral dose conformity, confirming their suitability for treating deep-seated and radioresistant tumors.Electrons contribute a non-negligible superficial dose within the first 2 mm of skin, requiring protective measures to prevent acute skin reactions.Gamma rays have negligible dose and do not require special protection.These results provide a foundation for optimizing ^{12}C ion therapy plans and radiation protection protocols, ultimately improving patient outcomes and safety. Future work should focus on heterogeneous phantoms, neutron dose analysis, and biological modeling to further advance the field.

Reference

[1] ICRU. Measurement of dose equivalents from external photon and electron radiation. ICRU Report No. 47. USA: ICRU, 1992.
[2] Walker E, Jacobs R. The response of selected survey instruments to various types and energies of beta radiation. Washington, DC, USA, 1983: 15–18.
[3] Herbaut Y, Rodriguez NA, Petel M, et al. Response of different survey instruments in beta and gamma radiation fields. Radiation Protection Dosimetry. 1986, 14(2): 199.
[4] Martz DE, Rich BL, Johnson LO. A portable beta spectrometer for tissue dose measurement. Radiation Protection Dosimetry. 1986, 14(2): 183.
[5] Dereje N, et al. Global burden of 369 diseases and injuries in 204 countries and territories, 1990–2019: a systematic analysis for the Global Burden of Disease Study 2019. The Lancet. 2020, 396(10258): 1204–1222.
[6] Li Yexiong, Wang Hua. History and development of tumor radiotherapy. China Cancer. 2008, 17(9): 775–779.
[7] Wilson R. Radiological use of fast protons. Radiology. 1946, 47(5): 487–491.
[8] Bongrand A, Busato E, Force P, et al. Use of short-lived positron emitters for in-beam and real

time β+ range monitoring in proton therapy[J]. Physica Medica. 2020, 69:248-255.
[9] Particle Therapy Centers [Internet]. (2021-09-30) [cited 2021-10-16]. Available from: https://www.ptcog.ch
[10] Wang T, Niu M, Huang C, et al. Design and simulation of a helmet brain PET system[J]. Nuclear Instruments and Methods in Physics Research Section A Accelerators Spectrometers Detectors and Associated Equipment. 2020, 978:164470.
[11] Schdart D, et al. Tumor therapy with high-energy carbon ion beams. Nuclear Physics A. 2007, 787(1–4): 633–641.

TOPICAL SESSION 4. Development of a Total Organic Carbon Analyzer Based on Supercritical Water Oxidation and Preliminary Experimental Validation

Anyuan Hu, Yi Liu, Suning Ma, Wenxu Yin

Department of Nuclear Safety and Environmental Engineering Technology, China Institute of Atomic Energy, Beijing, China

Abstract: Monitoring of total organic carbon (TOC) is critical for water quality assessment in environmental and industrial applications. Nevertheless, conventional TOC analyzers exhibit limitations in oxidation efficiency, interference resistance, and analysis speed. To address these constraints, this study developed a novel TOC analyzer utilizing supercritical water oxidation (SCWO) technology. Water under supercritical conditions exhibits unique properties including high diffusivity and potent oxidizing capacity, enabling complete degradation of organic compounds—a principle inherently aligned with TOC measurement methodology. Preliminary experimental results demonstrate that within the instrument's calibration range, the measurement error of TOC is maintained within ±2%, with a single analysis duration of <20 minutes. While the current system demonstrates robust operational stability, its portability and integration level require further optimization. This work comprehensively details the instrument's design rationale, construction process, and initial performance metrics, while proposing potential avenues for future enhancements.

Keywords: Total organic carbon (TOC); Supercritical water oxidation (SCWO); Analytical instrumentation; non-dispersive infrared detector (NDIR)

TOPICAL SESSION 4. β-γ Discrimination Using a Phoswich Detector for Radiation Monitoring

Qianyu Pan[1,2], Weizhong Sun[1,2], Meiying Zhu[1,2], Tao Jin[1,2], Yao Wu[1,2]

[1]China Nuclear Power Research and Design Institute, Chengdu, China,

[2]Sichuan Province Retired Governance Engineering Laboratory,

Chengdu, China,

Abstract: The refined requirements for occupational exposure management in nuclear facilities pose am urgent technical challenge for the effective discrimination of radiation types in β-γ mixed-fields. To address this need, a design study was conducted for a β-γ mixed-field discrimination detector based on multilayer scintillators, and experimental verification was performed in a laboratory environment. This paper investigates three aspects: detector materials, the number of detector layers and discrimination scheme, and detector dimensions. The study determined a three-layer detector structure: 0.5mm plastic scintillator + 16mm BC444 + 25mm NaI(Tl), with a side length of 30mm. Preliminary experiments using ^{90}Sr-^{90}Y, ^{241}Am, and ^{137}Cs sources were conducted in the laboratory. The results indicate that the detector successfully responded the sources in the lab environment and simultaneously obtained energy spectra for both types of radiation. The β misidentification rate was 0.66%, and the γ misidentification rate was 0.43%, meeting the design specifications.

Key words: Mixed β-γ Field; Radiation Detection; Radiation Protection; Occupational exposure

TOPICAL SESSION 4. Study on α Energy Spectrum Fitting Technology for Radioactive Aerosols

Tao Ma[1,2,3], Fu Shen[1,2,3], Yi Yang[1,2,3], Yanting Zhang[1,2,3], Liu Yang[1,2,3] , Nan Yang[1,2,3], Fuguo Zhang[1,2,3]

[1]China Institute for Radiation Protection, Taiyuan, China

[2]Shanxi Key Laboratory of Radiation Safety and Protection, Taiyuan, China

[3]CNNC Key Laboratory of Radiation Protection Technology, Taiyuan, China

Abstract: In the continuous monitoring of artificial nuclide aerosols, the traditional ratio method has obvious limitations in applicability in scenarios where the background, such as radon, thorium and their daughters, fluctuates greatly. Based on the accumulated operation data of the self-designed new-type artificial nuclide radioactive aerosol monitor for more than 10 years, this paper carries out the research on α energy spectrum fitting technology for background subtraction. By comparing with the preset fixed ratio method, it is found that the proposed fitting subtraction method shows better background subtraction ability in application scenarios where the subtraction ratio changes greatly. This study lays a solid foundation for the development of subsequent online monitoring instruments and has high application value.

Keywords: radon and thorium daughters; high radon; radioactive aerosols; α energy spectrum; fitting

Radioactive aerosols are suspended particles composed of radioactive substances, with a wide particle size range from nanoscale to micrometer scale. These aerosols can enter the human body through inhalation, ingestion, and other pathways, posing potential hazards to health and even causing diseases such as cancer [1, 2, 3]. Especially in the event of a nuclear accident, the diffusion of radioactive aerosols may lead to large - scale environmental pollution and population exposure. Therefore, the monitoring and evaluation of radioactive aerosols are crucial for ensuring public safety. In addition, during the normal operation of nuclear facilities, it is also necessary to continuously monitor the emitted radioactive aerosols to ensure compliance with environmental protection standards.

1 Introduction

In the online continuous monitoring of artificial radioactive aerosols in nuclear industry facilities or sites, the monitoring is interfered by natural radioactive aerosols formed by radon, thoron, and their progeny in the air, among which radon and thoron progeny are the main interference factors. At

present, online instruments usually adopt the ratio method to deduct the influence of radon and its progeny. In view of the obvious differences between radon - thoron progeny and artificial nuclide aerosols, aerosol monitoring technologies or instruments that use particle size separation and a thin air layer that blocks particles can be employed to reduce the interference of radon, thoron, and their progeny on artificial nuclides, thereby improving the detection performance [3, 4]. However, the current technologies inevitably require pre - setting deduction coefficients and conducting a large number of deduction coefficient tests. Meanwhile, in most cases, technologies such as particle size separation have insufficient applicability. The deduction coefficients of radon and thoron progeny are extremely prone to deduction failure due to changes in the environment where the monitor is located. Based on the newly developed artificial nuclide aerosol monitor studied in this paper, a reasonable fitting deduction method is studied, which can effectively reduce such failures.

1.1 Materials

The newly developed artificial nuclide aerosol monitor [4] was used in this paper (as shown in Figure 1). Measurements and tests were carried out in accordance with the measurement methods and principles to provide research data for the study. As shown in Figure 1, the instrument is not equipped with a particle size separation device and operates in an automated manner. The instrument mainly consists of an aerosol sampling device and an α (Alpha) energy spectrum measurement system.

1.2Aerosol Sampling Device

Large - flow air sampling is usually used for the sampling of radioactive aerosols. The newly developed artificial nuclide aerosol monitors sucks aerosols onto a filter membrane through a high - performance pump. The filter membrane can effectively capture particles in the air, including radioactive aerosols. Common filter membrane materials include glass fiber filter membranes and polypropylene filter membranes. In this paper, a thin - film filter membrane with little influence on the penetration of α particles was selected, and the material was PTFE (Polytetrafluoroethylene). The sampling time is determined according to the radioactive activity level in the air and the required lower limit of detection, usually ranging from several hours to several days.

Figure 1 On - line New Type Artificial Nuclide Aerosol Monitor

2. α Energy Spectrum Measurement System

The α energy spectrum measurement system for radioactive aerosols consists of a PIPS detector, a preamplifier, a main amplifier, a multichannel analyzer (MCA), and data acquisition and analysis software.

The measurement process is as follows: A PIPS silicon detector with high energy resolution and low noise detects radiation signals. Subsequently, the preamplifier converts the weak charge pulses output by the detector into voltage pulses and performs initial amplification. Then, the main amplifier further amplifies and shapes the signals to improve the signal - to - noise ratio. The formed signals are then sent to the multichannel analyzer (MCA) for analog - to - digital conversion and energy channel division, forming a digital energy spectrum. After that, the compiled data acquisition and analysis software controls the MCA, collects energy spectrum data, and realizes energy spectrum display, storage, and data processing. The data acquisition and analysis software runs on an industrial computer.

2.1 α Ratio Deduction Measurement Method

The α particle energy range of radioactive nuclide aerosols involved in radioactive nuclide aerosol measurement is from 4 MeV to 8.8 MeV. However, in most cases, the α energy of natural radioactive nuclides in aerosols is mostly in the range of 6 MeV ~ 8.8 MeV, while the energy range of artificial radioactive nuclides is less than 6 MeV. Artificial radioactive nuclides can be distinguished from natural radioactive nuclides through this energy difference [3, 4], as shown in Figure 2. N1 is the count of artificial nuclides, and its corresponding region is the artificial nuclide region. Both N2 and N3 are the α particle counts of natural radioactive aerosols, and their corresponding regions are the α particle count regions of natural radioactive aerosols. Typically, N2 is mainly the count of ^{218}Po, and N3 is mainly the count of ^{214}Po and ^{212}Po.

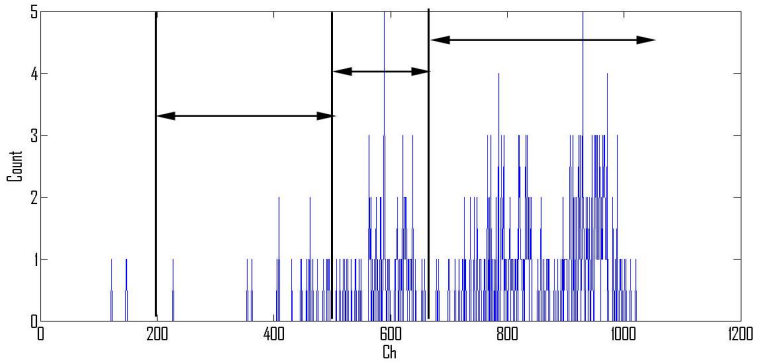

Figure 2 Aerosol Monitoring Spectrum

Typically, the α particles of natural radioactive aerosols in Zone 2 and Zone 3 will cause tailing due to air, filter paper, detector packaging, and other factors, leading to their counts extending into Zone 1 and thus affecting the results of Zone 1. Methods such as the ratio method are used to deduct this interference based on the relationship between N2, N3, and N1 to reduce the impact. The expression is as follows:

$$Na = N1 - f * (N2 + N3) \quad (1)$$

Na is the count of artificial radionuclides; N1 is the count in the artificial radionuclide region; f is the deduction ratio. Typically, N2 is mainly the count of ^{218}Po; N3 is mainly the count of ^{214}Po and ^{212}Po.

2.2.α Energy Spectrum Fitting and Deduction Measurement Method

As a classic radioactive analysis method, α-particle energy spectrum analysis is widely used in nuclear industry, nuclear medicine, environmental radioactive analysis, nuclear waste treatment and other fields due to its advantages of high energy resolution, clear spectral peaks and strong nuclide identification ability. Compared with β spectrum or γ spectrum, α spectrum has concentrated energy and less backscattering, which enables better high-precision quantitative measurement.

Typical α energy spectrum measurement usually uses semiconductor detectors (such as silicon PIN detectors, silicon drift detectors (Si-SSD), etc.) or gas ionization chambers, combined with a data acquisition system to form a complete spectrum shape. However, in practical applications, the α energy spectrum is affected by various factors such as statistical fluctuations, electronic noise,

detector response function broadening, and peak shape overlap, making spectrum fitting complex. This requires the use of effective energy spectrum fitting algorithms to model and decompose experimental data, thereby achieving accurate nuclide identification and quantification.

The current mainstream α energy spectrum fitting methods mainly include Gaussian model fitting, Voigt function fitting, empirical tailing function, maximum likelihood estimation (MLE), Bayesian spectrum shape analysis, etc. The nonlinear optimization algorithm based on the least square method is the most common one among them. In recent years, with the improvement of computing capabilities and the introduction of AI algorithms, machine learning and deep learning methods have also begun to be tried for spectral peak identification and fitting. The emerging new methods currently require strong computing power support and are mostly still in the stage of theoretical research, which makes them difficult to apply to continuous online measurement using industrial computers. At present, there is no automatic energy spectrum fitting for continuous online measurement in radioactive aerosol continuous monitors in China. Therefore, based on the computing performance of the industrial computer of the newly developed artificial nuclide aerosol monitor in this paper, research on fitting based on the Gaussian model is carried out.

The fitting function used is as follows:

$$F(x)=A*\exp\{-[(x-C)/T]^2\} \quad (2)$$

In the formula, A, C, and T are obtained through fitting.For simple α energy spectra, the above Gaussian function can be directly used for fitting. This method is simple and easy to implement; however, when spectral peaks overlap or background noise is relatively high, the fitting effect will be affected. In such cases, multiple Gaussian functions are used for fitting.

$$F(x)=\Sigma (A_i*\exp\{-[(x-C_i)/T_i]^2\} \quad (3)$$

When the fitting method is adopted, the count to be deducted can be obtained through energy spectrum fitting.

$$N_a = N_a = N_1 - N_1\_f$$

Na is the count of artificial radionuclides; N1 is the count in the artificial radionuclide region; N1_f is the count in the artificial radionuclide region of the fitted spectrum.

Figure 2 Schematic Diagram of Multi - Gaussian Function Fitting

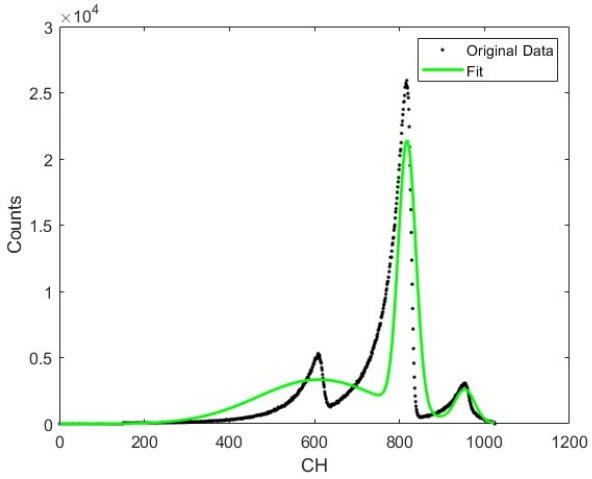

2.3 Activity Calculation

After the α count of artificial radionuclides in radioactive aerosols is determined, the radioactive aerosol concentration of the monitored nuclear facility can be obtained through Formula (2) under the condition that the sampling and collection efficiency is 1.

$$Ca=Na/(\eta \cdot Q \cdot T) \quad (4)$$

Ca is the concentration of artificial radionuclides; Na is the count of artificial radionuclides; η is the detection efficiency; Q is the sampling volume; T is the measurement time.

When in an environment without artificial radionuclides, run the background test program of the monitoring instrument. After the time reaches the time cycle set by the user, the minimum detectable activity can be obtained automatically. The minimum detectable activity concentration (MDAC) is calculated using Formula (5).

$$MDAC=3+k \cdot \sigma/(\eta \cdot Q \cdot T) \quad (5)$$

MDAC is the minimum detectable activity concentration of nuclide n at energy E; k is the confidence factor,and k is usually taken as 4.65 in Formula (5); σ is the counting deviation of T, and the calculation method is shown in Formula (6); η is the detection efficiency; T is the measurement time period; Q is the sampling volume.

$$\sigma = \sqrt{\frac{\sum_{i=1}^{n} Na(i) - \overline{Na}}{n-1}} \quad (6)$$

σ is the counting deviation of T; Na(i) is the measured count of artificial radioactive aerosols after deducting the interference of radon and thoron progeny in the i-th measurement; is the mean value; n is the number of measurements.

3 Main Performance Tests

3.1 Deduction Ratio

In accordance with the theoretical Formula (2), the newly designed and manufactured artificial nuclide aerosol monitor was operated for nearly 100,000 hours in environments with a radon concentration of 20–2000 Bq/m³, including on-site locations and laboratories [3, 4, 5, 7]. A large amount of data was collected and organized into a figure (note: the original text mentions but does not specify the figure number; it is recommended to supplement the figure number such as "Figure X" if available). It can be seen from the figure that the data has relatively high correlation. Using the least square method, results with a data accumulation time of more than 10,000 hours were selected to ensure the correlation coefficient was greater than 90%. The corresponding relationship between radon and thoron progeny and the deduction ratio were obtained. The ratios were organized and numbered according to the obvious differences in variations, and the results are shown in Table 1. Generally, significant changes in radon and thoron concentrations and a wide coverage range of equilibrium factors [5] both have a significant impact on the deduction effect.

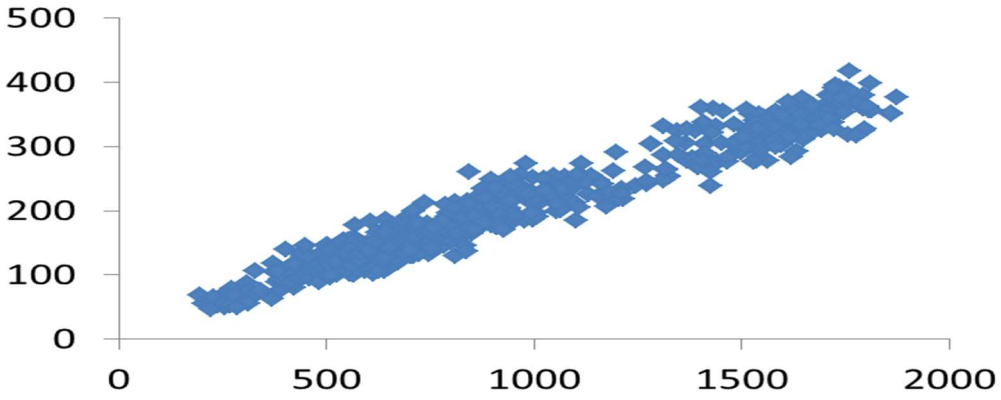

Figure 3 Deduction Test Data

Table 1 Deduction Ratios

Serial Number	Ratio	Remarks
Ratio Deduction1	0.0211	Radon concentration :20～200Bq/m³
Ratio Deduction2	0.1593	Radon concentration :20～200Bq/m³
Ratio Deduction3	0.2148	Radon concentration :20～200Bq/m³
Ratio Deduction4	0.2795	Radon concentration :1000～2000Bq/m³
Ratio Deduction5	0.3725	Radon concentration :1000～2000Bq/m³
Ratio Deduction6	0.4107	Radon concentration :1000～2000Bq/m³

3.2 Radon Deduction Effect

The instrument operated normally in an environment with a radon concentration of 20 Bq/m³–200 Bq/m³, and the corresponding aerosol energy spectra were measured. By adopting the fitting method described in the theory, the energy spectra were fitted using the optimal fitting parameters obtained within 30 seconds under the constraint of the industrial computer's operating capacity. The results are shown in the figure below (note: the original text mentions but does not specify the figure number; it is recommended to supplement the figure number such as "Figure X" if available). By calculating the difference between the original spectrum and the fitted spectrum, and in accordance with the zoning shown in Figure 1 and the fitting measurement principle, the data in Zone 1 after deduction was obtained as the measured data.

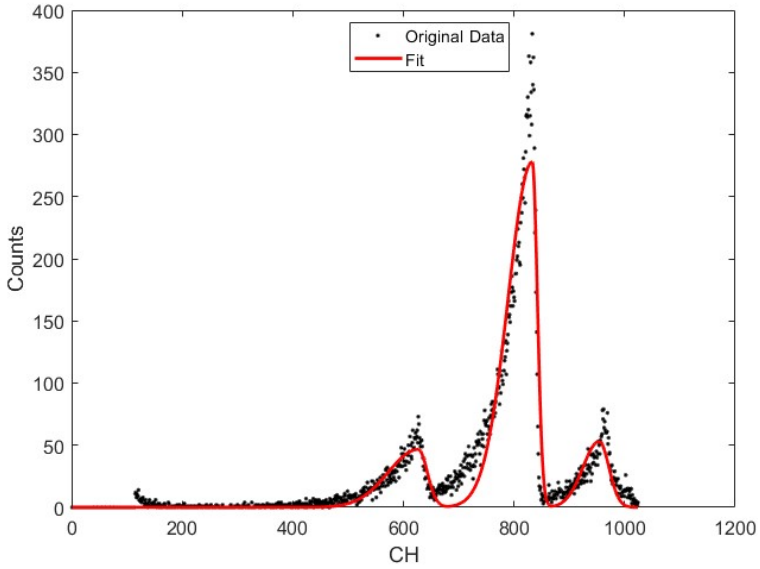

Figure 4 Automatic Fitting Status

During the tests in this study, a fitting correlation coefficient greater than 85% was selected as a certain convergence condition. However, the program still generated multiple solutions during operation; therefore, manual assistance was required to select the results with relatively ideal performance, which were then recorded and compared with the results of the ratio method. Finally, tests were conducted for three scenarios: no deduction, ratio deduction, and fitting deduction, and the results were organized into Table 2.

In this operation, the scenario corresponded to Ratio Deduction 3; thus, Ratio Deduction 3 achieved the best performance, with a deduction efficiency of 89.5%. In actual operation, since the deduction coefficient must be preset in advance, if there are significant changes in radon, thoron, or other factors, the tested deduction coefficient may not correspond to Ratio Deduction 3 but could be one of the other ratio scenarios. In such cases, except for individual scenarios (e.g., Ratio Deduction

4, whose performance is close to that of Ratio Deduction 3 and still acceptable), the deduction efficiency of other ratio methods is below 80%.

In contrast, the fitting method takes 30 seconds to run. Although its performance cannot match that of Ratio Deduction 3, its deduction efficiency has reached over 80%, which is better than the performance of most ratio deduction scenarios except Ratio Deduction 3. Therefore, under conditions where various factors lead to poor performance of the preset ratio deduction method, although the fitting deduction method cannot match the optimal ratio deduction performance obtained under specific corresponding scenarios, it is closer to the actual ratio deduction method compared with other preset ratio deduction parameters and thus has high practical value.

Table 2 Comparison Table of Fitting Deduction and Other Deduction Effects

(Concentration Unit: Bq/m³)

Deduction Method	Measured Concentration	Deduction Efficiency
No Deduction	1.137596	0.0%
Ratio Deduction1	1.037838	8.8%
Ratio Deduction2	0.382655	66.4%
Ratio Deduction3	0.119634	89.5%
Ratio Deduction4	-0.18699	83.6%
Ratio Deduction5	-0.62772	44.8%
Ratio Deduction6	-0.80876	28.9%
Fitting Deduction 1	0.164748	85.5%
Fitting Deduction 2	0.180389	84.1%
Fitting Deduction 3	0.203328	82.1%

4. Conclusions

Aiming at the problems that the measurement of artificial radioactive aerosols in nuclear facilities is easily significantly affected by radon and thoron progeny (especially leading to obvious changes in deduction coefficients), and that the previously studied methods for improving detection performance (such as particle size separation and ratio measurement methods) are limited in

application, this study developed a multi-Gaussian function fitting method based on the computing performance of the industrial computer in the existing radioactive aerosol monitor. The feasibility of the fitting deduction technology was studied under specified time and correlation coefficient conditions.

Preliminary research shows that although this technology cannot achieve the same effect as the ratio method under specific conditions or optimized scenarios, it can achieve better deduction results than the non-targeted ratio deduction method when the radon-thoron deduction coefficients change significantly or preset ratio parameters are not feasible. The test results of this study indicate that under the conditions of a 30-second time window and an 85% correlation coefficient, a deduction efficiency of more than 80% can be achieved. This method lays a foundation for on-site implementation. After further reducing manual intervention, it is expected to replace the ratio deduction method and be widely applied in online continuous monitoring systems.

References：

[1] Eisenbud, M., & Gesell, L. *Environmental Radioactivity*. Academic Press, 1997.

[2] UNSCEAR. *Sources and Effects of Ionizing Radiation*. United Nations Scientific Committee on the Effects of Atomic Radiation, 2008 Report to the General Assembly.

[3] Fu Shen. CAM Test Studying，ISORD-8[R]. Radiation Detection and Sensor Technology (I) R2-O-4，2015.

[4] Shen F. Design of a New Type of Artificial Nuclide Aerosol Monitor [J]. 2020.

[5] Ma Y H, Shen F, Xi P P, et al. Application Research on a New Type of Continuous Monitor for ^{222}Rn, ^{220}Rn and Their Progeny Concentrations [J]. Nuclear Electronics & Detection Technology, 2022, 42(1): 4.

[6] Shen F, Fu C M, Ma Y H, et al. A Testing Method and System for a Radioactive Aerosol Monitoring Technology Device: 201510952277 [P]. 2025-07-18.

TOPICAL SESSION 4. Establishment of a Mobile Pulsed γ-Ray Generation Device

Jiaoyu Zhang [1,2,3], Yingjing Wei [1,2,3], Ke Li [4], Yuanhao Zhao [5], Zhihui Tang [1,2,3], Jianxu Chen [1,2,3]

[1]China Institute for Radiation Protection, Taiyuan, China; [2]Shanxi Key Laboratory of Radiation Safety and Protection, Taiyuan, China; [3]CNNC Key Laboratory for Radiation Protection Technology, Taiyuan, China; [4]96036 Unit, Sanmenxia, China; [5]Shandong Nuclear Power Co., Ltd., Haiyang, China

Abstract: To address the difficulty of validating the effectiveness of fixed nuclear-criticality-alarm systems at nuclear facilities—owing to their complex structures, which make on-site removal and laboratory calibration impractical, and to the lack of a portable source capable of generating pulsed radiation—we developed the first mobile pulsed-γ irradiator in China. The unit employs a ^{137}Cs source and produces pulsed γ-rays by precisely moving the source inside an optimized shielding assembly. A 3.7×10^9 Bq ^{137}Cs capsule was selected; the lead thicknesses for both the source-storage and source-motion sections were calculated analytically. After commissioning the pulsed-γ generator, we built a dose-measurement system and a time-measurement system to characterize its performance. The device delivers single γ-ray pulses with widths adjustable from 34 ms to 998 ms, an air-kerma rate of 165 μGy h^{-1} to 215 μGy h^{-1}, and a relative expanded uncertainty of 5.4 % (k = 2). Its modular, dismountable design allows easy transport to nuclear facilities, enabling on-site verification of installed criticality-alarm systems.

Key words: Nuclear criticality accident; Pulsed γ-ray generation device; Air kerma; Pulse width

0 Introduction

Criticality safety in nuclear facilities is a unique and overriding concern for the nuclear industry. Once natural uranium is enriched to produce enriched uranium, or irradiated in reactors to yield plutonium, every subsequent processing, handling, and utilization step is accompanied by the ever-present risk of nuclear criticality. A documented criticality accident, for example, produced fission bursts every ~10 min over several hours, each lasting no more than 0.5 s [1]. To mitigate the consequences of potential criticality events, GB 15146.9—Criticality Safety for Fissile Materials Outside Reactors—mandates that "within any independent area, operations involving more than 700 g of ^{235}U, 520 g of ^{233}U, 450 g of plutonium, or any combination thereof must be evaluated for the need to install a criticality accident alarm system"[2]. The radiation emitted during a criticality accident is characteristically pulsed; alarm systems are therefore deployed to detect and quantify such pulses.

To guard against severe accident consequences, facilities handling nuclear fuel are extensively equipped with criticality alarm systems. These systems are structurally complex and permanently installed. Owing to the absence of on-site pulsed-γ calibration sources, their effectiveness can be verified only by cumbersome dismounting and laboratory shipment—an approach that is labor-intensive and limited to small batches, whereas large-scale dispatch is impractical. The lack of a pulsed-radiation device further undermines confidence in field test results. To ensure that alarm

equipment responds accurately at the instant of an accident, this work developed China's first mobile pulsed-γ facility based on a ^{137}Cs source. Key parameters and experimental protocols were determined through calculation, the hardware was constructed, and both dosimetric and timing systems were integrated to measure pulse width and air kerma. The facility supplies on-site test capability for production debugging and operational monitoring of alarm equipment, safeguarding their effectiveness and accuracy.

1 Design of the mobile pulsed γ-ray generation device

Research on pulsed radiation can be traced to the 1970s, when Janardhanan et al. (India) built a pneumatically driven device capable of generating pulsed γ rays with widths around 100 ms[3]; however, pneumatic instability precluded precise source-speed control, yielding non-reproducible pulses. Xi'an Jiaotong University and the Northwest Institute of Nuclear Technology later designed a dual-disc, differential-chopping system [4], but the resulting pulses were strictly periodic, unlike those of a criticality accident. More recently, Fang Dengfu et al. (China Institute for Radiation Protection) employed a gravity-driven shutter combined with a collimating aperture to slice a continuous γ beam into millisecond-scale adjustable pulses [5], yet the setup is unsuitable for field calibration. Drawing on these precedents, this paper proposes an overall design for a mobile pulsed-γ facility. The ^{137}Cs-based device generates adjustable pulsed γ rays by controlled motion of the source within a purpose-designed shield. To enhance mobility, the assembly is modular and readily disassembled. The main components are: (1) source and drive mechanism, (2) shielding, and (3) shield aperture, each detailed below.

1.1 Selection of Source and Drive

Pulsed γ rays with millisecond or longer durations are conventionally produced from a steady source by moving either the source itself or an external shutter. Because γ shielding typically employs high-density lead or tungsten, mobility demands a compact source. A ^{137}Cs source, Φ8 mm × 10 mm overall with a Φ4 mm × 4 mm active pellet and activity 3.7 × 10^9 Bq, was selected. Provided the distance to the dose point exceeds ten times the source's largest dimension, the source may be treated as a point source [6]. Equation (1) is used to calculate the air-kerma rate.

$$\dot{K}_a = \frac{A \cdot \Gamma_k}{R^2} \qquad (1)$$

In the equation, $\dot{K}_a$ is the air dose rate, units Gy/h; A is the activity of the radioactive source, units Bq; Γ_k is the air dose rate constant; R is the distance from the radioactive source, units m. Given the activity of the radioactive source and the air dose rate constant available in the literature, the air dose rate at a distance of 6 cm from the source can be calculated using formula (1) to be 5.65 × 10^{-2} Gy/h. In practical applications, when the charged particle equilibrium condition is satisfied, it can be assumed that the absorbed dose rate at a given point is numerically equal to its dose rate [7]. The dose rate measurement range of domestic nuclear criticality alarm devices is 0.1 μGy/h to 30 Gy/h, with a minimum alarm threshold of 0.1 mGy/h. Therefore, the selected radioactive source can meet the testing requirements of on-site nuclear criticality alarm devices. When selecting the power source, it is necessary to consider a power transmission device that matches parameters such as the radioactive source's movement speed, pulse width, pulse shape, and pulse dose rate. Additionally, considering the stability of the movement speed and the reproducibility of the experiment, an electric cylinder driven by electricity is selected as the drive device, with the movement speed adjustable within the range of 0 to 1000 mm/s.

1.2 Shielding Design

The shielding section of the entire device can be divided into two parts: the source storage end for holding the ^{137}Cs source when not in use, and the moving section where the source performs linear back-and-forth motion during operation. Considering shielding effectiveness, ease of processing, and manufacturing costs, lead was selected as the material for the shielding layer. For the storage end, according to the relevant standards in the standard document GBZ 125-2009 “Radiation Hygiene Protection Requirements for Instruments Containing Sealed Sources” [8], the maximum surrounding dose equivalent rate at the surface of the lead layer is 2.5 μGy/h. Given that the surrounding dose equivalent rate of the source without shielding is 5.65×10^{-2} Gy/h, the required attenuation factor K is calculated as $K = 5.65\times10^{-2} / 2.5\times10^{-6} = 22{,}600$. Given that the lead half-value layer for ^{137}Cs is 0.65 cm, the number of half-value layers required is $n = \ln K/\ln 2 \approx 14$. Based on the above theoretical calculations, the thickness of the lead shielding is determined to be $14 \times 0.65 = 9.37$ cm, which is the thickness of the lead shielding layer at the source storage end.

For the moving part of the source's linear back-and-forth motion, in order to achieve the device's mobility, the lead layer is kept as thin as possible. When operating the pulse device, a remote-control system is used, which provides the conditions for the feasibility of thinning the lead layer. Assuming the radius of the shielding body of the moving part is 6 cm (R_2), the dose rate on the inner surface of the lead layer is 2.18×10^{-5} Gy/s ($\dot{K}_2$). The minimum alarm threshold of the critical alarm device is 0.1 mGy/h, i.e., 2.78×10^{-8} Gy/s ($\dot{K}_l$). According to formula (2), R1 is approximately 1.67 m, meaning that at a distance of 1.67 m from the device, the critical alarm system will not trigger an alarm when the lead shielding layer thickness is zero.

$$\frac{\dot{K}_l}{\dot{K}_2} = \frac{R_2^2}{R_l^2} \qquad (2)$$

When the lead layer has a certain thickness, the distance between the device and the alarm system can be further reduced. From equation (1), the dose rate at a distance of 1 m from the radiation source is 5.6×10^{-8} Gy/s. It is known that a 2 cm thick lead layer can attenuate the dose rate of γ-rays by a factor of 8, resulting in a dose rate of 7.0×10^{-9} Gy/s. Therefore, when the lead layer thickness of the moving part is set to 2 cm, it will not trigger the critical alarm device.

1.3 Shielding opening design

The design of the shielding opening requires careful consideration, as the opening in the lead shielding layer directly affects the duration of the pulsed γ-rays, thereby determining the dose rate of the pulsed rays. The design of the opening primarily considers two aspects: position and size. For the position of the opening, it can be placed at the center of the moving part. The length of the opening is denoted by l, and the width by d. Based on the size of the radiation source, d is set to 1 cm. Here, assuming the duration of the pulsed radiation is t and the speed of the radiation source passing through the opening is v, then $t = l/v$. Therefore, the value of l is determined by the duration of the radiation t. According to GB/T 12787-2020 “Radiation Protection Instruments - Critical Incident Alarm Devices” [9], the pulse width of the pulsed radiation used to test the critical alarm device is 1 ms to 3 s, meaning that the range of t is 1 ms to 3 s. The maximum operating speed of the electric cylinder is 1 m/s, so the value of l is not fixed.

Based on this, the initial value of l is set to 10 cm, i.e., a 1 cm wide and 10 cm long opening is made on the shielding body, and a lead plate with a length of 10 cm, a width of 1 cm, and a thickness of 2 cm is installed at the opening. By adjusting the relative position of the lead plate and the opening, the

value of *l* can be changed to produce pulse radiation with different durations. Since the opening itself is narrow, theoretical control of the beam without an additional collimator is feasible. The final mechanical structure of the pulse γ-ray generator is shown in Figure 1.

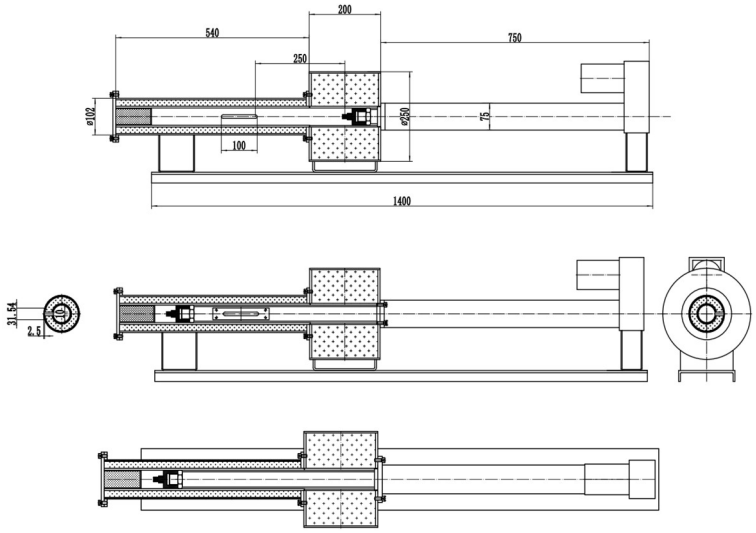

Figure 1 Engineering drawing of pulse γ radiation device (from top to bottom: front view, left-side view, top view)

2. Assembly of the mobile pulsed γ-ray generation device

The design and manufacturing drawings of the device are shown in Figure 2. The entire device can be divided into nine sections according to the annotations in Figure 2: 1. PLC control box, used to control the operational status of the electric cylinder; 2. Electric cylinder, used to drive the movement of the radioactive source; 3 and 4 are signal lines between the electric cylinder and the PLC box, respectively serving to supply power to the electric cylinder and limit the position of the electric cylinder's lead screw; 5. Network cable, connecting the PLC to a computer for remote control; 6. Source storage compartment, where the radioactive source is normally stored; 7. Source movement mechanism; 8. Opening, composed of two lead blocks, which can be moved to create openings of different sizes; when all lead blocks are removed, the opening can reach up to 10 cm in length; 9. Base, sturdy and reliable, providing stable support for the entire shielding section.

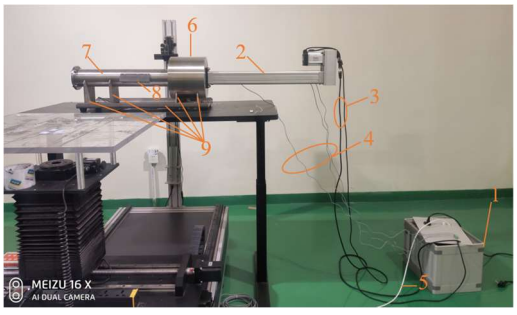

Figure 2 Photograph of the mobile pulsed-γ radiation device

3 Performance verification results of the pulsed γ-ray generation device

3.1 Air-kerma experiment

A dosimetry system consisting of a TW32002 spherical ionization chamber with 1 L sensitive volume and a PTW UNIDOS webline electrometer was used to determine air kerma via cumulative-charge measurements. Before the main experiment, the correlation between air kerma and cumulative charge under pulsed radiation was verified with pulsed X-rays. The verification kept the tube current constant while varying only the pulse width of the pulsed X-rays, and monitored the charge collected by the ionization chamber [10]. Following GB/T 12162.1, the N-60 narrow-spectrum (N-series) radiation quality was established. Cumulative charges were measured at pulse widths of 20 ms, 32 ms, 40 ms, 50 ms, 100 ms, and 200 ms under this quality, yielding the results shown in Table 1.

Table 1 Cumulative charge measurement results of pulsed X-rays in N-60 radiation medium

Pulse width/ ms	Cumulative charge/ pC
20	30.9
32	40.3
40	61.4
50	76.6
100	156
200	310

Performing a linear fit on the data in Table 1 yields Figure 3. Figure 3 shows how the accumulated charge measured with the TW32002 varies with pulse width under the N-60 radiation quality.

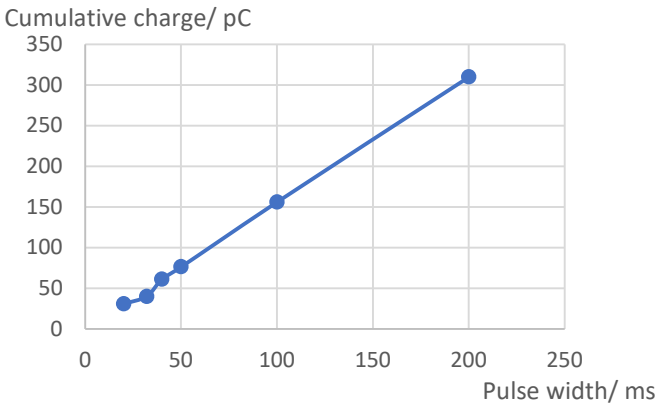

Figure 3 Linear correlation between cumulative charge and pulse width for the N-60 radiation quality

As shown in Figure 3, the cumulative charge recorded by the TW32002 ionization chamber exhibits a linear relationship with the tube current of the pulsed X-ray source, with a correlation coefficient of 0.998. This result indicates that the linear response of the TW32002 when measuring the cumulative charge of a single X-ray pulse is independent of the pulse width; in other words, the chamber possesses sufficient time-resolution capability for such measurements.

Using the validated measurement system, the cumulative charge Q in a steady-state γ-radiation field and the air kerma K_a were measured to derive their fitted relationship; the results are listed in Table 2.

Table 2 Measured cumulative charge and air kerma in the steady-state γ-radiation field

Cumulative charge, Q / pC	Air kerma, K_a/nGy
1.29	33.3
1.65	42.1
2.14	54.9
4.24	108
6.61	168
7.53	192
9.31	237
11.8	301

Linear fitting of the data in Table 2 gives the fitted relationship between air kerma K_a and cumulative charge Q:

$$K_a=25.5\cdot Q-0.07 \quad (3)$$

The measurement system was then used to measure the pulsed γ-radiation field. Under various aperture sizes and source speeds, the cumulative charge of the pulsed γ radiation was recorded and substituted into Eq. (3) to obtain the corresponding air kerma, with the results listed in Table 3.

Table 3 Measured cumulative charge and air kerma in the pulsed γ-radiation field

Aperture size / mm	Source speed / mm·s^{-1}	Nominal pulse width / ms	Cumulative charge / pC	Repeatability / %	Air kerma / nGy
100	100	1000	1.94	2.8	49.5
80	100	800	1.49	4.5	37.8
100	200	500	0.944	3.0	24.0
20	100	200	0.474	3.7	12.0
10	100	100	0.265	1.9	6.69
8	250	32	0.109	4.2	2.71

The repeatability in Table 3, calculated as the standard deviation divided by the mean of multiple measurements of the pulsed-γ cumulative charge, characterizes the stability of the pulsed-γ facility. It can be seen from the results that the air kerma measured with the ionization chamber increases with pulse width, ranging from 2.71 nGy to 49.5 nGy, and the repeatability does not exceed 4.5 %.

3.2 Pulse-width measurement of pulsed γ-rays

Pulsed signals exhibit a rapid rise to peak energy. The pulse width, t_w, i.e., the pulse duration, is defined as the time interval between the points on the leading and trailing edges at which the voltage reaches half of its maximum value [11]. The time-measurement system consists of a TW32002 ionization-chamber detector, a pre-amplifier circuit, and an oscilloscope. γ-rays passing through the ionization chamber generate voltage or current pulses, which, after amplification by the pre-amplifier, are displayed on the oscilloscope; the processed waveform is shown in Figure 4.

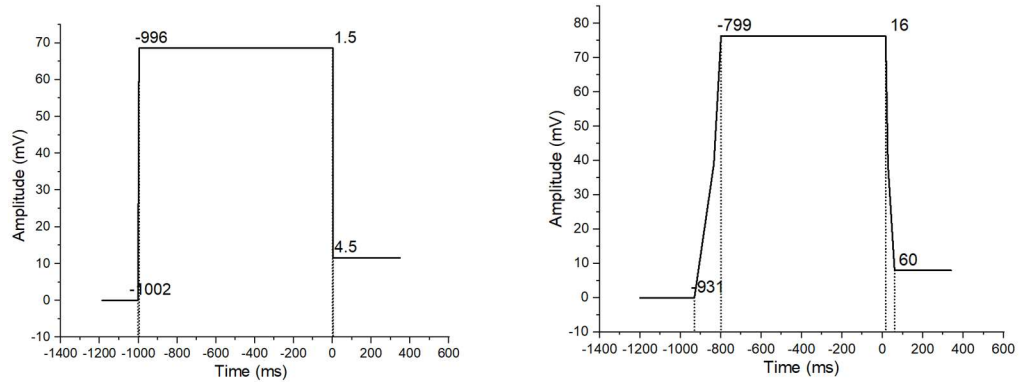

a) Nominal pulse width: 1000 ms b) Nominal pulse width: 800 ms

Figure 4 Measured waveform of the pulsed γ-radiation pulse width

The time-measurement system was then positioned in front of the pulsed γ-radiation source, and the pulse width was measured. During the experiment, the sensitive volume of the ionization chamber was suspended in air and aligned with the central axis of the source beam. Six nominal pulse widths were set—1000 ms, 800 ms, 500 ms, 200 ms, 100 ms, and 32 ms—and the corresponding actual pulse widths were recorded; the results are listed in Table 4.

Table 4 Measured pulse widths of the pulsed γ-radiation

Aperture size / mm	Source speed / mm·s^{-1}	Nominal pulse width / ms	Measured pulse width / ms	Relative deviation / %
100	100	1000	998	0.2
80	100	800	824	3.0
100	200	500	502	0.4
20	100	200	201	0.5
10	100	100	103	3.0
8	250	32	34	6.3

Table 4 shows that the relative deviation between measured and nominal values is small, with measured pulse widths generally exceeding the nominal widths. The larger deviation at short widths is likely due to: (1) greater statistical fluctuations when the ionization chamber measures narrow pulses; (2) millimetre-scale aperture sizes making the point-source approximation less valid; and (3) the linear actuator's actual velocity falling short of the preset value, so the source does not traverse the aperture for the intended duration.

3.3 Dose-rate measurement and uncertainty analysis of pulsed γ-rays

After determining the air kerma K_a and pulse width t_w of the pulsed γ-rays, the air-kerma rate ($\dot{K}_a$) is obtained by substituting these values into Eq. (4), as listed in Table 5.

$$\dot{K}_a = \frac{K_a}{t_w} \qquad (4)$$

Table 5 Dose-rate data for the pulsed γ-radiation field

Aperture size / mm	Source speed / mm·s^{-1}	Air kerma / nGy	Measured pulse width / ms	Air-kerma rate / μGy·h^{-1}
100	100	49.5	998	178
80	100	37.8	824	165
100	200	24.0	502	172
20	100	12.0	201	215
10	100	6.69	103	200
8	250	2.71	34	186

When analyzing the measurement uncertainty, corrections and contributions from temperature, pressure, radiation energy, actuator operation, ion-chamber positioning and calibration factor, cumulative-charge measurement, and pulse-width measurement were all taken into account; the combined results are summarized in Table 6.

Table 6 Uncertainty budget for dose rate in pulsed γ field

Source of uncertainty	Uncertainty / %	
	Type A uncertainty	Type B uncertainty
Temperature	0.39	
Pressure	0.06	
Actuator runtime		0.20
Radiation energy correction	0.29	
Ionization chamber positioning	0.58	
Ionization chamber calibration factor		1.6
Energy required to produce an elementary charge		0.2
Conversion process	0.5	
Pulse-width value	2.0	

Combining the results in Table 6 and applying Eq. (5), the combined standard uncertainty is calculated as u_c = 2.7 %. Consequently, the relative expanded uncertainty of the dose rate is U_{rel} = 5.4 % (k = 2). Combined standard uncertainty:

$$u_c = \sqrt{(\text{Type A uncertainty})^2 + (\text{Type B uncertainty})^2} \qquad (5)$$

In summary, the average air-kerma rate of the pulsed γ radiation at 1 m from the source ranges from 165 μGy/h to 215 μGy/h with a relative expanded uncertainty of 5.4 % (k = 2); the achievable pulse-width range is 34 ms to 998 ms.

4. Conclusion

A nuclear criticality accident can have severe consequences, so nuclear-fuel-related facilities are equipped with numerous criticality alarm systems. These systems are structurally simple but permanently installed; they cannot readily be dismantled for laboratory calibration, and the absence of practical pulsed-radiation sources has cast doubt on the validity of on-site measurements. To verify

the effectiveness of fixed alarm systems in situ, this study proposes a mobile pulsed γ-radiation device. Lead shielding thicknesses for the source storage and moving ends were calculated according to theoretical formulas, resulting in China's first mobile pulsed γ device. Dose and timing measurement systems were established, and pulsed γ-dosimetric experiments were conducted. Results show single-pulse air kerma values of 2.71 nGy–49.5 nGy, pulse widths of 34 ms–998 ms, and air-kerma rates of 165 μGy/h–215 μGy/h with a relative expanded uncertainty of 5.4 % (k = 2). The device features stable, adjustable source speed, good repeatability, a wide pulse-width range, and a modular design that facilitates transport to sites for on-site testing.

References

[1] Liu Xinhua, Wu Deqiang, Liu Hua, et al. Characteristics and consequences of nuclear criticality accidents [J]. Radiation Protection, 2001, 21(6): 369.

[2] State Bureau of Quality and Technical Supervision. GB 15146.9-1994 Nuclear criticality safety for fissile materials outside reactors: Performance and testing requirements for nuclear criticality accident detection and alarm systems [S]. Beijing: China Standards Press, 1994.

[3] Janardhanan S, Dabhadkar S B, Soman S D. Device for criticality monitor calibration, 1972.

[4] Qiao Fengpu, Jing Minqing, Liu Heng, et al. Study on pulsed X/γ radiation field generator [J]. Nuclear Electronics & Detection Technology, 2011, 31(9): 999-1003.

[5] Fang Dengfu, Tang Zhihui, Wei Yingjing, et al. Establishment of a high-dose-rate pulsed γ radiation facility [J]. Nuclear Electronics & Detection Technology, 2025, 45(02): 154-161.

[6] Xia Yihua, Chen Ling, Zhang Hongjian, et al. Advanced Course on Ionizing Radiation Protection [M]. Harbin: Harbin Engineering University Press, 2019.

[7] Xu Yang, Gao Fei, Zhao Rui, et al. Monte Carlo simulation of H*(10)/K_a conversion coefficients for mono-energetic photons and narrow spectra from 15 keV to 1.5 MeV [J]. Isotopes, 2022, 35(04): 311-316.

[8] Ministry of Health of the People's Republic of China. GBZ 125-2009 Radiological protection requirements for sealed-source gauges [S]. 2009.

[9] State Administration for Market Regulation. GB/T 12787-2020 Radiation protection instrumentation—Criticality accident alarm equipment [S]. Beijing: China Standards Press, 2020.

[10] Liu Chuanfeng, Zhang Xiaole, Li Dehong, et al. Dose measurement method for pulsed X-rays [J]. Journal of Harbin Engineering University, 2022, 43(11): 1642-1648.

[11] ISO/TS 18091-2015, Radiological protection—Characteristics of reference pulsed radiation—Part 1: Photon radiation [S]. 2015.

TOPICAL SESSION 5. 3D Radiation Mapping Using 3-D Pixelated CZT Detectors

Brian Kitchen, PhD [1]; Reid Sobota [1]; Chris Wahl, PhD [1]; Daivid Nestle [1]; Weiyi Wang, PhD [1 *]

[1] H3D, Inc., Ann Arbor, Michigan, USA

H3D, Inc. has developed a technique to combine the gamma-ray imaging capabilities that have been developed for 3D CZT detectors with spatial-awareness sensors to enable 3D radiation mapping. A prototype system was developed that achieves better than 1.1% FWHM at 662 keV, which enables the system to provide high accuracy isotope identification as well as quantification algorithms to determine the activity of each isotope present. The excellent spectroscopy also enables isotope-specific imaging of gamma-ray sources. The prototype system performs 3D imaging using two imaging modalities: coded aperture imaging for sources below 500 keV and Compton Imaging for sources above 250 keV.

This 3D imaging is achievable using spatial-awareness sensors to determine the position and orientation of the CZT detectors in relation to the surrounding environment. A LIDAR sensor is the primary sensor, and it also generates a point-cloud map of the area. The 3D radiation image that is generated is then overlaid onto the LIDAR map to enable the user to visualize where the gamma-ray sources are located. In real time, a top-down 2D projection of the room is shown to the user along with an overlay of the radiation image onto that projection. The data can then be transferred to a computer where it can be post-processed to generate 3D pictures of the radiation environment as well as perform additional analysis. Algorithms are under development to combine quantitative-analysis techniques that have been developed for use with 3D CZT gamma-ray imaging spectrometers with the results from the 3D imaging. This work will present the technology that was developed and how it works along with results collected from early testing of this prototype at commercial nuclear power plants and other facilities.

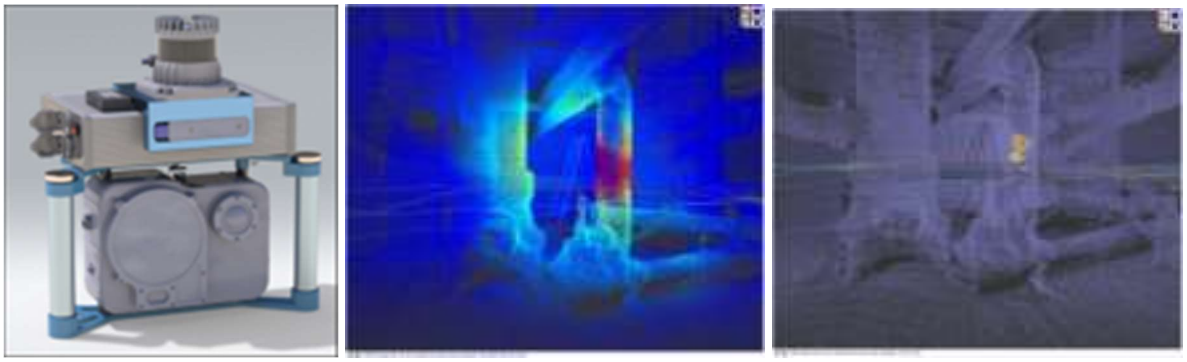

Figure 1: The prototype system (left); 3D surface reconstruction of a primary coolant pipe at a nuclear power plant (middle); full 3D reconstruction of the same pipe (right)

TOPICAL SESSION 6. The Development of the Self-Service WBC System and Its Application

Liye Liu[a], Xiaodun Li[a], Yunshi Xiao[a], Kairui Zhou[a], Yue Wang[b], Binjun Hou[c], Na Liang[b], Yu Wang[a], Yuan Zhao[a], Xiaofeng Guo[a]

[a] China Institute for Radiation Protection (CIRP), China

[b] Qinshan Nuclear Power Co., Ltd., China

[c] Jiangsu Nuclear Power Co., Ltd., China

Whole-body counter（WBC） is the most commonly used method for routine internal monitoring in nuclear power plants. And this measurement system mainly consists of the standing whole-body counter, such as ORTEC-StandFAST II, CANBERRA-FASTSCAN and CIRP-StandWBC. They are primarily designed for fast and accurate measurement of internal contamination of radionuclides with medium and high energy photons. However, the monitoring process is carried out by professional radiation protection staff who need to complete the entire process of personnel identity verification, measurement, result analysis, internal contamination confirmation, re-testing, personnel authorization, and other operations. The total measurement time for a single person is about 5 minutes, and the running time of the measurement system is limited by working hours, which cannot meet the temporary measurement needs.

This paper presents a self-service and automatic unattended WBC system. Under the premise of ensuring measurement quality, the WBC system has been optimized by adding self-service appointment systems, access control systems, automated measurement systems, sound and light signal guidance systems, etc., to achieve full process self-service operation for personnel to be measured, which can reduce labor costs in nuclear power plants, improve measurement efficiency and reduce operating costs. At present, the self-service WBC system has been applied to Qinshan Nuclear Power Plant and Jiangsu Nuclear Power Plant.

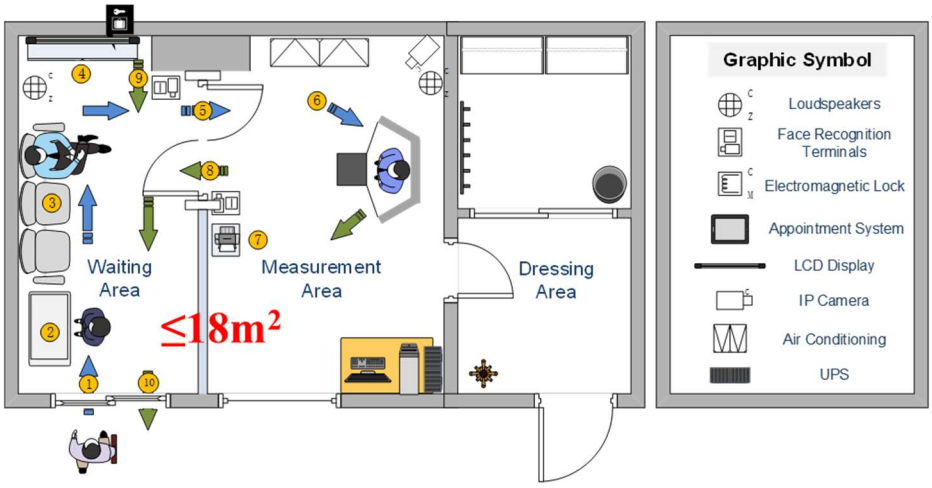

Features of the self-service WBC system include：

- 24-hour unattended operation.
- Automated process: appointment, measurement, analysis, and result submission.

- Remote monitoring and management.
- Low labor costs.
- Total measurement time for a single person is less than 3 minutes.

TOPICAL SESSION 6. Design of Thyroid/Lung Counter and Monte Carlo Simulation Study on Detection Efficiency

Yunpeng Wang [1,2,3], Qinjian Cao [1,2,3], Yuan Zhao [1,2,3], Yu Wang [1,2,3], Yunshi Xiao [1,2,3], Xiaodun Li [1,2,3], Yicong Liu [1,2,3], Yihai He [1,2,3]

[1] China Institute for Radiation Protection, Taiyuan, China

[2] Shanxi Key Laboratory for Radiation Safety and Protection, Taiyuan, China

[3] CNNC Key Laboratory for Radiation Protection Technology, Taiyuan, China

Abstract: In nuclear energy and radioactive operations, internal radiation monitoring is crucial to ensuring the health of occupational workers. In this study, a seat-type measurement system with thyroid and lung contamination monitoring capabilities was designed to address the internal exposure monitoring needs of nuclear facility personnel. Through structural design and Monte Carlo simulation, the lead shielding structure was optimized by determining the appropriate thicknesses of the collimated lead, floor shielding lead plates, and rear shielding plates, all while minimizing weight to ensure the system's portability and rapid on-site assembly. The design was validated to ensure that, within the 500 keV energy range, the detection efficiency of radioactive sources inside the human body model significantly exceeds the contribution from environmental sources. The Monte Carlo simulations were employed to establish the CIRP-RPT-1 torso model and IAEA/ANSI neck model, as shown in Figure 1. Detection efficiencies of the system across varying energy levels were calculated, and the simulation results were validated against experimental data. The results indicate that experimentally measured detection efficiencies in the low-energy region (e.g., 40 keV for lung counting and 31 keV for thyroid counting) exceeded Monte Carlo predictions by approximately 17–20%. At energies above 100 keV, discrepancies remained within 10%, demonstrating good agreement between experimental and computational results. The relatively large deviation observed in the low-energy region may be attributed to limitations in the accuracy of the geometric modeling and material parameter settings. More precise structural measurements and material characterization could enhance the simulation's accuracy, providing an important basis for subsequent instrument optimization and improvements in calibration methods.

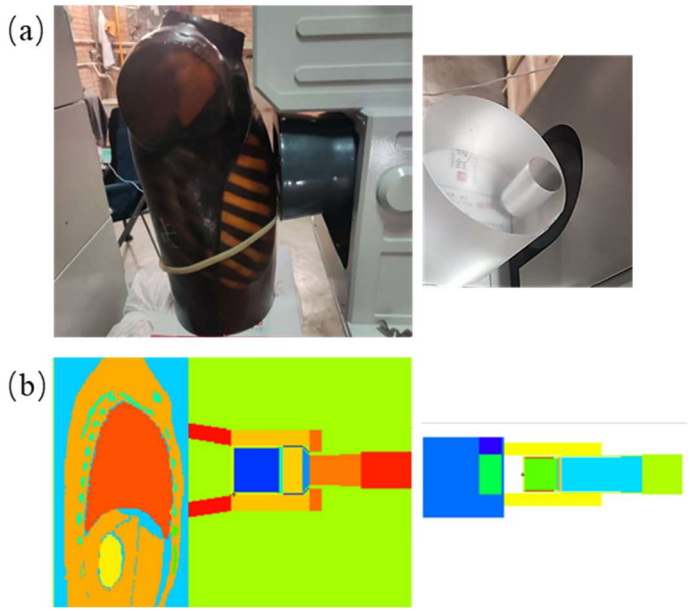

Figure 1 CIRP-RPT-1 torso model and IAEA/ANSI thyroid model experimental measurement and Monte Carlo simulation modeling.

Keywords: Thyroid/Lung Counter; Monte Carlo simulation; Detection Efficiency; Internal radiation monitoring

TOPICAL SESSION 6. Development of a New Skull Phantom for Calibrating In Vivo Monitoring Systems for Pb-210 Internal Contamination

YiCong Liu [1], WanChun Xiong [1], YunShi Xiao [1], XiaoDun Li [1]

[1]China institute for Radiation Protection, Taiyuan, China

Abstract: The internal exposure dose estimation formula is E=I·e(g), where I is the intake, and e(g) is the dose coefficient. Therefore, the intake I directly determines the committed effective dose, and the main purpose of internal exposure monitoring is to obtain the value of the intake I by measuring the retained activity in order to improve the accuracy of the intake I, a more effective measure is to calibrate the monitor to improve the measurement accuracy. In this paper, a new anthropometric skull phantom has developed and applied for calibration of skull counter.

The phantom's head circumference of is 56.18 cm, the total head height is 23.31 cm, the maximum head breadth is 15.76 cm, and the maximum head length is 19.23 cm which conform to the reference Chinese male [1] . The phantom consists of bone substitute and soft tissue substitute, the soft tissue substitute is polyurethane, and the hard bone substitute is a mixture of epoxy resin and calcium carbonate. At 46.5keV, the relative deviations between the mass attenuation coefficients of the two tissue equivalent materials and the reference values given by the ICRP [2] are 0.86% and -2.98%, respectively. The relative deviation of the mass attenuation coefficient of brain tissue and soft tissue at 46.5 keV is 5.03%, so soft tissue substitute can be used instead of brain tissue. The phantom was made by pouring. The mold is made by 3D printing.

In order to restore the bone-seeking nuclide distribution, the authors decided to simulate the surface source by evenly distributing point sources on the skull surface. The solution of the radioactive source was dropped on the filter paper, and after drying the filter paper was cut and attached to the corresponding position on the skull, and then the skull was suspended in the head mold. After the positioning was completed, soft substitute was poured and the radioactive sources sealed. The total Pb-210 content in the point sources is 4203 Bq.

The skull counter is a HPGe with the model of GEM40P4-76-S. The entrance window made of carbon. The crystal's radius is 40mm and length is 30mm. The measurement was carried out in a low-background laboratory, which is is 5m deep, surrounded by 0.5m concrete, embedded with 0.4m steel plates inside. The core part is composed of 20cm thick iron plates. The internal space is 2.3m long, 1.8m wide and 2.2m high. The dose rate in the core part is 26nGy/h. In order to ensure the consistency of multiple measurements, a limit device was designed for the phantom. The detector plane was close to the scalp during measurement. The average detection efficiency after three replicate measurements, was 3.07×10^{-4}cps/Bq. When the measurement time is 15min, the MDA is 378Bq

In this paper, an anthropometric skull phantom that conforms to the reference Chinese male is designed and manufactured. Using this model, the efficiency of the skull counter was evaluated, for accurate acquisition of Pb-210 retained in the radiation worker.

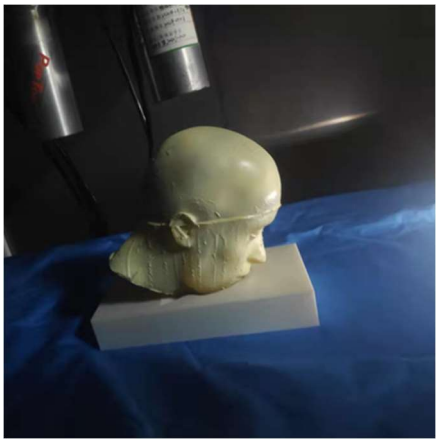

Figure 1. Photos of skull phantom measurement.

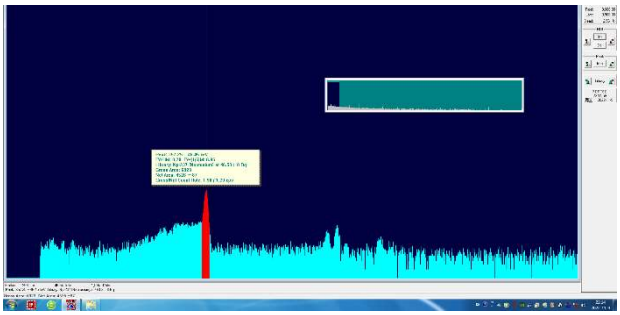

Figure 2. Spectrum using the skull phantom and HPGe system.

Keywords: anthropometric phantom, in vivo measurement, calibrating.

TOPICAL SESSION 6. Standardization Research on Analytical Monitoring Technology for ^{241}Am in Urine

Yipin Zhang, Hailin Lou, Zhiping Luo, Lixia Ren, Yifan Zheng, Rili Cong, Shaolin Wang
Department of Nuclear Safety and Environmental Engineering Technology, China Institute of Atomic Energy, Beijing, China

Abstract: ^{241}Am belongs to the alpha nuclides of the extremely toxic group, which will cause internal exposure hazards when inhaled into the human body. Urine sample measurement is one of the important methods for monitoring and evaluating the internal exposure of workers. In this paper, the analysis and monitoring techniques of internal irradiation urine samples were established by studying the pretreatment, separation and purification, electroplating and other factors of large volume urine samples. At the same time, the research on the monitoring and evaluation technology of the analysis technology in ^{241}Am was investigated. The results show that the chemical recovery rate of the established internal urine sample analysis and monitoring technology is 86.2%, the precision is 3.88%, the accuracy is less than 10%, the decontamination coefficient for Pu is greater than 1.0×10^{3}, the detection limit is 3.18×10^{-5} Bq/L. For 1.6 L 24 h urine sample, 360 d monitoring regular cycle, corresponding minimum measurable effective dose is 0.13 mSv, lower than the routine monitoring 2 mSv survey level. The analysis and monitoring techniques of internal irradiation urine samples is suitable for routine monitoring of urine samples in professional ^{241}Am and dose evaluation. The research results provide support for establishing the technical standard for the analysis and monitoring of ^{241}Am in urine.

Key words: ^{241}Am; urine sample; internal dose; routine monitoring and evaluation； Standard

TOPICAL SESSION 6. Study on the Standardization of Tritium Analysis in Urine and Internal Exposure Dose Assessment

Jinfeng Li, Hailin Lou, Mingyu Li, Rili Cong, Jingshun Pan, Man Zhang, Yi Liu, Shaolin Wang, Zhiping Luo, Lixia Ren

Department of Nuclear Safety and Environmental Engineering Technology, China Institute of Atomic Energy, Beijing, China

Abstract: During the processes of nuclear power plant operation, nuclear reprocessing, nuclear technology application, nuclear decommissioning, and nuclear fusion research, the generation and release of tritium (^{3}H) are inevitable. Tritium is a low toxicity β radionuclide, but it is highly diffusible. It can enter the human body through inhalation, ingestion, and other pathways, causing internal exposure hazards. The International Commission on Radiological Protection (ICRP) recommends urine measurement to estimate tritium intake and internal exposure dose. In this study, the oxidation distillation and liquid scintillation counting were used to measure the tritium activity concentrations in urine. The results show that for a 1 L urine sample, after distillation, 8 mL of the sample was taken for liquid scintillation counting measurement, with a sample measurement time of 180 min, and the taction limit was 3.13 Bq/L. This detection limit meets the requirements for routine monitoring of tritium internal exposure and dose assessment for workers. The results provide support for the establishment of technical standards for tritium analysis and monitoring in urine as well as internal exposure dose assessment.

Key words: ^{3}H; urine sample; internal dose; routine monitoring and evaluation; standard

TOPICAL SESSION 6. Analysis of the Establishment of Monitoring Period and Measurement Duration for Personal Dose Of Internal Exposure

Zheng Lu, Yuqin Li

China Institute of Atomic Energy, Beijing, China

Abstract: To develop a reasonable personal dose monitoring plan for internal exposure, this paper introduces three representative types of radionuclides and their associated monitoring methods for personal dose assessment using direct measurement techniques. This introduction is based on relevant domestic and international standards and considers available internal exposure measurement equipment. The paper summarizes the derivation process for determining the monitoring period and measurement duration. First, the maximum monitoring period is analyzed for each radionuclide according to its retention characteristics and reporting standard requirements, satisfying the conditions $m(1)/m(T/2) \leq 3$ and $m(T/2)/m(T) \leq 3$ (where m(t) is the retained activity at time t). Second, the corresponding instrument's lower detection limit (LDL) is derived based on the monitoring period and the nuclide's Annual Limit on Intake (ALI), ensuring this LDL is lower than the nuclide's Derived Minimum Detectable Level (DMDL). Finally, the required instrument measurement time is derived from the instrument's LDL and the maximum monitoring period. This derivation process provides a valuable reference for formulating personal dose monitoring plans for internal exposure.

Keywords: Internal exposure monitoring；Monitoring period；Measurement duration；Personal dose

With the development of the nuclear industry, radiation protection for radiation workers is continuously improving. Based on relevant standards, regulations, and reporting parameters for internal exposure monitoring, this paper addresses uncertainties in personal internal dose monitoring using direct measurement methods and explores how to establish the monitoring period and measurement duration in individual internal dose monitoring plans.

1 Materials and Methods

Based on the characteristics or types of radionuclides potentially ingested by monitoring subjects, we selected three representative radionuclides as examples:

I-131 (short half-life/thyroid deposition);

Cs-137 (artificial nuclide/whole-body distribution);

Am-241 (transuranic nuclide/low-energy γ-rays).

The instruments used for monitoring these nuclides correspond to three measurement devices:

Thyroid I-131 Counter.

Whole-Body Counter.

Lung Counter.

These instruments monitor radionuclides deposited in different body parts and with different deposition patterns. Instrument parameters are listed in Table 1:

Table 1 Parameters of the moniting instrument

Instrument Name	Thyroid I-131 Counter	Whole-Body Counter	Lung Counter
Purpose	I-131 internal exposure measurement in thyroid	Whole-body internal exposure measurement	Internal exposure measurement in lungs
Typical Measured Nuclide	I-131	Cs-137	Am-241
Detector Crystal Type	NaI(Tl)	NaI(Tl)	BEGe
Energy Resolution	8.33%(661.7keV)	8.07%(661.7keV)	2.382keV(1332.5keV)
Calibration Model	Thyroid Model (IAEA/ANSI)	Whole Body Model (BOMAB)	Lung Model (LLNL)
Detection Efficiency	4.02E-02 (364.5keV)	3.54E-03 (661.7 keV)	6.59E-03 (59.5 keV, chest wall thickness 3 cm)
Background Count Rate	0.09 cps (I-131 energy region/public sample)	3.76 cps (Cs-137 energy region/public sample)	12.72 cps (Am-241 energy region/public sample)
Detection Limit	24Bq(I-131/300s)	124 Bq (Cs-137 / 600 s)	26 Bq (Am-241 / 600 s)

1.1 Thyroid I-131 Counter

Used for monitoring I-131 deposited in the thyroid. Measurement involves aligning the instrument with the neck. The probe uses a sodium iodide (NaI) crystal. Calibration follows IAEA/ANSI-N13.44-2014 standards. Background: 0.09 cps (average of 10 public samples). Detection limit: 24 Bq (300 s).

1.2 Whole-Body Counter

Used for monitoring uniformly distributed radionuclides. Measurement is a head-to-toe scan. Calibration uses a BOMAB phantom and Cs-137 sources. Background: 3.76 cps. Detection limit: 124 Bq (600 s).

1.3 Lung Counter

Used for monitoring radionuclides deposited in the lungs. Measurement uses two detectors aligned with the lungs. The probe uses a Broad Energy Germanium (BEGe) crystal. Calibration uses an LLNL lung model and Am-241 sources. Background: 12.72 cps. Detection limit: 26 Bq (600 s).

2 Results

The derivation process for monitoring period and measurement duration is as follows:

1. Establish the maximum monitoring period based on nuclide retention characteristics and standard requirements to satisfy:$m(1)/m(T/2)\leq 3$, $m(T/2)/m(T)\leq 3$;
2. Derive the instrument's required detection limit from the monitoring period and Annual Limit on Intake (ALI), ensuring it is below the Derived Monitoring Detection Limit (DMDL);
3. Calculate the measurement time based on the instrument’s detection limit and the maximum monitoring period.

2.1 Factors in Monitoring Period Design

2.1.1 Impact of Intake Estimation Uncertainty

International standards (ICRP-54, ICRP-78, IAEA-RS-G-1.2) and Chinese standard GBZ 129-2016 require that uncertainty due to unknown intake timing within the monitoring period should not exceed a factor of 3. For routine monitoring, intake is assumed to occur at the period midpoint. Extreme cases (intake at period start/end) demonstrate:

Intake at period end → Overestimation by factor $m(1)/m(T/2)$.

Intake at period start → Underestimation by factor $m(T/2)/m(T)$.

To limit bias to ≤3, the monitoring period T must satisfy:

$$m(1)/m(T/2)\leq 3 \text{ ， } m(T/2)/m(T)\leq 3$$

Maximum Monitoring Periods Under Constraints are listed in Table 2:

Table 2 Maximum Monitoring Periods Under Constraints

Nuclide & Type	I-131/Thyroid/Inhalation (F, AMAD=5 μm)		Cs-137/Whole Body/Inhalation (F, AMAD=5 μm)		Am-241/Lungs/Inhalation (M, AMAD=5 μm)	
Reference Standard	GBZ129-2016	ICRP-137	GBZ129-2016	ICRP-137	GBZ129-2016	ICRP-141
m(1)	1.20E-01	1.60E-01	6.00E-01	6.30E-01	5.80E-02	5.80E-02
m(T/2)	4.34E-02	6.80E-02	2.00E-01	2.10E-01	1.93E-02	1.94E-02
m(T)	2.59E-02	2.50E-02	9.07E-02	7.65E-02	7.57E-03	9.08E-03
Max Monitoring Period	26d	23d	252d	279d	228d	232d

2.1.2 Limitations from Instrument Performance

The instrument's detection limit must be below the DMDL, derived as:

$$ALI = \frac{0.001}{e(50)}$$

$$DMDL = \frac{0.95 \times ALI \times T \times m(T/2)}{365}$$

where e(50) = committed effective dose coefficient (Sv/Bq).

DMDL Under Constraints are listed in Table 3:

Table 3 DMDL Under Constraints (Committed Dose Limit = 0.001 Sv)

Parameter	I-131/甲状腺/吸入/F 类 /AMAD=5 μm		Cs-137/全身/吸入/F 类 /AMAD=5 μm		Am-241/肺部/吸入/M 类 /AMAD=5 μm	
DMDL (Bq)	2.67E+02	3.70E+02	1.96E+04	1.64E+04	4.24E-01	1.46E+00
Lab Instrument DL (Bq)	24(300s)		124(600s)		26(600s)	

The lab's instruments meet DMDL requirements for I-131 and Cs-137 but not for Am-241. Solutions: upgrade equipment, shorten monitoring period, increase measurement time, or switch to bioassay (e.g., urine monitoring).

2.2 Optimization of Measurement Duration

Increasing measurement time reduces the detection limit. For Am-241 lung monitoring:

$$MDA = \frac{4.65\sqrt{N_b} + 2.71}{t \cdot \varepsilon \cdot p_\gamma}$$

where N_b = background counts, t = measurement time (s). Required Measurement Time for Am-241 are listed in Table 4:

Table 4(a) Required Measurement Time for Am-241 (Dose Limit = 0.001 Sv)

Reference Standard	Monitoring Period (d)	DMDL (Bq)	Detection Efficiency	Measurement Time (s)
GBZ129-2016	228	4.24E-01	6.59E-03	1.94E+06
ICRP-141	232	1.46E+00	6.59E-03	1.65E+05

Table 4(b) Required Measurement Time for Am-241 (Dose Limit = 0.02 Sv)

Reference Standard	Monitoring Period (d)	DMDL (Bq)	Measurement Time (s)
GBZ129-2016	228	8.48	5200
ICRP-141	232	229.3	480

Note: For Am-241/lungs/inhalation (M, AMAD=5 μm).

3 Discussion

Establishing the monitoring period and measurement duration is critical for credibility and cost efficiency. This paper provides a systematic derivation process:

1. Determine maximum monitoring period based on retention and standards.
2. Derive DMDL from the period and ALI.
3. Calculate measurement time from DMDL and instrument performance.

This methodology can applies to other nuclides or γ-ray monitoring scenarios. Current standards for internal exposure monitoring in China need further refinement to align with international updates.

References

[1] International Commission on Radiological. ICRP Publication 54. Individual Monitoring for Intakes of Radionuclides by Workers: Design and Interpretation[R]. 1988.

[2] International Commission on Radiological. ICRP Publication 78. Individual Monitoring for Internal Exposure of Workers[R]. 1997.

[3] International Atomic Energy Agency. IAEA Safety Reports Series No. RS-G-1.2 Assessment of Occupational Exposure Due to Intakes of Radionuclides[R]. Vienna：IAEA, 1999.

[4] International Atomic Energy Agency. IAEA Safety Reports Series No.37(2004), Methods for Assessing Occupational Radiation Doses Due to Intakes of Radionuclides[R]. Vienna：IAEA, 2004.

[5] 国家卫生和计划生育委员会. GBZ 129—2016 职业性内照射个人监测规范[S].2016.

National Health and Family Planning Commission of PRC. GBZ 129—2016 Specifications for individual monitoring of occupational internal exposure [S].2003.

[6] International Commission on Radiological. ICRP Publication 137 publication Occupational Intakes of Radionuclides:Part 3[R]. 2017.

[7] International Commission on Radiological. ICRP Publication 141 publication Occupational Intakes of Radionuclides:Part 4[R]. 2019.

[8] 国家质量监督检验检疫总局. GB 18871—2002 电离辐射防护与辐射源安全基本标准[S]. 北京：中国标准出版社，2003.

General Administration of Quality Supervision, Inspection and Quarantine of the People's Republic of China. GB 18871—2002 Basic standards for protection against ionizing radiation and for the safety of radiation sources [S]. Beijing: Standard press of China ,2003.

[9] 国家卫生和计划生育委员会. WS/T 584—2017 人体内放射性核素全身计数测量方法[S].2017.

National Health and Family Planning Commission of PRC. WS/T 584—2017 Methods for measuring radionuclides in the human body with whole body counts [S].2017.

TOPICAL SESSION 6. Impacts of Legacy Uranium Sites on Agricultural Ecosystems

Chenxiao Wang[1, 2, *], Qifan Wu[1], Senlin Liu[2], Jiaqing Guo[3], Shoulong Xu[1,4], Xiaogang Li[5,6]

[1]Department of Engineering Physics, Tsinghua University, Beijing, China

[2]China Institute of Atomic Energy, Beijing, China

[3]Minnan Normal University, Zhangzhou, China

[4]University of South China, Hengyang, China

[5]Fudan University, Shanghai, China

[6]Jiangxi Provincial Radiation Environment Supervision Station, Nanchang, China

To address radiological issues surrounding a legacy uranium mining and milling site, this study systematically evaluates the migration behavior of Uranium-238 (^{238}U) within the "soil–irrigation water–rice" system and its organ-specific distribution within rice plants. Effluents from uranium ore processing are discharged, after treatment, into rivers that irrigate nearby paddy fields. Over time, soils have absorbed ^{238}U from these waters, leading to elevated radioactivity levels. Rice grown in the area accumulates ^{238}U from both soil and irrigation water, showing increased activity concentrations across different plant tissues.

To quantify this, field samples of river water, agricultural soil, and rice plants were collected. Activity concentrations of uranium isotopes were analyzed to assess the regional radioecological profile. Background radioactivity levels in the local water body—measured at the highest-elevation drinking water source—were 15–32 mBq/L for gross α, 71–91 mBq/L for gross β, and 3.7–15.4 mBq/L for ^{238}U. In total, 16 river water samples were collected across the study area, with ^{238}U activity concentrations ranging from 0.25 to 2.55 Bq/L—approximately 10 to 100 times higher than background levels. Six soil-rice paired samples were obtained, with soil ^{238}U concentrations between 50 and 580 Bq/kg, representing 1.5 to 17.6 times the national soil average (33 Bq/kg). In rice, dry straw samples exhibited ^{238}U levels of 0.1–9.1 Bq/kg, while polished rice grains ranged from 0.074 to 0.457 Bq/kg. Although these values exceed typical global grain reference levels by one order of magnitude, they remain well below China's regulatory limits for food radioactivity.

Using the measured transfer factors, the average annual effective dose from ^{238}U ingestion via rice consumption by local adults was estimated. Notably, disregarding the differential uptake between edible (grain) and non-edible (straw) parts would result in an overestimation of population doses by approximately one order of magnitude.

A multi-compartment kinetic transfer model was established. Using differential equations, the model simulates time-dependent radionuclide migration pathways within the soil–plant system. Model predictions for ^{238}U distributions in straw and grain aligned well with measured values, demonstrating its utility in forecasting radionuclide uptake kinetics under varying environmental scenarios.

TOPICAL SESSION 7. Optimization Suggestions for Classified Collection and Treatment Methods of Scrapped Protective Articles in Nuclear Power Plants

Yu Zhang[1], Yuan Hu[1], Quanlu Gou[1]

[1]Shandong Nuclear Power Company Ltd, Haiyang, Shandong, China

Abstract: Among the radioactive dry waste generated by nuclear power plants (NPPs), various types of scrapped personal protective articles (PPE) from the radiation control area account for a relatively high proportion. According to statistical data from one NPP, scrapped PPE can account for over 15% of the total radioactive dry waste generated. Establishing detailed implementation rules for targeted classified collection, disassembly, sorting, detection, and cleaning/decontamination for different types of scrapped PPE enables the following: some scrapped PPE can be directly treated as non-radioactive waste after detection; some can be reused as cleaning rags in the radiation control area after simple treatment; and most PPE can meet clearance standards and be cleared. Compared with traditional radioactive dry waste treatment methods (such as supercompaction with grouting or incineration), this approach can significantly reduce the amount of radioactive waste generated, lessen the environmental impact, reduce NPP operating costs, and comply with HAD 401/08-2016 "Guideline on Minimization of Radioactive Waste from Nuclear Facilities".

Keywords: Scrapped protective articles; Classified treatment; Reuse; Clearance

TOPICAL SESSION 7. A Brief Introduction of Thermal Treatment and Clearance Technology of Radioactive Wastes for Nuclear Power Plants

Ming Han

Huaneng Shandong Shidao Bay Nuclear Power Co., Ltd., Rongcheng,China

Abstract: According to administrative requirements of minimizing radioactive wastes,and the rules of thermal treatment and clearance of radioactive wastes,combined with experience of thermal treatment and clearance,the report analyzes the technology of thermal treatment and clearance of radioactive wastes produced by nuclear power plants,and give suggestions for improvement.

Key words: nuclear power plant;thermal treatment;burning;Plasma;clearance

Introduction

The CPC Central Committee mentioned the requirement of developing clean energy in the report of the 20th National Congress, and in April 2022, the National Energy Administration and the Ministry of Science and Technology jointly put forward the requirement of actively and orderly safe development of nuclear power. China's nuclear power industry ushered in a new development opportunity, in the process of the development and use of nuclear energy will inevitably produce radioactive waste, if these radioactive wastes cannot be safely and properly dealt with will become a key factor restricting the development of nuclear power, in order to ensure the safe and healthy development of nuclear energy safety science and technology to provide high quality, clean and efficient energy for the national economy, it is necessary to safely deal with the radioactive wastes produced by the nuclear power plant.

After decades of development of China's nuclear industry, the recognition and treatment technology of radioactive waste generated by nuclear power plants have also been continuously upgraded, from the previous compression of temporary storage in landfills, to the back of the solidification and fixation technology, and even the use of HIC high-integrity containers, the radioactive waste of nuclear power plants have been more safely handled. However, the concept of radioactive waste minimisation, which is widely recognised internationally, has challenged the capacity-enhancing waste fixation technology. For this reason, China's nuclear power engineers and technicians, combined with the practice of foreign counterparts and their own research, have put forward specific treatment measures of heat treatment and clean decontamination, which have greatly reduced the volume of waste, and at the same time, through the operation and overhaul period of good source control, the initial volume of waste generated by the nuclear power plant has also been controlled. According to statistics, the proportion of decontrollable materials in the operation process of nuclear facilities is about 20-30%, and the radioactive waste generated by the operation and overhaul of large-scale nuclear power plants that can be cleaned and decontrolled accounts for about 80% of the total volume of the waste, so the radioactive waste of nuclear power plants has a broad potential for clean decontrol.

At the beginning of this century, European and American countries carried out a long period of research on clean decontrol, formulated relevant technical guidelines and carried out a variety of radioactive waste materials clean decontrol practices, including heat treatment operations. IAEA also

summarised the international practice, further promoting the research and application of clean decontrol technologies, including heat treatment, greatly promoting the minimisation of radioactive waste and safeguarding the healthy development of the nuclear power industry. healthy development of the nuclear power industry. This report will analyse and explain the international status of thermal treatment and CDC management, as well as the domestic research and application of the technologies, and make recommendations for improvement.

1 International status of thermal treatment and CDM

1.1International status of thermal treatment technology development

The thermal treatment mentioned in this report is the technology that uses the principle of high-temperature pyrolysis and incineration to treat radioactive wastes. Thermal treatment is the most effective volume reduction technology for combustible wastes with a low specific activity and produces ash that can be easily processed into a stable form suitable for disposal. Thermal treatment is an exothermic reaction. In many cases, the combustion of the waste itself provides sufficient heat to sustain the thermal reaction. In some cases, supplementary fuels such as natural gas are required. Thermal treatment is a promising technology that is currently being used in many foreign countries, such as Switzerland, Japan, Korea, Australia, the United States, the United Kingdom and Canada, as a means of treating combustible (organic containing) wastes.

The combustibility of organics makes thermal treatment an ideal technology for the complete destruction of organics, with the ability to achieve high reduction ratios, e.g. more than 25:1 in plasma melting theory, and to convert the waste into a form suitable for immobilisation and disposal (fly ash slag). Fully thermally treated wastes have carbon dioxide, water and oxides consisting of other components such as nitrogen, sulphur and metal oxides. Thermal treatment can be used for both dry and wet wastes.

As thermal treatment cannot change the radioactive elements, the activity level during thermal treatment needs to be controlled below the personal dose limit level. Since the tail gas produced by thermal treatment contains radioactivity, it requires a well-equipped tail gas purification system, which results in high investment and operating costs.

At present, the main types of thermal waste treatment facilities put into application abroad are incinerators and plasma melting furnaces. Now some typical application facilities are introduced. (1) the United States Los Alamos National Laboratory controlled air incinerator (CAI) for uranium and mixed fissile material containing waste treatment, which mainly includes incinerator equipment (the main combustion chamber, the intermediate combustion chamber and the second combustion chamber), the exhaust gas treatment system and the relevant auxiliary systems, the results of its long-term operation shows that the annual average release of mixed fissile material and plutonium concentration fluctuations in the detection limit or so. (2) The Rocky Flatts Fluidised Bed Incinerator (FBI) in the United States recovers plutonium mainly from large quantities of waste. Its exhaust gas treatment system consists of a set of sintered metal filters, a process gas heat exchanger and a four-stage HEPA filter. The FBI has only been tested intermittently (over two years) and has been assessed to have very low measured radionuclide concentrations of less than 10 nCi/g, with a waste volume reduction multiplier of 23:1.(3) The Karlsruhe Nuclear Research Centre (KFK) incinerator in Germany Designed by NUKEM, one incinerates β/γ nuclide-contaminated solid waste and one incinerates α nuclide-contaminated solid waste. The former of these is a typical vertical excess air incinerator. The furnace body is 6 m high, lined with refractory bricks after 0.5 m, with an inner

diameter of 1 m at the top and shrinking to 0.4 m at the bottom. The heat of combustion of the waste keeps the furnace temperature at 1000°C. The waste is cleaned by the exhaust gas cleaning equipment. The flue gas purified by the exhaust gas cleaning equipment is mixed with the ventilation exhaust of the workshop after the induced draft fan and discharged through a 70m high chimney.The KFK incinerator does not require crushing and strict sorting of the waste. The ash produced by the incinerator is first loaded into 180L thin-walled steel drums, and then pressed into cakes with a 1500t compactor, and a number of cake bags are loaded into a 200L steel drum, and finally 14 such drums are put into a 7.2m3 square steel container, with the voids filled with cement slurry, and the total volume reduction ratio is 45.(4) In order to deal with the different organic radioactive wastes, the German company REW NUKEM has designed a pebble bed high-temperature pyrolysis incinerator, which is very successful in converting organic matter into chemically inactive products. The reactor can be operated as a decomposer, evaporator or dryer. This versatility makes it possible to treat all types of liquid wastes and organic solid wastes. The dried products from the incineration can be stored directly in suitable containers or fixed immediately, because the pyrolysed resins are chemically stable, they can be mixed with cement at a higher inclusion factor than untreated resins, and the final volume of the cement curing is significantly reduced by a factor of greater than 5 for spherical resins, and a factor of greater than 5 for powder resins. The incinerator is also divided into feeding system, high temperature reactor, flue gas cleaning and fine filtration system, the incinerator can be operated continuously 24 hours a day, 5 days a week.

Plasma incineration, a novel thermal treatment technology, uses a plasma arc to generate temperatures in excess of 2,000°C. This high temperature supports the combustion of the organic components of radioactive waste and the melting of inert waste components. The exhaust gases from the plasma treatment of the waste pass through an afterburning chamber or a catalytic converter (for complete combustion), followed by appropriate treatment of the exhaust gases. The slag, which contains most of the radioactivity, is transferred to an external container for cooling. Usually, the solid residue is considered suitable for direct storage and disposal, and glass packets are usually added to the melting furnace to induce the slag to form a stable glass solid, which can be easily immobilised for disposal. Fly ash from the tail gas treatment process as secondary waste will be the feed to the plasma incinerator. The first international industrial plant for the treatment of LLRW, the Plasma Centrifuge Treatment Facility PACT, was built at the ZWILAG plant in Sweden. Similar installations include the KAERI plasma waste treatment facility in Daejeon, Korea, and the Japan Atomic Power Company (JAPC) plasma arc centrifugal LLRW treatment facility, where the suitability of the melted and immobilised products for disposal was verified prior to the treatment of LLRW mixed solid waste from a nuclear power plant, and the results of the technology have been satisfactory in terms of the containment of radionuclides. For the treatment of radioactive waste resins, Fuji Electric Power Co. Ltd. of Japan has developed a system for volume reduction of resin wastes by low-pressure plasma. The process consists of two steps: in the first step, plasma gas-phase oxidation. Low volume reduction (1/4-1/5) is achieved; the second part directly oxidises the ion exchange resin to achieve high volume reduction (1/10-1/20). Volume reduction to 1/20th of the original waste is achieved at a waste treatment rate of 2 L/h. PGM plasma gasification melting systems have also been developed by SIA RADON of Russia, a major nuclear power, and are planned by the plant, Pluton, for the co-processing of solid organic wastes with waste insulation, concrete, glass fragments, construction waste and other fusible materials. The waste is added to the shaft furnace until it is full and remains at that level for the duration of the operation. The shaft furnace is heated with a plasma generator. Inside the shaft furnace the waste is progressively dried, gasified, burned, slag is formed and melted. The exhaust gases are cleaned by means of an exhaust gas treatment system. The exhaust gas treatment system consists of an afterburner, a chemical gas neutralisation unit, a catalytic toxic gas neutralisation unit

and a two-stage radioactive aerosol trap. The main advantage of the shaft furnace is the ability to process unsorted waste with a high reduction ratio.

1.2 International Status of Cleaner Decontamination Management

1.2.1 IAEA Technical Guidelines on Cleaner Decontamination

The 2004 safety guideline IAEA-RS-G-1.7 specifies that the primary radiological basis for the development of activity concentration limits for cleaner decontamination is an annual effective dose to an individual of less than or equal to 10 uSv. Consideration is given to the occurrence of low-probability events that may result in higher radiation exposures, and an additional guideline is used that the annual effective dose resulting from such low-probability events should be no more than 1 mSv. The annual effective dose resulting from such a low probability event should not exceed 1 mSv, with an equivalent dose criterion of 50 mSv/a to the skin.

The basic safety standard BSS GSR-Part 3 published by IAEA in 2014 proposes that the guideline for the clean decontrol level is the personal irradiated dose. It defines the clean decontrol level as "the value, expressed in terms of activity concentration, specified by the regulatory authority, at or below which a radiation source in recorded or authorised practice may no longer be subject to regulatory control". Clean decontrol should therefore be a regulatory process prescribed by the regulator.

Based on the BSS GSR-Part 3 Basic Safety Standard published in 2014, IAEA revised the IAEA-RS-G-1.7-2004 Safety Guidelines in 2018, in which clean decontrol is discussed separately in the guideline DS500, which covers the following main topics: the regulatory framework for clean decontrol, the process of clean decontrol, the different physical forms of materials for DS500 mainly covers the following contents: cleaning and decontrol management framework, cleaning and decontrol process, decontrol of materials in different physical forms, conditional cleaning and decontrol and other related contents.

1.2.2 Management of CDD in Europe and the US

The US Nuclear Regulatory Commission (NRC) (formerly the Atomic Energy Commission (AEA)) has been researching the CDD of minor radioactive contaminants since the 1940s. In 1957, the AEA developed a radiation protection standard that exempted materials from regulatory control if their radionuclide concentration was below a certain value. 1964 saw an attempt in the US to establish a uniform standard for CDD but it was limited to surface contamination. In the 1980s and 1990s, the NRC developed dose guidelines for cleanup and decontamination, as well as activity limits for surface and body contamination of radionuclides, which were promulgated as national standards. 2003 saw the promulgation of the NRC's NURGE-1640 series of reports on the evaluation of radioactivity in cleanup and decontamination of materials generated at nuclear facilities, which provide a complete description of the potential individual-year risk factors associated with cleanup and decontamination of a given material. The NURGE-1640 recommended decontamination levels are greater than the IAEA recommended limits. Ultimately, the NRC developed the concept of "negligible dose levels" and recommended a personal dose guideline of 10 uSv/a for solid material cleaning and decontamination.

The European Commission EC has issued a series of requirements for radiation protection RPs to implement exemptions and clean decontrol, and the 1996 Council Regulation (EC) "Establishment of Basic Safety Standards for the Protection of Workers and the Public Against the Risks posed by Ionising Radiation to Their Health" put forward guidelines for clean decontrol limits of 10uSv/a.

France classifies radioactive waste into six categories without the concept of clean decontrol, and manages all lower level wastes according to the very low level wastes; Germany classifies radioactive wastes into four categories, and manages all wastes below the low level using clean decontrol. Germany classifies radioactive waste into four major categories and manages all waste below the low level with CDD, proposing that unconditional CDD applies to buildings, building rubble and sites, and conditional CDD applies to incineration waste, building demolition and molten metal, etc. In 2010, the EC published the RP Series No. 157, which compares the level of CDD with the IAEA system, and it can be seen that the two systems have different levels of CDD and the level of cleanliness. The comparison shows that both adopt the dose guideline of 10uSv/a for clean decontrol, the difference is that the IAEA system mainly considers clean decontrol according to different exposure paths, while the EC system is divided into unconditional decontrol and conditional decontrol.

Europe and the United States through the practice of radioactive waste treatment in power plants, gradually on the exemption and clean decontrol of the formation of the corresponding management regulations and guidelines, although the understanding of different countries on the clean decontrol of slightly different, but all point to the personal dose guideline of 10uSv/a, which makes the nuclear power plant on the treatment of very low level of radioactive waste has a new option, through the decontamination of the disposal of radioactive wastes can be better achieved by minimising. The decontrol can better minimise the disposal of radioactive waste. Europe and the United States nuclear power plants on the practice of clean decontrol also provides a strong basis for waste minimisation. The waste package generation of pressurised water reactor (PWR) nuclear power plants in Europe and the United States is shown in Table 1.

Table 1 Median and optimal level of annual generation of single-unit waste packages of pressurised water reactor (PWR) nuclear power plants in the world's major nuclear energy countries

Country	United States	France	Japan	Spain	Belgium	South Korea
Median annual generation of single-unit waste package, m^3	20	84	8	46	23	52
Optimal level of annual generation of single-unit waste packages,m^3	7	45	6	30	21	11

2 Development status of domestic thermal treatment and clean decontamination

2.1 Domestic waste management standards and requirements

The Clean Decontamination Level for Recycling and Reuse of Iron and Steel, Aluminium, Nickel and Copper from Nuclear Facilities (GB/T 17567-2009), which was promulgated and implemented by the State General Administration of Quality Supervision, Inspection and Quarantine (AQSIQ) in 2009, stipulates the clean decontamination level for the recycling and reuse of Iron and Steel, Aluminium,

Nickel and Copper materials, equipment and tools generated from the operation and decommissioning of nuclear facilities. Decontamination level, including surface pollution and body pollution level. The surface contamination level stipulated in this standard is consistent with that in GB 18871-2002, and the body contamination level mentioned in this standard is derived from 10uSv/a individual dose and 1 person Sv/a collective dose for the purpose of recycling and reuse through the possible reuse pathways of different metal materials. This standard is also the reference basis for conditional clean decontamination in China.

The activity concentration of radionuclides in materials exempted from radiation protection supervision (GB 27742-2011) promulgated and implemented by AQSIQ in 2011 stipulates that the activity concentration of radionuclides exempted from radiation protection supervision refers to the IAEA Safety Guidelines on "Application of the concepts of exclusions, exemptions and decontrols" (IAEA RS -G-1.7-2004), which can be regarded as unconditional clean decontrol limits.

In 2016, the National Nuclear Safety Administration (NNSA) issued "Radioactive Waste Minimisation at Nuclear Facilities" (HAD 401/08-2016), which provides guidance on radioactive waste minimisation at nuclear facility design, construction, operation and decommissioning units. It requires separate collection of solid waste at the place of generation, setting up necessary sorting devices and equipping radiation monitoring instruments with applicable accuracy to facilitate the sorting of wastes with different activity levels, especially the sorting of non-radioactive wastes and wastes slightly contaminated by radionuclides that can be cleaned and decontrolled after storage decay from radioactive wastes, so as to reduce the amount of radioactive waste generated. For low-level radioactive combustible waste, it is appropriate to give priority to inorganic and stabilising treatment technologies such as incineration.

2.2 Domestic waste heat treatment research and application

At present, there is no mature radioactive waste heat treatment engineering practice in China, and heat treatment has been applied to a certain extent in the treatment of non-radioactive waste such as municipal hazardous wastes and medical wastes.The Hazardous Waste Incineration Pollution Control Standards (GB 18484-2020) promulgated and implemented in 2020 provides the environmental protection requirements for the treatment of hazardous wastes by applying incineration technology It provides mandatory regulations to ensure the sustainable use of incineration technology.

Relevant domestic research institutes and enterprise units have carried out the practice of hazardous waste plasma melting by drawing on foreign plasma melting technology, among which Jiangsu Tianying Company and Wuxi Nengzhihui Company have carried out the hazardous waste plasma demonstration project, and the practice shows that the plasma incineration technology can well realise the pyrolysis and melting and harmless treatment of hazardous wastes, and can realise a higher volume reduction ratio. China Guangdong Nuclear Research Institute and the Southwest Institute of Physics of the Nuclear Industry have independently developed plasma incineration technology for low-level radioactive wastes in nuclear power plants, of which the former adopts plasma gasification and combustion technology, and the latter adopts plasma pyrolysis and melting technology, and are currently carrying out engineering demonstrations in Gansu Jinta Dongfang Ruilong Environmental Protection and Governance Company and Hainan Changjiang Nuclear Power Plant, respectively, and at present, Dongfang Ruilong has already obtained the operation licence, and will soon carry out incineration of low-emission solid waste, and the plasma melting demonstration project at Hainan Changjiang Nuclear Power Plant has completed its design and development, and is under engineering construction, and is expected to be put into operation in 2025. The China Institute of Radiation

Protection conducted research on incinerators and completed the construction of a prototype mobile incinerator prototype in 2023. The prototype equipment draws on the practical experience of foreign counterparts and has been improved with its own research. The successful development of this prototype provides a model for the adoption of incineration technology for radioactive waste in domestic nuclear power plants.

2.3 Domestic Research and Achievements in Clean Decontamination

At present, in accordance with the requirements of radioactive waste minimisation management and the "Clean Decontamination Levels of Steel, Aluminium, Nickel and Copper Recycling and Reuse in Nuclear Facilities" (GB/T 17567-2009) as well as the practical experience of foreign countries, the domestic nuclear power plant operating units have carried out the practice of clean decontamination of very low-level radioactive wastes, including the adoption of biodegradable materials, very low-level waste sorting and storage decay decontamination, decontamination decontamination, and disposal of waste that has reached the decontamination level using ordinary industrial waste disposal methods. And the recyclable scrap metal to take metal smelting to achieve waste reuse.

In the past ten years, the domestic nuclear power plants have carried out a wide range of radioactive pollutants material cleaning and decontrol practices, and achieved some good management experience:

(1) The clean decontamination of radioactive minor pollutant materials is mainly based on the clean decontamination limit values stipulated in GB 27742-2011, and the materials to be decontaminated are subject to radiation level measurements, decontamination compliance evaluation and application for decontamination.

(2) For different types of pollutant materials in different nuclear facilities, the evaluation and application for decontrol adopts the "one-issue-one-negotiation" method. At present, China has already established a clean decontrol process for materials such as waste resin of the evaporator sewage system and metal frames of the waste air filters.

(3) Cleaning and decontrol materials have been expanded to include work clothes, work shoes, safety helmets, buildings, waste oil and waste organic solvents.

3 Improvement Suggestions for Thermal Treatment and Clean Decontamination

Although the research and application of thermal treatment and clean decontamination have been carried out in China's nuclear power plants, there still exists a big gap compared with the nuclear energy developed countries in Europe and the United States, and in order to achieve waste minimisation, the research and practice of thermal treatment and clean decontamination of radioactive waste need to be carried out continuously. The following are some suggestions for improvement:

(1) It is appropriate to carry out research on automatic rapid measurement technology of nuclide activity concentration and rapid estimation of radionuclide concentration in specific wastes for radioactive light pollutant materials, in order to improve the efficiency of clean decontamination evaluation.

(2) At present, China has issued cleaning and decontrol standards for metals, but has not yet issued cleaning and decontrol specifications for other different types of pollutants, which is not conducive to the development of cleaning and decontrol of other minor pollutant materials by the operating units of

nuclear power plants, and it is advisable to speed up the issuance of cleanliness and decontrol standards and specifications for different materials in accordance with international standards.

(3) Domestic standards for thermal treatment are missing, there are no technical standards for incineration of radioactive waste and technical specifications for plasma incineration, which is not conducive to the practical application of incineration and plasma waste treatment technology, and it is recommended that relevant technical standards be introduced as soon as possible in line with international standards.

(4) The relevant IAEA standards have increased the radioactive level basis for conditional clean decontamination and the interpretation of clean decontamination for gas and liquid, but there are no relevant technical standards in China and very few practices, it is recommended to carry out relevant theoretical research to make up for the shortcomings in this area.

References:

[1] Xu Kan, Xiong Kouhong, et al. Radioactive minor pollutants clean decontamination management practice and thinking[J]. Radiation Protection, 2023,43(4):360-363.

[2] GUO Zhimin. Radioactive solid waste treatment technology [M]. Beijing: Atomic Energy Press, 2007.5

[3] WANG Ping, WEI Guoliang, et al. clean decontamination of radioactive materials[J]. Nuclear Safety, 2015,14(2):6-12.

TOPICAL SESSION 7. Introduction to a Plasma Melting Treatment Process for Radioactive Sludge

Ming Han

Huaneng Shandong Shidao Bay Nuclear Power Co., Ltd., Rongcheng,China

Abstract: This thesis is on the utility model patent [ZL 202320023684.1]: a radioactive sludge waste treatment system process.The patent aims to use plasma high temperature melting technology, through the process of fully automatic control means, to achieve sludge receiving, pre-treatment, temporary storage, melting into glass, and exhaust gas cooling and purification and discharge, and ultimately realise reliable treatment and waste minimisation of radioactive sludge.The final goal is to achieve reliable handling and waste minimisation of radioactive sludge. The treatment process in this thesis is suitable for the treatment of soil wastes with radionuclides or contaminated with radionuclides.The treatment process in this thesis is valuable for the treatment of soil wastes with radionuclides or contaminated by radionuclides.

Key Words: plasma, sludge, nuclear power plant, capacity reduction

Introduction

Currently, nuclear power plants and nuclear steam and heat plants have been developed in China due to their non-greenhouse gas production, high energy density, safe and controllable.

However, the treatment and disposal of radioactive pollutants is also an inherent challenge. Especially for the treatment of large-volume low-level radioactive waste,there is a time-consuming, labour-intensive and safety-regulatory burden, and there is an urgent need for advanced treatment processes to treat LLRW and minimise waste to meet regulatory requirements.

At a nuclear power plant, cement curing of radioactive sludge has been carried out since 2004, resulting in a total of 54.6 m^3 of cement cured radioactive sludge.

During the period from 2017 to 2019, 43.4m^3 (59 barrels in total) were sent to the Northwest Disposal Site of CNNC Qingyuan Environmental Technology Engineering Co.

The remaining 11.2m^3 of cement curing body is temporarily stored in the temporary storage of radioactive waste of the power plant.

On 21 March 2022, an inspection by the East China Nuclear and Radiation Supervision Station (ECNRSS) found that the cement curing body of radioactive sludge sent for disposal by the nuclear power plant had not completed the performance test in accordance with the requirements of the "Performance Requirements for Curing Bodies of Low- and Medium-Level Radioactive Wastes - Cement Curing Bodies" (GB14569.1), and the results of some of the performance tests carried out on the radioactive silt curing body showed that the deviation of its compressive strength exceeds the standard requirement of ±20%; more than 80 per cent of the specimens showed varying degrees of fragmentation in impact resistance; the performance tests for irradiation resistance, freeze-thaw resistance and immersion resistance have not yet been completed. Failure to meet the requirements of

section 8.8 of the Operational Safety Requirements for Nuclear Power Plants. Section 8.8 of the "Operational Safety Requirements for Nuclear Power Plants" states that "the handling and intermediate storage of radioactive wastes must be strictly controlled to ensure that they comply with the requirements for the final safe disposal of radioactive wastes".

The above case shows that radioactive sludge, as a kind of low-level radioactive waste commonly found in nuclear power plants, is mainly found in the groundwater of nuclear islands and in the scale on the bottom of radioactive containers.

It contains both inorganic and organic components, and the organic component means that it can be treated by incineration technology. The conventional cement curing process has its technical drawbacks, i.e. the low technical reliability of the curing body (as described in the case study) and the lack of volume reduction.

After studying the practical experience of power plants overseas, plasma melting was found to be a superior waste treatment process.

In foreign countries, plasma melting has been practically applied in the treatment of hazardous and discharged wastes, and its operation experience shows that plasma has the advantages of high energy density, strong melting power, small secondary pollution, fully melting inorganic materials and burning organic materials with good capacity reduction performance, etc., which makes it has a broad application prospect in the treatment of radioactive sludge..

1 Process Flow Description

The unit used in this process is shown below.

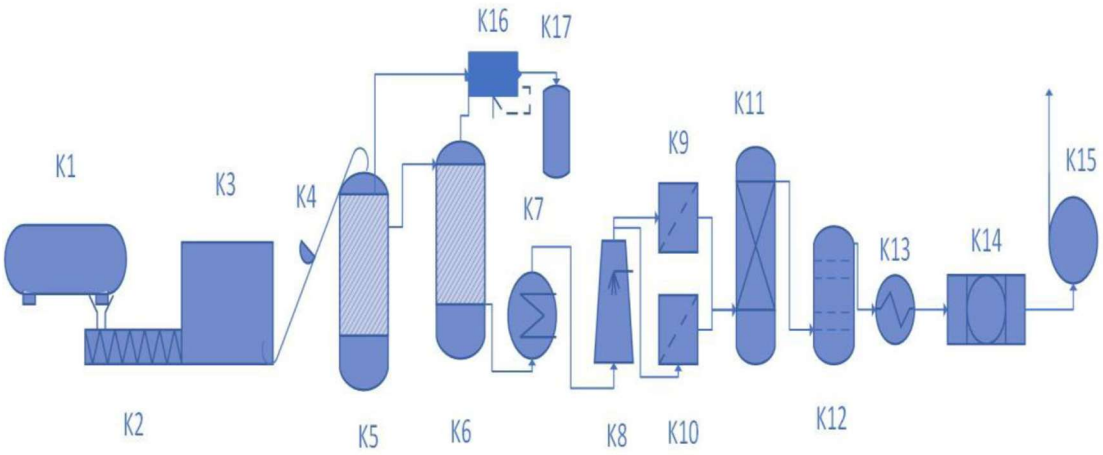

K1 Waste pre-treatment unit; K2 Waste conveyor; K3 Waste packet storage box; K4 Waste packet lifter; K5 First combustion chamber; K6 Second combustion chamber; K7 Heat exchanger; K8 Emergency cooling tower; K9/10 Bag filter; K11 Caustic washing tower; K12 Mist eliminator; K13 Flue gas heat exchanger; K14 High efficiency adsorber; K15 Exhaust fan; K16 Rapid pressure relief valve; K17 Emergency water sealing tank

Fig. 1 Process device diagram

The device mainly includes waste pretreatment and feeding system, plasma high temperature melting system, exhaust gas cooling and purification system, slag and glass curing system, ash unloading and

discharging system as well as corresponding connecting pipelines. The collected radioactive sludge to be treated is transported to the waste pre-treatment unit K1 for sorting, to remove the metal in the sludge or waste that cannot be melted, then drying, cutting, weighing and packaging, and transported via the waste conveyor K2 to the waste package holding tank K3, where it is stored until a certain amount is reached, pending the ignition of the main plasma process system.

After ignition of the main plasma process system, the packaged waste (5kg) and the glass formula packages (1:2 ratio) are transported to the First combustion chamber K5 via the waste pack elevator K4.

After preheating and pyrolysis of the radioactive sludge, the organic matter becomes combustible gas and is sent into the second combustion chamber K6, and the inorganic matter in the radioactive sludge is oxidised in the lower part of K5 and then enters into the melting zone to be melted into slag, which is melted into a vitreous body together with glass formula.The combustible gases enter K6 and are fully combusted by adding oxygen.

The resulting exhaust gas passes through the heat exchanger K7 and the rapid cooling tower K8, cools down step by step, and then passes through the bag filters K9/10 arranged in parallel, through which the filter bags fully filter the exhaust gas.

The filter bag fully filters the particulate impurities in the exhaust gas, and the exhaust gas is sent to K11 alkali washing tower after filtration to fully neutralise the NOx and sulphide in the exhaust gas, and then through the mist eliminator, the water vapour and small droplets that may exist after heat exchange are removed from the exhaust gas through the wire mesh material.The exhaust gas then passes through the flue gas heat exchanger K13 to further condense the water vapour in the flue gas.

The condensed exhaust gas passes through the high-efficiency particle adsorber K14.After adsorption, the toxic and harmful substances in the exhaust gas are efficiently absorbed by the high efficiency adsorber K14 with a front heater and then discharged to the atmosphere through the chimney monitored by exhaust fan K15. In addition, the unit is equipped with a quick pressure relief valve K16, which is used in case of overpressure in the first or second combustion chamber.

In addition, the unit is equipped with a quick pressure relief valve K16, which is used to quickly relieve the pressure in case of high pressure in the first or second combustion chamber, and then discharged into the emergency water sealing tank K17 for overpressure protection.

2 Detailed descriptions of treatment equipment

2.1 Waste pre-treatment device K1

Pre-treatment device K1 is a combined device, which undertakes the functions of sorting, drying, cutting, weighing and packing of waste sludge respectively.

The sorting is operated by artificial glove box, and the drying is provided by hot air device with electric heating wire to provide drying heat source. Before weighing and packing, biodegradable plastic bags are provided.

Before weighing and packing, biodegradable plastic bags are provided to pack the waste sludge after cutting to avoid contamination of the weighing table, and the pretreatment process ensures that the sludge meets the plasma melting requirements.

The pre-treatment process ensures that the sludge meets the requirements of plasma melting.

2.2 First combustion chamber K5

The first combustion chamber K5 is a plasma heating and melting device with a core temperature of 1000-1200 degree Celsius and a heat-resistant crucible as furnace material with corrosion-resistant coating.

It is made of heat-resistant crucible, lined with corrosion-resistant coating and cooled by water-cooled walls on the outside. A nitrogen plasma torch (which can be replaced periodically) is located on the lower left and upper right. The first combustion chamber K5 is divided into preheating, pyrolysis, oxidising and melting zones according to the temperature gradient (of which the the preheating zone is approximately 200 degrees Celsius, the pyrolysis zone is approximately 400-500 degrees Celsius, the oxidation zone is typically 600-800 degrees Celsius, and the melting zone is typically 1000-1200 degrees Celsius).

The sludge is pyrolysed in the pyrolysis zone and the organic matter is combusted to a certain extent in the oxidation zone to form a mixture of combustible gases, which are sent to the second combustion chamber. The inorganic material in the sludge enters the melting zone, and after combustion, it melts with the glass formula to form a glass body.

2.3 Dual combustion chamber K6

The secondary combustion chamber K6 is a plasma-oxygenated combustion unit with a core temperature of 800-900 degrees Celsius. The mixed combustible gases formed in the first combustion chamber K5 are combusted in an oxygenated environment using the second combustion chamber K6 to form an exhaust gas, which is discharged to the exhaust gas treatment system. A small amount of fly ash is returned to the first combustion chamber K5 via the fly ash collection device.

2.4 Emergency Pressure Relief Valve and Emergency Water Seal Tank

An emergency pressure relief valve K16 and an emergency water sealing tank K17 are provided for overpressure protection in the primary and secondary combustion chambers. In case of high temperature and pressure in the first and second combustion chamber, the pressure relief valve opens quickly and discharges the excess gas into the emergency water sealing tank, providing overpressure protection for the first and second combustion chambers.

2.5 Heat exchanger and emergency cooling tower, bag filter

The plant is set up to reduce the temperature of the exhaust gases by two-stage heat exchange using heat exchanger K7 and rapid cooling tower K8, and the exhaust gases are fully filtered by bag filters K9/10.The heat exchanger is a water-cooled contact heat exchanger, in which the cooling water comes from the bottom of the heat exchanger and contacts the exhaust gas from the top in a counter-current process. The cooling water is heated and then cooled again by the external heat exchanger and circulated to cool the exhaust gas. The cooled exhaust gas enters the rapid cooling tower and is rapidly cooled to 200 degrees by spraying and atomising cold water. The cooled exhaust gas enters a bag filter, which uses a pocket filter to retain the particulate impurities in the exhaust gas.

2.6 Alkali washing tower

The plant uses a lye scrubber K11 to neutralise the NOx and sulphides in the exhaust gas to avoid environmental pollution. The lye solution is dilute NaOH solution.

2.7 Mist eliminator and flue gas heat exchanger

The plant uses a mist eliminator K12 and a flue gas heat exchanger K13 for further dehumidification and cooling of the exhaust gas. The mist eliminator removes water vapour entrained in the exhaust gas and any small droplets that may be present after heat exchange.

The flue gas heat exchanger exchanges heat with cold water to further condense the water vapour in the flue gas.

2.8 High efficiency adsorber

A high efficiency particle adsorber (HEPA) K14 with a front electric heater is used to avoid damping of the HEA cartridge due to the low temperature of the exhaust gases, which may affect the filtration effect.

High-efficiency particle adsorber (HEPA) realizes efficient capture of toxic and hazardous substances.

3 Superiority of the process

(1) Plasma has many characteristics such as high energy density, fast reaction speed, wide range of application, small secondary pollution, small amount of exhaust gas, etc. It is recognised by the IAEA as a waste treatment method that can be applied on a large scale, and it has the experience of treating radioactive solid waste in nuclear power plants in foreign countries, but it is mainly used for treating hazardous wastes such as municipal wastes, medical wastes, and so on, domestically. According to the radioactive sludge contains organic and inorganic components, and the plasma has the characteristics of melting and oxygenated combustion, which can achieve the melting treatment of radioactive sludge and achieve the effect of volume reduction. Experiment simulations have demonstrated a volume reduction ratio of up to 20:1, which fully achieves the objective of waste minimisation.

(2) In order to reduce the exposure of personnel to the radioactive sludge decontamination workshop, the device makes full use of automatic control principal technology to achieve the automation of the device operation.

(3) The process is equipped with a perfect exhaust gas treatment system, which can achieve the emission standard of exhaust gas.

(4) This process adopts the glass formula and waste package according to a certain weight proportion of formula feeding, to achieve a high degree of reliability of the performance of the glass body.

(5) The process is equipped with an emergency explosion relief system, i.e., quick pressure relief valve K16 and emergency water sealing tank K17, which can realise the overpressure protection of the first combustion chamber K5 and the second combustion chamber K6, so as to guarantee the safety of the plant equipment and personnel.

(6) The equipment parts used in this process are all commercially available items to achieve cost control.

4 Conclusion

Radioactive sludge plasma melting treatment process adopts advanced plasma high temperature melting heat treatment process to realise the inorganic material melting vitrification, organic material fully combustion and monitoring emission of the treatment purpose, and through automatic control technology, to achieve the reduction of personnel operation and intervention to protect personnel radiation safety.

Through experimental analysis and research, it can achieve a high reduction effect of 20:1, which is a kind of waste treatment with broad application prospects, and has application and promotion value for solid waste of nuclear power plants, as well as radioactively contaminated and even hazardous and medical wastes.

LIST OF EXHIBITORS

■China Institute of Atomic Energy

No. 1 Sanqiang Road, Fangshan District, Beijing, 102413

China

■Nuclover Technology (Beijing) Co.,Ltd.

Room 1107-1109, Building A, No.36 North Third Ring East Road,Beijing

China

■H3D, Inc.

812 Avis Drive,

Ann Arbor, MI 48105

USA

■Chiyoda Technol Corporation

1-7-12, Yushima,

Bunkyo-ku, Tokyo, 113-8681

Japan

LIST OF PARTICIPANTS

Last Name	First Name	Country	Company
Walschaerts	Benedicte Clement	Belgium	Tractebel
Nguyen	Loc	Canada	Self
Zhang	Ye	China	NEA
Feng	Youcai	China	Nuclear and Radiation Safety Center, MEE
Yang	Duanjie	China	Nuclear and Radiation Safety Center, MEE
Li	Bing	China	Nuclear and Radiation Safety Center, MEE
Zhu	Hao	China	Nuclear and Radiation Safety Center, MEE
Fang	Yuan	China	Nuclear and Radiation Safety Center, MEE
Zeng	Chao	China	Nuclear and Radiation Safety Center, MEE
Li	Anqi	China	Nuclear and Radiation Safety Center, MEE
Zhou	Yaocen	China	Eastern Regional Office of the Nuclear and Radiation Safety Inspection,MEE
Lv	Huaquan	China	Huaneng Shandong Shidao Bay Nuclear Power Co.,Ltd
Chen	Liqiang	China	Huaneng Shandong Shidao Bay Nuclear Power Co.,Ltd
Liu	Ying	China	Huaneng Shandong Shidao Bay Nuclear Power Co.,Ltd
Han	Ming	China	Huaneng Shandong Shidao Bay Nuclear Power Co.,Ltd

Last Name	First Name	Country	Company
Xu	Gaoxiang	China	Huaneng Shandong Shidao Bay Nuclear Power Co.,Ltd
Hu	Yangxing	China	Huaneng Hainan Changjiang Nuclear Power Co., Ltd
Jiang	Jianqi	China	CNNP Nuclear Power Operations Management Co., Ltd.
Huang	Hao	China	CNNP Nuclear Power Operations Management Co., Ltd.
Shen	Yanyun	China	CNNP Nuclear Power Operations Management Co., Ltd.
Shen	Haiju	China	CNNP Nuclear Power Operations Management Co., Ltd.
Chen	Quanli	China	Jiangsu Nuclear Power Corporation
Hou	Mingjun	China	Sanmen Nuclear Power Co.,Ltd
Shen	Jingyi	China	China Nuclear Power Engineering Co.,Ltd.
Tian	Yingnan	China	China Nuclear Power Engineering Co.,Ltd.
Wang	Chuan	China	Nuclear Power Operations Research Institute
Liang	Weimin	China	Nuclear Power Operations Research Institute
Dong	Bing	China	Nuclear Power Operations Research Institute
Hong	Yanan	China	China Institute of Atomic Energy
Lu	Zheng	China	China Institute of Atomic Energy
Zhang	Yipin	China	China Institute of Atomic Energy

Last Name	First Name	Country	Company
Du	Xiaohui	China	China Institute of Atomic Energy
Miao	Caixia	China	China Institute of Atomic Energy
Shi	Haijiang	China	China Institute of Atomic Energy
Li	Jinfeng	China	China Institute of Atomic Energy
Chen	Chao	China	China Institute of Atomic Energy
Yuan	Guojun	China	China Institute of Atomic Energy
Li	Shiyao	China	China Institute of Atomic Energy
He	Yuan	China	China Institute of Atomic Energy
Wu	Jianhua	China	China Institute of Atomic Energy
Wang	Chenxiao	China	China Institute of Atomic Energy
Wu	Yihua	China	China Institute of Atomic Energy
Zhu	Fan	China	China Institute of Atomic Energy
Deng	Shuai	China	China Institute of Atomic Energy
Chen	Ran	China	China Institute of Atomic Energy
Cui	Chunsheng	China	China Institute of Atomic Energy
Yuan	Bangzheng	China	China Institute of Atomic Energy

Last Name	First Name	Country	Company
Song	Weijie	China	China Institute of Atomic Energy
Li	Yuejun	China	China Institute of Atomic Energy
Duan	Yunsen	China	China Institute of Atomic Energy
Li	Xiaodun	China	China Institute for Radiation Protection
Li	Hui	China	China Institute for Radiation Protection
Ma	Ji	China	China Institute for Radiation Protection
Sun	Bowen	China	China Institute for Radiation Protection
Shen	Fu	China	China Institute for Radiation Protection
Liu	Ruiwen	China	China Institute for Radiation Protection
Pan	Zhiji	China	China Institute for Radiation Protection
Wang	Chongyang	China	China Institute for Radiation Protection
Li	Hua	China	China Institute for Radiation Protection
Pan	Qianyu	China	China Nuclear Power Research and Design Institute
Li	Xiuchuan	China	Liao Ning Hong Yan He Nuclear Power Co.,Ltd
Qu	Bing	China	Liao Ning Hong Yan He Nuclear Power Co.,Ltd
He	Weihua	China	Taishan Nuclear Power Joint Venture Co., Ltd

Last Name	First Name	Country	Company
Ren	Xueming	China	Taishan Nuclear Power Joint Venture Co., Ltd
Li	Pingwei	China	Yangjiang Nuclear Power Co.,Ltd.
Jiang	Zhao	China	China General Nuclear Power (Shenzhen) Operational Technology & Radiation
Wu	Zhifeng	China	China General Nuclear Power (Shenzhen) Operational Technology & Radiation
Huang	Qianqian	China	China Nuclear Power Engineering Co., Ltd
Fu	Yaru	China	Shanghai Nuclear Engineering Research & Design Institute
Gou	Quanlu	China	Shandong Nuclear Power Company Ltd
Zhang	Yu	China	Shandong Nuclear Power Company Ltd
Zhang	Lizhi	China	State Nuclear Power Demonstration Plant Co.,Ltd
Yang	Ceming	China	State Nuclear Power Demonstration Plant Co.,Ltd
Schieber	Caroline	France	CEPN, ISOE European Technical Centre
Soos	Tamas	Hungary	MVM Paks Nuclear Power Plant Ltd.
Pinak	Miroslav	IAEA	ISOE IAEA Technical Centre
Ma	Jizeng	IAEA	ISOE IAEA Technical Centre
Naka	Motoki	IAEA	ISOE IAEA Technical Centre
Suzuki	Akiko	Japan	Nuclear Regulation Authority

Last Name	First Name	Country	Company
Ozawa	Shingo	Japan	Chiyoda Technol Co., Ltd.
Akaza	Taro	Japan	Chiyoda Technol Co., Ltd.
Suzuki	Toshikazu	Japan	TEPCO
Theune	Andries	Netherlands	EPZ N.V.
De Meij	Semmi	Netherlands	EPZ N.V.
Ekong	Godwin Bassey	Nigeria	Nigeria Nuclear Regulatory Authority
Ahmad	Rana Iftikhar	Pakistan	Pakistan Atomic Energy Commission
Hoffmeister	René	Switzerland	Leibstadt Nuclear Power Plant
Wang	Weiyi	USA	H3D, Inc.
Mazyopa	Bupe Abraham	Zambia	Radiation Protection Authority